Cooperative Assembly with Autonomous Mobile Manipulators in an Underwater Scenario

Davide Torielli

DIBRIS - Department of Computer Science, Bioengineering, Robotics and System Engineering

University of Genova

In partial fulfillment of the requirements for the degree of

Robotics Engineering

30th August, 2019

“Choose a job you love,
and you will never have to work a day in your life”
Confucius (maybe)

Acknowledgements

I would like to thank my mother, my father, and my whole family, without whom I would not be here. I would to thank my sweetheart and my love, Sara (aka Cucurucho) which has always supported me and always will do. She was also really important for reviewing my English.
I would like to thank the Spanish lab, IRSLab, especially Javier, whom really help me a lot despite every morning at 10:12 he distracted me with Spanish almuerzos. I would also to thank professors from my home country, Professor Giuseppe Casalino, and Ernico Simetti, my two thesis relators. I want also to remember my Spanish Supervisors, Professor Pedro J Sanz and Professor Raul Marin Prades.
I think that I have to thanks also my colleague and friend, Fabio. Also him distracted me a lot with very long telephone calls, anyway they were useful for him to learn something from me =) . *Maybe*, *sometimes* it was also useful for me.
Last but not least, I have to thank myself, because I'm great. Bravo Tori.

Abstract

Robotics is spreading in all the relevant sectors of the human life. The importance of studying this field is confirmed by all the various applications where robots are used: exploration of space and sea, industry, healthcare, transportation and so on. This thesis aims to improve the current state of art in a particular field: Underwater Robotics. Currently, the research in this area focuses on improving robots capabilities to make them more and more efficient in performing missions autonomously. A particular advancement is towards the cooperation between multiple agents. With cooperation the robotics systems can perform more and more difficult tasks, such as carrying a long and heavy object in an unstructured environment.
Specifically, the problem is an *assembly* one known as the *peg-in-hole* task. In this case, two autonomous manipulators have to carry *cooperatively* (at kinematic level) a *peg* and have to insert it into an *hole* fixed in the environment. Even if the *peg-in-hole* is a well-known problem, there are no specific studies about when two different autonomous manipulators are used, especially in underwater scenarios. Among all the possible investigations towards this problem, this work focuses mainly on the kinematic control of the robots. The methods used are part of the Task Priority Inverse Kinematic (TPIK) approach, with a cooperation scheme that permits to exchange as less information as possible between the agents (that is really important being water a big impediment for communication). A force-torque sensor is exploited at kinematic level to help the insertion phase. The results show how the TPIK and the chosen cooperation scheme can be used for the stated problem. The simulated experiments done consider little errors in the hole's pose, that still permit to insert the *peg* but with a lot of frictions and possible stucks. It is shown how can be possible to improve (thanks to the data provided by the force-torque sensor) the insertion phase performed by the two manipulators in presence of these errors.
Another part of the thesis deals with computer vision algorithms: a third robot exploits robotic vision methods to estimate the *hole*'s pose. Different techniques are compared to *detect* and to *track* the *hole*, considering the error they provide in the pose's estimation.
Even if the problem is simplified (due to its complexity), this thesis could help further works. The focus is on the particular problem stated, but the methods and tools exploited can be useful also for other applications, not only underwater-related.

Contents

List of Figures

Chapter 1

Introduction

Nowadays, Robotics is spreading in any considerable area of human life. Fields such as exploration of deep space and sea, healthcare, industrial application, transportation, show more and more usage of robotics systems. The research has the responsibility to tackle the increasing needs that these many application have.
The underwater environment is one of the field where Robotics is in a fast escalation, being the sea so important, from industry to environmental issues. Nowadays, different kinds of robot are largely used for underwater missions. A particular type of submarine robot is the Underwater Vehicle Manipulator System (UVMS): an autonomous underwater vehicle (AUV) capable of accomplishing tasks that require a certain level of dexterity, thanks to single or multiple arms.
A really innovative field for underwater missions is the analysis of cooperation between multiple agents, which permits to extend their flexibility. Cooperative robots are two or more robots, identical or different, that coordinate themselves autonomously (i.e. without human intervention) to accomplish various objectives, from mapping an area to assembling an object.

This thesis focuses on a totally unexplored environment: cooperative *peg-in-hole* assembly with underwater manipulators. It is part of the TWINBOT project [TWINBOT (2019)], which is devoted to make a step forward to missions in complex scenarios. Effort is devoted to extend the capability of robots to be able to solve strategic missions.

Part of this thesis is developed at IRSLab at Universitad Jaume I, Castellòn de la Plana, Spain, during the time I spent as an Erasmus+ 2018/19 student, under the supervision of Professor Pedro J. Sanz and Professor Raúl Marín Prades. The IRSLab is the coordinator of the cited TWINBOT project.
Another part of the work is done at GRAAL at Università degli Studi di Genova, Italy, under the supervision of Professor Giuseppe Casalino and Professor Enrico Simetti.

The architecture is implemented in C++ and the code is avaible on GitHub at

the following link: https://github.com/torydebra/AUV-Coop-Assembly.

This thesis is structured as follows. Chapter 1 introduces the problem, recaps the previous work in this field, and states objectives of the work. Chapter 2 defines the theory behind the work. Chapter 3 applies the theory explained to the actual problem, introducing new methods for the stated problem. In Chapter 4 the simulation set-up is described and results are discussed. Chapter 5 focuses on the vision part, explaining methods and examining results. In Chapter 6, conclusions are given. In Appendix A further explanation about the code are given, and in Appendix B discarded methods (but maybe useful for other purposes) for Vision are briefly presented.

1.1 State of the Art

Robots have been massively introduced in various fields to help humans in different tasks. Nowadays, there are various strategies to use them in underwater environments. A manipulator (robot arm) is considered to be the most suitable tool for executing sub-sea intervention operations. Hence, unmanned underwater vehicles (UUVs), such as remotely operated vehicles (ROVs) and autonomous underwater vehicles (AUVs), are equipped with one or more underwater manipulators.

During the last 20 years, underwater manipulators have been used for many different sub-sea tasks in various fields, for example, underwater archaeology [Bingham *et al.* (2010); Drap (2012)], marine geology [Wynn *et al.* (2014); Urabe *et al.* (2015)], and military applications [Capocci *et al.* (2017)].

There are many specific tasks where the underwater manipulators are important, from salvage of sunken objects [Cheng Chang *et al.* (2004)] to mine disposal [Fletcher (2000); Djapic *et al.* (2013)]. One particular scenario is towards the oil and gas industry, where underwater manipulators are used for pipe inspection, opening and closing valves, drilling, rope cutting [Christ & Wernli (2013)], and, in general, to reduced field maintenance and development costs [Gilmour *et al.* (2012)]. A recent survey explored the market related to this technology for oil and gas industry [Diaz Ledezma *et al.* (2015)].

1.1.1 Previous Works in Underwater Missions

Since early '90s, research in marine robotics started focusing on the development of underwater vehicle manipulator systems (UVMS). ROVs have been largely used, but they have high operational costs. This is due to the need for expensive support vessels, and highly qualified man power effort. In addition, the pilot which operates

the vehicle and the arm experiences heavy fatigue in order to carry out the manipulation task.

For the above reasons, the research started to increase the effort toward augmenting the autonomy level in underwater manipulation. For example, to reduce the operator's fatigue, some autonomous control features were implemented in work class ROVs [Schempf & Yoerger (1992)]. Another solution is to completely replace ROVs with autonomous underwater vehicles (AUVs).

Some pioneering projects in this field carried out in the '90s. The AMADEUS project [Lane *et al.* (1997)] developed grippers for underwater manipulation [Casalino *et al.* (2002)] and studied the problem of dual arm manipulation [Casalino *et al.* (2001)].

The UNION project [Rigaud *et al.* (1998)] was the first to perform a mechatronic assembly of an autonomous UVMS.

Early 2000s showed many field demonstrations. The SWIMMER project [Evans *et al.* (2001)] developed a prototype autonomous vehicle to deploy a ROV mounted on an AUV. This permitted to remove the need of long umbilical cables and continuous support by vessels on sea surface.

This work was followed by the ALIVE project [Evans *et al.* (2003); Marty (2004)], that achieved autonomous docking of Intervention-AUV (I-AUV) into to a sub-sea structure not specifically created for AUV use.

The SAUVIM [Yuh *et al.* (1998); Marani *et al.* (2009)] project carried out the first autonomous floating underwater intervention. It focused on the searching and recovering of an object whose position was roughly known a priori. Here, the AUV weighted 6 tons, and the arm only 65 kg, so the dynamics of the two subsystems were practically decoupled and the two controllers were separated. The mission consisted in the AUV performing station keeping while the arm was recovering the object.

After SAUVIM, a project called RAUVI [Prats *et al.* (2012)] took a step further. Here, the AUV performed a hook-based recovery in a water tank. Again, the control of the vehicle and the arm was separated, even if the Girona 500 light AUV and the small 4-degrees-of-freedom (DOF) arm used had more similar masses than the ones used in SAUVIM.

A milestone was the TRIDENT project [Sanz *et al.* (2012)]. For the first time, the vehicle and the arm were controlled in a coordinated manner [Casalino *et al.* (2012)] to recovery a black-box mockup [Simetti *et al.* (2014a)]. The used task priority solution dealt with both equality and inequality control objectives, although the inequality ones were only-scalar, except for the joint limits. This permitted to perform some manipulation tasks *while* considering also other objectives, for example,

keeping the object centred in the camera frame. In this project, only the kinematic control layer (and not also a suitable dynamic one) was implemented.

The PANDORA project [Lane *et al.* (2012)] focused on increasing the autonomy of the robot, by recognizing failures and responding to them. The work combined machine learning techniques [Carrera *et al.* (2014)] and a task priority kinematic control approach [Cieslak *et al.* (2015)]. However it dealt with only equality control objectives, with a specific ad-hoc solution to manage the joint limit inequality task.

The TRIDENT concepts were enhanced within the MARIS project [Casalino *et al.* (2014)]. The used task priority framework [Simetti & Casalino (2016)] permitted to *activate* and *deactivate* equality/inequality control objectives of any dimension (not only scalar ones). This project also extended the problem to cooperative agents [Simetti & Casalino (2017)].

TRIDENT and MARIS concentrated on using the control framework to perform only grasping actions. Recent work [Simetti *et al.* (2018)] analyses how the method can be used in different scenarios, like pipeline inspection and deep sea mining exploration.

The DexROV project [Di Lillo *et al.* (2016)] is studying latencies problems which arise de-localizing on the shore the manned support to ROV operations.

The PROMETEO project [PROMETEO (2016)] plans to improve the use of underwater robotics in archaeological sites. It investigates the manipulation capacity when occlusions of objects can occur and with a wireless communication system to use the robot without umbilical cable.

The ROBUST project [ROBUST (2016)] aims to explore and to map deep water mining sites, through the fusion of two technologies: laser-based in-situ element-analysing, and AUV techniques for sea bed 3D mapping.

1.1.2 The Control Framework

In the '90s, industrial robotics researches focused on how to specify control objectives of a robotic system. This was done especially for redundant systems, i.e. systems with more degree of freedoms (DOFs) than necessary. This surplus is useful to perform multiple, parallel tasks; for example, avoiding an obstacle with the whole arm while the end-effector is reaching a goal. Given that such systems need to complete different goals, it has become important to have a simple and effective way to specify the control objectives.

The task-based control [Nakamura & Hanafusa (1986)], also known as operational space control [Khatib (1987)], defined the control objectives in a coordinate system that is directly linked to the tasks that need to be performed. This idea was

followed by the concept of task priority [Nakamura (1990)]. In this theory, a more important task is executed together with a less important task. To accomplish the whole action, the secondary task is attempted only in the null space of the primary one. This means that the secondary task is executed *only if* it does not go against the accomplishment of the first.

This concept was later generalized to multiple task priority levels [Siciliano & Slotine (1991)]. These works putted the position control of the end-effector as the highest prioritized one, while safety tasks (like joint limits) were only *attempted* at lower priority level.

First studies in control of redundant manipulators [Yoshikawa (1984); Maciejewski & Klein (1985)] managed the free residual DOF in such a way to solve the problem of singularity and obstacle avoidance for an industrial manipulator. Another work [Khatib (1986)] introduced the use of potential functions in industrial manipulators and mobile robots.

A different solution [Chiaverini (1997)] proposed a suboptimal approach. The secondary task was solved as if it was alone, but after it was projected in the null space of the higher priority one. To deal with singularities, a variable damping factor was used [Nakamura & Hanafusa (1986)]. This solution was later enhanced and called null-space-based behavioural control [Antonelli *et al.* (2008)].
The approach does not deal with the problem of algorithmic singularities that can occur due to rank loss caused by the projection matrix. Further works [Marani *et al.* (2003); Flacco *et al.* (2012)] focused on this problem.

Since those times, the task priority framework has been applied to numerous robotic systems, other than redundant industrial manipulators. Some examples includes mobile manipulators [Antonelli & Chiaverini (1998); Antonelli & Chiaverini (2003); Zereik *et al.* (2011)], multiple coordinated manipulators [Padir (2005); Simetti *et al.* (2009)], modular robots [Casalino *et al.* (2009)], and humanoid robots [Sentis & Khatib (2005); Sugiura *et al.* (2007)]. Furthermore, a stability analysis for several prioritized inverse kinematics algorithms can be found in [Antonelli (2009)].

The problem of the classical task priority framework, evident in all the previous mentioned works, is that inequality control objectives (e.g. avoiding joint limits) were never treated as such. In fact, the corresponding tasks were always active, like the equality ones. So, for example, also when the joints are sufficiently far from their limits, the fact that the task is active uselessly adds constraints and "consumes" DOFs. Thus, without a transition, the safety control objectives like joint limits could be only considered as secondary. Otherwise, they would consume DOFs, and mission tasks, like reaching a position with the end-effector, can never be accomplished. This

led to an undesired situation where safety tasks have a lower priority with respect to non-safety ones.

The challenge in activating (inserting) or deactivating (deleting) a task is that these transitions would imply a discontinuity in the null space projector, which leads to a discontinuity in the control law [Lee *et al.* (2012)]. Thus, in the last decade, researches focused on integrate safety inequality control objectives in a more efficient way.

A new inversion operator was introduced [Mansard *et al.* (2009b)] for the computation of a smooth inverse with the ability of enabling and disabling tasks in the context of visual servoing. But the work only dealt with the activation and deactivation of the rows of a single multidimensional task (so, not including the concept of different levels of priority). The extension to the case of a hierarchy of tasks with different priorities was provided successively [Mansard *et al.* (2009a)]. However, the algorithm requires the computation of all the combinations of possible active and inactive tasks, which grows exponentially as the number of tasks increases.

Another work [Lee *et al.* (2012)] modified the reference of each task that was being inserted or being removed, in order to comply with the already present ones, and in such a way to smooth out any discontinuity. However, the algorithm requires $m!$ pseudo-inverses with m number of tasks. For this reason, the authors provided approximate solutions, which are suboptimal whenever more than one task is being activated or deactivated.

Another approach [Faverjon & Tournassoud (1987)] directly incorporated the inequality control objectives as inequality constraints in a Quadratic Program (QP). According to this, the idea was generalized to any number of priority levels [Kanoun *et al.* (2011)]. At each priority level, the algorithm solves a QP problem, finding the optimal solution (in a least-squares sense). Slack variables are used to incorporate inequality constraints in the minimization process. If the solution contains a slack variable different from zero, it will mean that the corresponding inequality constraint is not satisfied. Otherwise, the inequality constraints are propagated to the next level and transformed into an equality ones (to prevent lower priority tasks from changing the best least-square trade-off found). A similar process is done for the equality constraints. A drawbacks of this approach is that the cascade of QP problems can grow in dimension. Another issue is that the activation and deactivation of tasks are not considered. This last point is important when temporal sequences of tasks are used, for example when assembling objects [Nenchev & Sotirov (1994); Baerlocher & Boulic (2004)].

Instead of a cascade of QP problems, another research [Escande *et al.* (2014)] proposed to solve a single problem finding the active set of all the constraints at the same time. Due to its iterative nature, the authors proposed to limit the number

of iterations to achieve a boundary on the computation time, to be more suitable for a real-time implementation. But this solution is not optimal, and, again, activation/deactivation of equality tasks is not considered.

Improvements are made in the already cited TRIDENT project [Sanz *et al.* (2012); Simetti *et al.* (2014a)], where field trials proved how to consider activation and deactivation of scalar tasks. But the solution still lacks the ability to deal with activation/deactivation of multidimensional tasks, i.e. multiple scalar tasks at the same priority level.

The goal reached by TRIDENT are improved in the MARIS project [Casalino *et al.* (2014); Simetti *et al.* (2014b)], where, among the others accomplishment, task transitions were successfully implemented in the framework. In particular [Simetti & Casalino (2016)], possible discontinuities that can arise are eliminated by a task-oriented regularization and a singular value oriented regularization. Plus, the original simplicity of the task priority framework is retained thanks to pseudo-inverses.

1.1.3 The Peg-in-Hole Assembly Problem

The peg-in-hole is an essential task in assembly processes in various fields, such as manufacturing lines.

This task can be performed following the classical position control method. But this is possible only if precise position of the hole is provided, and the position control error of the robot is zero. In practice, these conditions can only be obtained in specialized scenario. In the case of more versatile robots, such as industrial or underwater manipulators, imprecisions and errors are unavoidable.

To deal with these problems, classical works exploit two kind of instruments: cameras and sensors. With camera(s), the robot can roughly recognize the objective (i.e. the hole) and inspect the overall process. Past researches [Miura & Ikeuchi (1998); Pauli *et al.* (2001)] use this idea to extract boundaries of the object. Another one [Chang *et al.* (2011)] uses visual feedback for a micro-peg-in-hole task (hole of $100\mu m$).

Other approaches perform precise assembly of the parts thanks to force/torque sensors installed on the wrist. A study [Shirinzadeh *et al.* (2011)] successfully accomplishes the assembly detecting the force of contact to compensate the positional uncertainty. Newman *et al.* study [Newman *et al.* (2001)] shows how sensors can be used to build map of force and torque values of each contact point. In another works [Dietrich *et al.* (2010); Abdullah *et al.* (2015)], the location of the hole was estimated using the measured reaction moment occurred by the contact. Another good aspect of the sensors [Oh & Oh (2015); Song *et al.* (2016)] is that they can guarantee stable contact through real-time contact force feedback.

Other proposals [Chhatpar & Branicky (2001); Lee & Park (2014)] try to esti-

mate the state of the contact using joint position sensor. This permits to not use the force/torque sensors on the wrist, which would need highly control frequency, and would increase overall cost and operation time. Some researchers [Park *et al.* (2013)] show that assembly task can be accomplished without contact force information and with inaccurate vision data. The proposed strategy mimics the human behaviour: the peg was rubbed in a point close to the object until the relevant objects mated using compliant characteristics. The compliance allows the robot to softly adapt to the hole [Lozano-PÃľrez *et al.* (1984); Xu (2015)]. A Similar, unexpensive, approach is tested experimentally [Park *et al.* (2017)], without the use of force/torque sensors (i.e. no force feedback), nor Remote-center-compliance devices, and with inaccurate hole information.

1.2 Motivation and Rationale

Sea plays an important role in our societies. Many examples are given in the previous section 1.1. When such kind of environment are so important, robotic usage and exploitation is necessary at different level.
This thesis aim to improve the current state of art in autonomy of underwater vehicles. Efforts in this direction can help the robots doing always more complicated tasks, substituting gradually the remotely operated version of them. The peg-in-hole is one example of these complicated tasks. In general, robotic assembly problems have been addressed and explored widely, but, to the best of this author's knowledge, no works have been done for cooperatively assembly in underwater scenarios, except for the TWINBOT project [TWINBOT (2019)], which this thesis is part of. Productions related to this problem can help to improve this actual lack and make the technology to advance. Cooperative agents augment the capability of the single, for example to carry an heavy object. It is important to notice that cooperation here is intended at *kinematic level*. So, for example, it is not intended to deal with swarms of robots. In this case, cooperation means two (or, in general, more than two) robots that share (in some way) their commanded system velocities (the usual output of the kinematic layer) to move together without, in this case, make the common tool fall or break. There is not "high level" reasoning with a planner, but only mathematical formulas to make the robot *cooperate*. Such improvements at kinematic level are important because reduce the effort at high level (i.e. the planner) that, in general, is always necessary but with this kind of method can be less complicated.

At the time this thesis was being developed, the TWINBOT project was in an early stage. So, this works evolves autonomously, always keeping an eye on the main objective of the project: improve capabilities of cooperative underwater intervention robots.

The aim is to developed a kinematic control framework suitable for the underwater *peg-in-hole* scenario. Task Priority Inverse Kinematic is exploited for the control of the single agent, for the cooperation part, and to exploit the information given by cameras and a force-torque sensor.
For the detection and pose estimation of the hole, computer vision algorithm are exploited. In particular, stereo-vision methods are implemented, using the cameras of a third robot, who acts exclusively for the vision part.
This pose is only an estimation: to correctly insert the peg into the hole during the final phase, a force-torque sensor is used and information provided by it shared between the two agents.

Chapter 2

Control Framework

Introduction

In this section, the control framework implemented is discussed. The architecture is constituted by two parts:

- The Mission Manager, which job is to supervision the execution of the overall mission. It provides the *action*, a list of control objective that the Kinematic Control Layer must satisfy.
- The Kinematic Control Layer (KCL) focus on provide the system velocities (i.e. vehicle and joint velocities), given the list of control objectives from the Mission Manager.

This architecture is build from the ones used in Simetti & Casalino (2017), Wanderlingh (2018), Simetti *et al.* (2018). The sections 2.1, 2.2, 2.3, 2.4, and 2.5 derive from these works and are here recalled.

2.1 Definitions

In this section, principal used notations are described.

- The system configuration vector of the robot $\boldsymbol{c} \in \mathbb{R}^n$, $\boldsymbol{c} \triangleq \begin{bmatrix} \boldsymbol{q} \\ \boldsymbol{\eta} \end{bmatrix}$, where $\boldsymbol{q} \in \mathbb{R}^l$ is the l-DOF arm configuration vector and $\boldsymbol{\eta} \in \mathbb{R}^6$ is the vehicle *generalized coordinate position vector*. The first three components of $\boldsymbol{\eta}$ are the position vector $\boldsymbol{\eta}_1 \triangleq \begin{bmatrix} x \\ y \\ z \end{bmatrix}$, with components in the inertial frame $\langle w \rangle$. The last

three components of η are the orientation vector $\boldsymbol{\eta}_2 \triangleq \begin{bmatrix} \phi \\ \theta \\ \psi \end{bmatrix}$ expressed in terms of the three angles roll, pitch, yaw (applied in the yaw-pitch-roll sequence Perez & Fossen (2007)). The singularity given by this Euler sequence that arise when $\theta = \pi/2$ is handled by a specific control objective (i.e. *horizontal attitude*). (TODO) From the explained definition, it results that $n = l + 6$

- The system velocity vector or the robot $\dot{\boldsymbol{y}} \in \mathbb{R}^n$, $\dot{\boldsymbol{y}} \triangleq \begin{bmatrix} \dot{\boldsymbol{q}} \\ \boldsymbol{\nu} \end{bmatrix}$, where $\dot{\boldsymbol{q}} \in \mathbb{R}^l$ are the arm joint velocities and $\boldsymbol{\nu} \in \mathbb{R}^6$ is the vehicle velocity vector. The first three component of $\boldsymbol{\nu}$ are the linear velocities $\boldsymbol{\nu}_1 \triangleq \begin{bmatrix} \dot{x} \\ \dot{y} \\ \dot{z} \end{bmatrix}$ and the last three are the angular velocities $\boldsymbol{\nu}_2 \triangleq \begin{bmatrix} p \\ q \\ r \end{bmatrix}$, both with components in the vehicle frame $\langle v \rangle$. The vehicle is considered fully actuated, so the vector $\dot{\boldsymbol{y}}$ coincides with the control vector used by the kinematic layer.

2.2 Control Objectives

Let us consider what the robot need to achieve. An *objective* is a job that the robot must accomplish during the mission. Different objectives can be requested at the same time, for example we want the joints to stay away from their physical limits, the robot to maintain an horizontal attitude, and the end-effector to reach a desired pose.

2.2.1 Control Objectives classification

Control objectives can be classified in order of importance in the execution of the mission. Some of them can be more important of others. For example, usually we prefer that the robot do not hurt humans over the reaching of a goal. Another example could be that the robot should first act to not damage itself while accomplish the mission. In general this give the idea that the more important objectives have to been satisfied first, and then, *if possible*, also the less important ones. A general classification based on the *priority* is given here (from the more important class to the less important one):

- *Physical Constraints* objectives. This include interaction with environment (e.g not push against a rigid surface, impose a cooperative tool velocity).
- *System Safety* objectives, e.g. avoiding joint limits or obstacles.
- *Prerequisite* objectives. This is for objectives needed to accomplish the mission, like focus the camera on the object to be grasped
- *Mission* objectives, the actual objective that define the mission, like reach an end-effector position.
- *Optimization* objectives, to choose, among the possible solution (if multiple ones exist) the best one. To example, to choose the one which has the best energy efficiency.

2.2.2 Equality and Inequality Objectives

We consider a variable $\boldsymbol{x}(\boldsymbol{c}) \in \mathbb{R}^m$, dependent on the robot configuration vector $\boldsymbol{c}$, with p the control objective *dimension*. The control objective can be of two types:

- *Equality control objective*, the requirement, for $t \to \infty$, that $\boldsymbol{x}(\boldsymbol{c}) = \boldsymbol{x}_0$.
- *Inequality control objective*, the requirement, for $t \to \infty$, that $\boldsymbol{x}(\boldsymbol{c}) < \boldsymbol{x}_{max}$ or $\boldsymbol{x}(\boldsymbol{c}) > \boldsymbol{x}_{min}$ or $\boldsymbol{x}_{min} < \boldsymbol{x}(\boldsymbol{c}) < \boldsymbol{x}_{max}$.

Please note that here symbols $=, <, >$ refers to element-by-element comparison of the vectors.

2.2.3 Reactive and non Reactive Control Task

For each control objective, there is always an associated *feedback reference rate*. The aim is to drive the variable $\boldsymbol{x}(\boldsymbol{c})$ toward a point $\boldsymbol{x}^*$ where the control objective requisite is satisfied. The used example of *feedback reference rate* is:

$$\dot{\tilde{\boldsymbol{x}}}(\boldsymbol{x}) \triangleq \gamma(\boldsymbol{x}^* - \boldsymbol{x}), \quad \gamma > 0 \tag{2.1}$$

That is a simple proportional law, where γ is a positive gain proportional to the desired convergence rate for the considered variable.

To link the considered variable $\boldsymbol{x}(\boldsymbol{c})$ to the system velocity vector, the following relationship is used:

$$\dot{\boldsymbol{x}} = \boldsymbol{J}\dot{\boldsymbol{y}} \tag{2.2}$$

that express how system velocity vector $\dot{\boldsymbol{y}}$ influences the rate of change of the variable. $\boldsymbol{J} \in \mathbb{R}^{m \times n}$ is the so-called *task-induced Jacobian*.
Having the actual $\dot{\boldsymbol{x}}$ as much as possible equal to the desired reference $\bar{\boldsymbol{x}}$ is called *reactive control task*.

There are situation where a task has not an associated control objective. For example, it happens when an external command (e.g. an human operator, or an imposed vehicle velocity) provide directly the reference velocities. In this case, there is no desired $\boldsymbol{x}^*$ to reach, and the reference is generated by something else. It this case, we speak about *non-reactive control task*.

2.2.4 Control Objectives Activation and Deactivation

During the execution of a mission, not always each inequality control control objective is relevant. As an example, maintaining joints away from their mechanical limits is a safety task which is needed only when the joints are actually near its limits. When a joint is sufficiently far away, there is no necessity to overconstrain the system imposing a velocity. To deal with this, we speak about *activation* and *deactivation* of control objectives and their relative control task. Let us define the following *activation function*:

$$a(x) \in [0, 1] \tag{2.3}$$

as a continuous, sigmoidal, function, which assumes 0 value outside the validity region of the control objective, and 1 inside it. In between, a smooth transition is present, to gently activate/deactivate the control objective.
For example, considering a scalar ($p = 1$) inequality control objective with the requirement $x(\boldsymbol{c}) > x_{min}$ the *activation function* is defined as:

$$a(x) \triangleq \begin{cases} 1, & x(\boldsymbol{c}) < x_{min} \\ s(x), & x_{min} \leq x(\boldsymbol{c}) \leq x_{min} + \Delta \\ 0, & x(\boldsymbol{c}) > x_{min} + \Delta \end{cases} \tag{2.4}$$

where $s(x)$ is a smooth decreasing function joining the two extreme value 1 and 0, and Δ a value to create a zone where the inequality is satisfied but the activation is between 1 and 0 to prevent chattering problems. Similar definition can be done for the other two kind of inequality control objectives.

In general, when multidimensional control objectives ($m > 1$) are present, the

activation takes the form of a diagonal matrix:

$$\boldsymbol{A} \triangleq \begin{bmatrix} a_1 & & \\ & \ddots & \\ & & a_m \end{bmatrix} \tag{2.5}$$

Obviously, for equality control tasks the activation is not defined, because they are always "active".

For *non-reactive* control tasks, the activation is simply $\boldsymbol{A} \equiv \begin{bmatrix} 1 & & \\ & \ddots & \\ & & 1 \end{bmatrix}$, being absent the variable $x(\boldsymbol{c})$

2.3 Task Priority Inverse Kinematics

We describe an *Action* $\mathscr{A}$ as list of prioritized control objectives. Each objectives is positioned at a defined priority level k. With this notation, the following symbols are defined:

- $\dot{\tilde{\boldsymbol{x}}}_k \triangleq \begin{bmatrix} \dot{\tilde{x}}_{1,k} & \cdots & \dot{\tilde{x}}_{k_m,k} \end{bmatrix}^T$ is the vector of the reference velocities for the control task k, of dimension k_m.
- $\dot{\boldsymbol{x}}_k \triangleq \begin{bmatrix} \dot{x}_{1,k} & \cdots & \dot{x}_{k_m,k} \end{bmatrix}^T$ is the current rate of change of the k task.
- $\boldsymbol{J}_k$ is the Jacobian relationship which relates the current rate-of-change $\dot{\boldsymbol{x}}_k$ with the system velocity vector $\dot{\boldsymbol{y}}$ as in equation (2.2).
- $\boldsymbol{A}_k \triangleq \text{diag}(a_{1,k}, \cdots, a_{k_m,k})$ is the diagonal matrix of all the activation functions described in section 2.2.4

It is important to notice that different objectives can have same priorities k. In this case, it is possible to simply stack the vectors and matrices to obtain a objective and a related task k that includes both objectives. Without loss of generality, different objectives will be considered always at different priority levels.

The aim of the kinematic layer is to find the system velocity vector $\bar{\boldsymbol{y}}$ that satisfies *as much as possible* the requirements of each objective of the action $\mathscr{A}$. Given the presence of different objectives with different priorities, it must be taken into account to satisfy higher priority objective first. To do this, a sequence of nested minimization problems must be solved:

$$S_k \triangleq \left\{ \arg\text{R-}\min_{\dot{\tilde{\boldsymbol{y}}} \in S_{k-1}} \left\| \boldsymbol{A}_k (\dot{\tilde{\boldsymbol{x}}}_k - \boldsymbol{J}_k \dot{\tilde{\boldsymbol{y}}}) \right\|^2 \right\}, \; k = 1, 2, \ldots, N, \tag{2.6}$$

where $S_0 \triangleq \mathbb{R}^n$, S_{k-1} is the manifold of solutions of all the previous tasks in the hierarchy, and N is the total number of priority levels. This is the so called *Task Priority Inverse Kinematic* (TPIK). The notation R-min is introduced in Simetti & Casalino (2016). The so called *iCAT* (inequality Constraints And Task transitions) framework solve the (2.6) with the algorithm 1.

Algorithm 1 iCAT

$\boldsymbol{\rho}_0 = \mathbf{0}$
$\boldsymbol{Q}_0 = \boldsymbol{I}$
for k=1 **to** N **do**
  $\boldsymbol{W}_k = \boldsymbol{J}_k \boldsymbol{Q}_{k-1} (\boldsymbol{J}_k \boldsymbol{Q}_{k-1})^{\#,\boldsymbol{A}_k,\boldsymbol{Q}_{k-1}}$
  $\boldsymbol{Q}_k = \boldsymbol{Q}_{k-1} (\boldsymbol{I} - (\boldsymbol{J}_k \boldsymbol{Q}_{k-1})^{\#,\boldsymbol{A}_k,\boldsymbol{I}} \boldsymbol{J}_k \boldsymbol{Q}_{k-1})$
  $\boldsymbol{\rho}_k = \boldsymbol{\rho}_{k-1} + \mathrm{Sat}\left(\boldsymbol{Q}_{k-1} (\boldsymbol{J}_k \boldsymbol{Q}_{k-1})^{\#,\boldsymbol{A}_k,\boldsymbol{I}} \boldsymbol{W}_k \left(\dot{\boldsymbol{x}}_k - \boldsymbol{J}_k \boldsymbol{\rho}_{k-1}\right)\right)$
end for
$\dot{\boldsymbol{y}} = \boldsymbol{\rho}_N$

The special pseudo inverse operator $(\cdot)^{\#,\boldsymbol{A},\boldsymbol{Q}}$ [Simetti & Casalino (2016)] manages some invariance problems of (2.6); the function Sat$(\cdot)$ [Antonelli *et al.* (2009)] controls the variable saturations. Details of the procedure can be found again in [Simetti & Casalino (2016)].

2.3.1 Notes on Conflicting Objectives

From section 2.2.1, it should be understood that lower priority task are not always satisfied. The problem with this arise when the main mission objective, that is not at the higher priority, can't be never accomplished, thus failing the general mission. This can be the case with an obstacle: the robot may stuck in a point of *local minima* (that is anyway better than crash into it). This is a general problem of all reactive controlling method. The solution must be found at the mission manager level, which should plan another path or another sequence of Actions. This problem is not considered in this work.

2.4 Arm-Vehicle Coordination Scheme

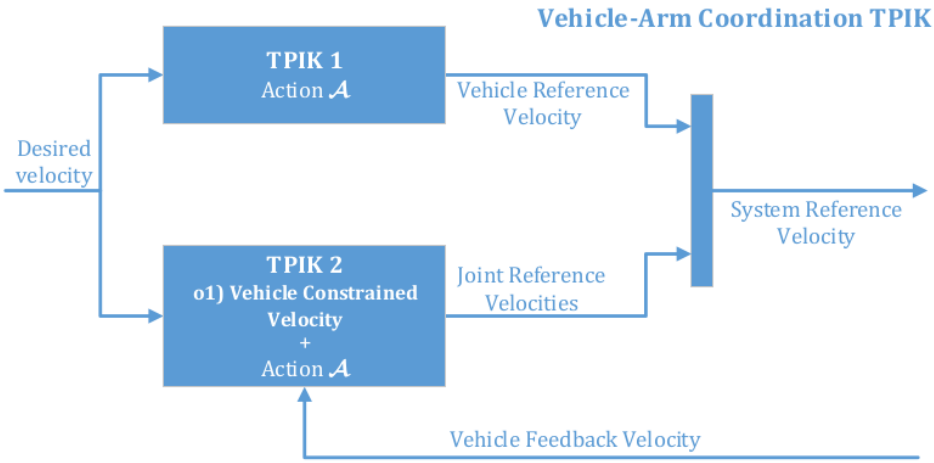

Figure 2.1: A scheme showing the two Task Priority Inverse Kinematics blocks for the arm-vehicle coordination implementation

Inaccuracy in velocity tracking for vehicle can have effects on the arm. A relevant problem arises when disturbances of the floating base, caused by thrusters or its large inertia, propagate and affect the end effector motions [Simetti & Casalino (2017)]. To solve this, a kinematic decoupling of arm and base is done, implementing it within the task priority approach The idea is to have two parallel TPIK as shown in 2.1:

- The first TPIK 1, given the Action $\mathscr{A}$ consider the vehicle together with the arm as a whole full controllable system. From its output $\dot{\mathbf{y}}$ only the vehicle reference velocity are taken.
- The second TPIK 2 consider the vehicle as totally non controllable. So, a *non-reactive* task (2.2.3) is used at the top of the priority list to *constrain* the output velocities of the vehicles to the actual one. From the total output $\dot{\mathbf{y}}$, only the manipulator part is taken.
  In this way, the manipulator velocity are *optimized* to follow *at best* the objectives of the action $\mathscr{A}$ considering the *measured* vehicle velocity and their influence on the objectives.

In general, a multi-rate control of arm and vehicle is used, which means that velocities for arm and vehicle are given at different frequency. This schema is suitable

for such an implementation: the TPIK 2 can run at higher frequency, updating the manipulator commanded velocities more frequently that the vehicle commanded ones.

2.5 Cooperation Scheme

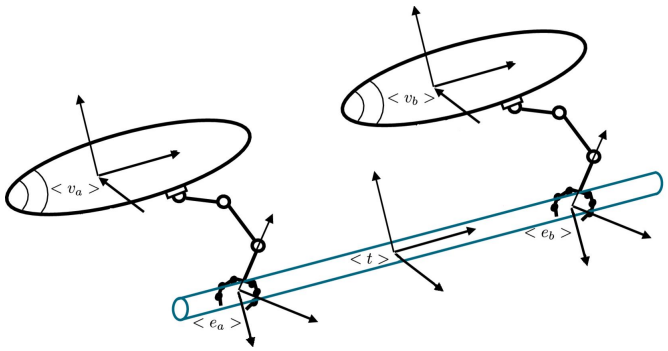

Figure 2.2: The frames of the two cooperative vehicles carrying a common object

The discussion about cooperation is here explained, limiting it to include only two cooperating robotic systems. This is used to transporting a common object. The coordination policy described take care of the bandwidth restriction in underwater scenario. Thus, it deals with the cooperation in a decentralized manner, limiting the exchange of information.
It is assumed that the object is held firmly by both agents, so no sliding happens during the missions. The two robots agree on a shared fixed frame, so, their respective tool frames $\langle t_a \rangle$ and $\langle t_b \rangle$ and the object frame $\langle o \rangle$ are coincident:

$$\langle t \rangle \triangleq \langle t_a \rangle = \langle t_b \rangle = \langle o \rangle$$

In the figure 2.2) the cited frames are shown. The firm grasp assumption imposes that

$$\dot{\boldsymbol{x}}_t = \boldsymbol{J}_{t,a}\dot{\boldsymbol{y}}_a = \boldsymbol{J}_{t,b}\dot{\boldsymbol{y}}_b \tag{2.7}$$

with $\dot{\boldsymbol{x}}_t$ the object velocity with component on $\langle t \rangle$, $\dot{\boldsymbol{y}}_a$ and $\dot{\boldsymbol{y}}_b$ the system velocity vectors of agents a and b as described in section 2.1, and $\boldsymbol{J}_{t,a}$ the system Jacobians of agents a and b with respect to $\langle t \rangle$. These Jacobians tells how the tool velocities $\dot{\boldsymbol{x}}_t$ are affected by system velocities $\dot{\boldsymbol{y}}_a$ and $\dot{\boldsymbol{y}}_b$. Due to the firm grasp assumptions, the tool velocities generates by $\dot{\boldsymbol{y}}_a$ and $\dot{\boldsymbol{y}}_b$ must be equal.

The equation (2.7) derived from the grasp constraint and can be expressed in the Cartesian space as:

$$\dot{\boldsymbol{x}}_t = \boldsymbol{J}_{t,a}\boldsymbol{J}^{\#}_{t,a}\dot{\boldsymbol{x}}_t = \boldsymbol{J}_{t,b}\boldsymbol{J}^{\#}_{t,b}\dot{\boldsymbol{x}}_t \tag{2.8}$$

$$(\boldsymbol{J}_{t,a}\boldsymbol{J}^{\#}_{t,a} - \boldsymbol{J}_{t,b}\boldsymbol{J}^{\#}_{t,b})\dot{\boldsymbol{x}}_t \triangleq \boldsymbol{C}\dot{\boldsymbol{x}}_t = \boldsymbol{0} \tag{2.9}$$

$$\dot{\boldsymbol{x}}_t \in ker(\boldsymbol{C}) = Span(\boldsymbol{I} - \boldsymbol{C}^{\#}\boldsymbol{C}) \tag{2.10}$$

The kernel of $\boldsymbol{C}$, called *Cartesian Constraint Matrix*, express the space of achievable object velocities at the current configuration.
The idea of the scheme is to put a non-reactive task at the top of the priority, to constrain the desired object velocity $\dot{\bar{x}}$in this subspace. In this way both agents can follow this desired object velocity despite the different situation caused by other objectives.

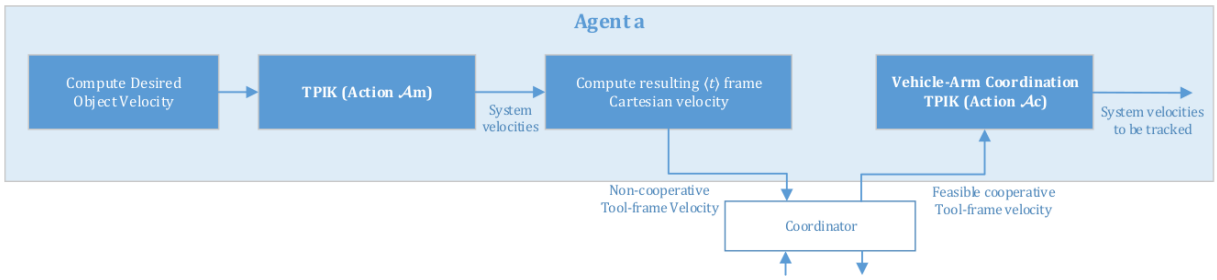

Figure 2.3: The cooperation algorithm with its different steps

The algorithm, sketched in fig. 2.3 proceeds as follows:

- In the first step, the two agents run the algorithm of 2.3 as they were the only to act. So, we have:

  $$\dot{\boldsymbol{x}}_{t,a} = \boldsymbol{J}_{t,a}\dot{\boldsymbol{y}}_a, \qquad \dot{\boldsymbol{x}}_{t,b} = \boldsymbol{J}_{t,a}\dot{\boldsymbol{y}}_b \tag{2.11}$$

  where, in general, the two *non cooperative* tool velocities are different: $\dot{\boldsymbol{x}}_{t,a} \neq \dot{\boldsymbol{x}}_{t,b}$.

- The tool velocities are exchanged (i.e. sent to the coordinator) and a *cooperative* tool velocity is computed:

  $$\dot{\hat{\boldsymbol{x}}}_t = \frac{1}{\mu_a + \mu_b}(\mu_a\dot{\boldsymbol{x}}_{t,a} + \mu_b\dot{\boldsymbol{x}}_{t,b}), \qquad \mu_a, \mu_b > 0 \tag{2.12}$$

$$\begin{aligned} \mu_a &= \mu_0 + \|\dot{\tilde{\boldsymbol{x}}}_t - \dot{\boldsymbol{x}}_{t,a}\| \triangleq \mu_0 + \|\boldsymbol{e}_a\|, \\ \mu_b &= \mu_0 + \|\dot{\tilde{\boldsymbol{x}}}_t - \dot{\boldsymbol{x}}_{t,b}\| \triangleq \mu_0 + \|\boldsymbol{e}_b\|, \\ \mu_0 &> 0 \end{aligned} \tag{2.13}$$

where $\dot{\tilde{\boldsymbol{x}}}_t$ is the ideal velocity that, if applied, would asymptotically take the tool to the desired goal.
The *cooperative* tool velocity is a *weighted* compromise between the two *non cooperative* ones. The *weights* μ_a, μ_b given more freedom to the robot which meet the highest error $\boldsymbol{e}$. This error is a way to understand how much one robot is in difficult in tracking the *ideal* tool velocity $\dot{\tilde{\boldsymbol{x}}}_t$.

- The new *cooperative* tool velocity $\dot{\hat{\boldsymbol{x}}}_t$ is not, in general, a *feasible* velocity that both vehicle can provide to the tool. So, an additional passage is required:

$$\dot{\tilde{\boldsymbol{x}}}_t \triangleq \left(\boldsymbol{I} - \boldsymbol{C}^{\#}\boldsymbol{C}\right)\dot{\hat{\boldsymbol{x}}}_t \tag{2.14}$$

  with $\boldsymbol{C}$ defined in (2.9).

- Each agent run a new TPIK procedure, identical to the first one, but with a *non-reactive* control objectives to track the *feasible cooperative* velocity $\dot{\tilde{\boldsymbol{x}}}_t$. The outputs of the two agents algorithm, $\dot{\hat{\boldsymbol{y}}}_a$ and $\dot{\hat{\boldsymbol{y}}}_b$ will be the final velocities which the kinematic layer provides.
  Moving the equality control objective to make the end effector reach the goal at the top of the hierarchy does not influence the safety tasks. This property is proven in Wanderlingh (2018).

In this described method, the only information that the agent must exchange are the *non-cooperative* velocities $\dot{\boldsymbol{x}}_{t,a}, \dot{\boldsymbol{x}}_{t,b}$, the feasible ones $\dot{\tilde{\boldsymbol{x}}}$ and the constraint matrix $\boldsymbol{C}$. Furthermore, even less data can be exchanged if the *coordinator* is a procedure which runs on a robot, and it is not on an external node.

Chapter 3

Control Architecture: Methods

In this chapter, the theory explained in the previous chapter 2 is exploited to the specific scenario stated for this thesis.
A specific objective, the *Force-Torque* objective (3.1), is added to the TPIK list. This permits to help the insertion phase, dealing with forces and torques *at kinematic level*.
Another section (3.3) describes another (additional) method to improve the performance of the mission. In brief, the goal frame inside the peg is, in general, not precise. This causes additional contacts between peg and inner hole. This collisions are used to modify the goal frame, reducing the error of the estimated goal pose.

3.1 Force-Torque Objective

Information from a force torque sensor can be exploited at kinematic level, inserting an additional control objective into the TPIK procedure. The aim of this objective is to zeroing the forces and torques acting on the peg. This is done generating properly joints and vehicle velocities to drive the peg in such a way the forces and torques decrease.
If we visualize the resultant of the forces caused by the collisions on the peg as a vector, moving *linearly* the peg along this vector will cause the forces itself to decrease. The same idea can be use with torques, *rotating*, along the resultant vector instead of moving linearly.

The *feedback reference rate* for this objective will be:

$$\dot{\tilde{\boldsymbol{x}}}_{ft} \triangleq \begin{bmatrix} \dot{\tilde{x}}_f \\ \dot{\tilde{x}}_m \end{bmatrix} \triangleq \begin{bmatrix} \gamma_f \\ \gamma_m \end{bmatrix} \begin{bmatrix} 0 - \|\boldsymbol{f}\| \\ 0 - \|\boldsymbol{m}\| \end{bmatrix} \qquad 0 < \gamma_f < 1, \quad 0 < \gamma_m < 1 \tag{3.1}$$

where $\|\boldsymbol{f}\|$ and $\|\boldsymbol{m}\|$ are the norms of the forces and torques vectors $\boldsymbol{f}$ and $\boldsymbol{m}$. Gains

smaller that 1 are necessary because big gains would mean too big velocities provided.
It can be noticed that, instead the full 3-dimensional vectors $\boldsymbol{f}$ and $\boldsymbol{m}$, the norms f and m are used. This is done to not overconstrain the system and to let more freedom to lower priority task. Even with norms, the control objective is obviously satisfied, because zeroing the norms brings each component of the vector to zero.

The *feedback reference rate* of equation (3.1) is intended to be like a velocity that the tool must follow. So, the Jacobian must be built considering this thing. For the *task-induced* Jacobian (section 2.3) of this new task, we have to take the linear and the angular part, and pre-multiplying them for the normal vector of $\boldsymbol{f}$ and $\boldsymbol{m}$ transposed:

$$\boldsymbol{J}_{ft} \triangleq \begin{bmatrix} \boldsymbol{J}_f \\ \boldsymbol{J}_m \end{bmatrix} \triangleq \begin{bmatrix} \left(-\frac{\boldsymbol{f}}{\|\boldsymbol{f}\|}\right)^T & {}^{lin}\boldsymbol{J}_t \\ \left(-\frac{\boldsymbol{m}}{\|\boldsymbol{m}\|}\right)^T & {}^{ang}\boldsymbol{J}_t \end{bmatrix} \tag{3.2}$$

where $\boldsymbol{J}_f, \boldsymbol{J}_m \in \mathbb{R}^{1\times l}$; J_t is the Jacobian which express how Cartesian velocity $\dot{\boldsymbol{x}}_t$ of the tool are affected by the system velocity vector $\dot{\boldsymbol{y}}$; lin, ang superscripts refer to *linear* (top three rows) and *angular* (bottom three rows) parts of J_t.

This objective can be considered as a *pre-requisite* one (section 2.2.1). So, it is put at higher priority than the *reaching goal objective*. This will cause the robot to, first, try to nullified the forces and torques (if collisions happened), and only after (i.e. *if possible*) to move the peg towards the goal.
Deactivating the task is necessary when the forces and/or torques are zero, to not generate system velocities for this task when they are not necessary. So a smooth activation function (section 2.2.4), $\boldsymbol{A} \in \mathbb{R}^{2\times 2}$ is used:

$$\begin{gathered} \boldsymbol{A}_{ft} \triangleq \begin{bmatrix} a_f & 0 \\ 0 & a_t \end{bmatrix} \\ a_f(\|\boldsymbol{f}\|) \triangleq \begin{cases} 0, & \|\boldsymbol{f}\| = 0 \\ s(\|\boldsymbol{f}\|), & 0 < \|\boldsymbol{f}\| \leq 0 + \Delta \\ 1, & \|\boldsymbol{f}\| > 0 + \Delta \end{cases} \\ a_m(\|\boldsymbol{m}\|) \triangleq \begin{cases} 0, & \|\boldsymbol{m}\| = 0 \\ s(\|\boldsymbol{m}\|), & 0 < \|\boldsymbol{m}\| \leq 0 + \Delta \\ 1, & \|\boldsymbol{m}\| > 0 + \Delta \end{cases} \end{gathered} \tag{3.3}$$

where $s(\cdot)$ is a smooth *increasing* function from 0 to 1, and Δ a constant to create the smooth zone.

3.2 Objectives Prioritized List

In this section, the objectives inserted into the TPIK procedure are listed and briefly explained.

The first task prioritized list, the one where the two robot acts independently to each other (section 2.5), is:

- **Joint Limits avoidance** (*reactive, inequality, safety*): this objective keep joint away for their mechanical limits. It must be at high priority because it is a safe task, and also must be an inequality objective to not overconstrain the system when joints are away from their limits.
- **Horizontal Attitude** (*reactive, inequality, safety*): to maintain the vehicle horizontal respect to the water surface. Most of the underwater vehicle are are passively stable in roll and pitch and these DOF are not controllable, so this objective is only needed for fully actuated vehicles (as stated in this case).
- **Force-Torque** (*reactive, inequality, pre-requisite*): to nullified the forces and torques acting on the peg during the insertion. This objective is detailed in section 3.1.
- **Tool position control** (*reactive, equality, mission*): this is the objective that define the mission. It is used to bring the tool towards the defined goal (i.e. inside the hole).
- **Preferred Arm Shape** (*reactive, inequality, optimization*): this is a low priority objective that, *if possible*, maintain the arm in a predefined shape. This shape permits the arm to have good dexterity but it is also useful to transport the peg in a natural way.

The categories (written in italic) are explained in section 2.2; further explanations on these and other objectives are available in Simetti & Casalino (2017), Wanderlingh (2018), Simetti *et al.* (2018). Please note that in the code there is also an additional *last task* which is used to cancel out any practical discontinuities during task activations [Simetti & Casalino (2016)].

The TPIK procedure is run two more times, one for the vehicle-arm coordination (section 2.4), the other for the cooperation between the two robots (section 2.5).

Respectively, two *non-reactive* objectives are put at the top of the hierarchy listed above, as explained in the cited sections.

Please note that some important objectives related to safe transportation (e.g. obstacle avoidance, minimum altitude from seafloor, minimum distance between robots), grasping (e.g. camera centring object) are not considered because they are not necessary in the particular experiment chosen, and also because they are explored in other works [Simetti & Casalino (2017); Simetti *et al.* (2018)].

3.3 The Change Goal Frame routine

In general, the frame where the tool is dragged by the control architecture (the *goal* frame) is known with some errors. This is the case when, for example, we have some computer vision algorithm to estimate the hole pose. This error between ideal goal and estimated one, along linear and angular component, can cause the peg to collide more with the hole. If the peg clashes against the hole structure face (i.e. outside the proper hole) it is pushed back and a stuck may happen. In the literature, various methods (cited in 1.1.3) have been explored to deal with this problem.
This thesis focuses only the final part of the problem, i.e. when the peg is inside the hole, but bad alignment causes lot of collisions between peg and hole's internal walls. In this case, the peg usually does not stuck in a intermediate position, because the forces and torques acting on the peg *naturally* drive it towards the goal (that is at a certain depth in the hole). In such a way, the peg continuously scrapes along the hole's walls, possibly damaging the pipe, the hole and also the robot which can suffer some stress. In practice there is a chattering problem: the peg continuously *bounces* because the control wants to drag it towards the erroneous pose, while the hole's walls cause forces in opposite direction.
The method explained in this section try to solve this problem, modifying the goal accordingly to the forces acting on the peg. Considering the cartesian coordinate of the origin ${}^w\boldsymbol{g} \in \mathbb{R}^3$ of the goal frame, projected on the world frame, we modify it, providing ${}^w\boldsymbol{g}' \in \mathbb{R}^3$ as:

$$\begin{aligned} {}^w\boldsymbol{g}' &= {}^w\boldsymbol{g} + {}^w\tilde{\boldsymbol{f}} \\ {}^w\tilde{\boldsymbol{f}} &= {}^w\boldsymbol{R}_t \, {}^t\tilde{\boldsymbol{f}} \\ {}^t\tilde{\boldsymbol{f}} &= k\,[0, f_y, f_z] \qquad 0 < k < 1 \end{aligned} \tag{3.4}$$

where $[0, f_y, f_z]$ is the vector which represent the resultant of the forces acting on the peg, projected on the *tool* frame, but with the component along x put to zero; ${}^w\boldsymbol{R}_t$ is the rotation matrix from world to tool; k a positive gain lesser than 1.

The component on x axis of the force is neglected. This because the x axis of the tool frame $\langle t \rangle$ is the one along the length of the peg. So, we do not want that this component modify the goal because can modify the wanted depth at which we want the peg to be inserted.
To proper utilize the force vector in the sum with the vector of the goal position, we must use a gain k. This gain is less than one change very slowly the goal position.
The formula (3.4) is used every time a force (not null) is detected.

To understand better the method, we can take as an example one where the estimated goal is a bit on the left of the ideal one, but not so much to make the peg miss the hole. In such a case, the control architecture drive the peg on the left of the hole, causing a lot of collisions with the left side of the inner hole. So, the peg suffers forces with an important component in the right direction. Thus, this method shifts the goal to the right.
From this example should be noticed that this approach could cause the same problem in the opposite direction, if the goal is modified too much on the right. For this reason, setting a suitable k is important.

Chapter 4

Control Architecture: Simulation Results

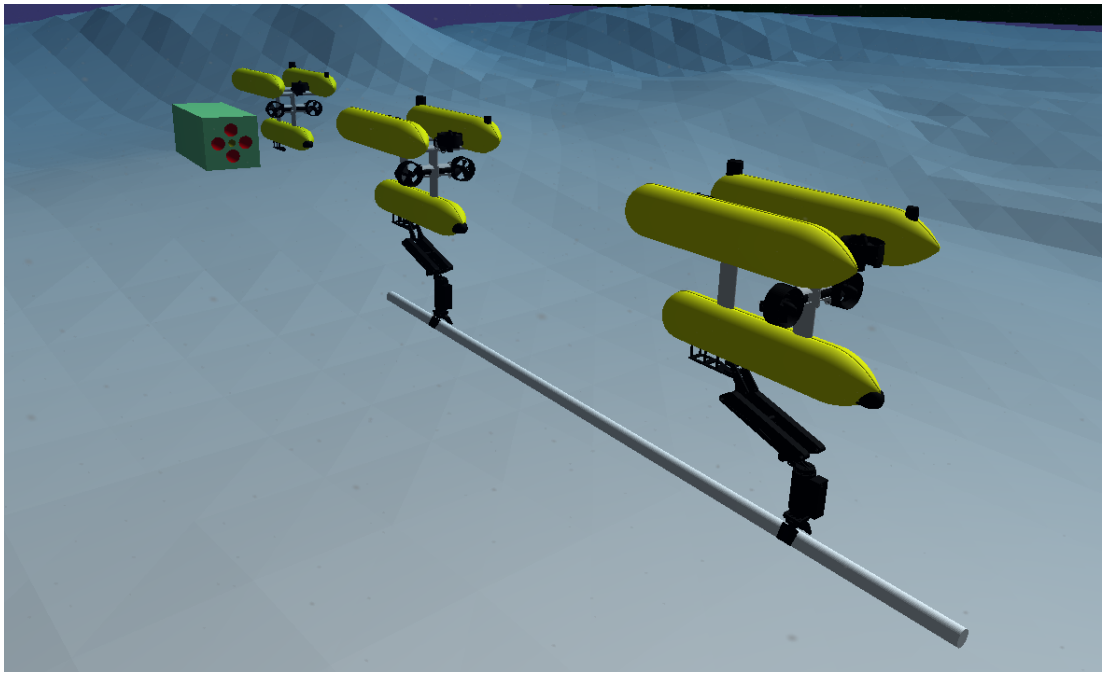

Figure 4.1: The Scenario of the experiment. The two twin robots are carrying the common peg, while the third robot is watching the hole to estimate its pose.

In this chapter, experimental set-up is described, and results are given and discussed. The code for the whole architecture is available at the following link: https://github.com/torydebra/AUV-Coop-Assembly; some details about it are discussed in section 4.5 and in appendix A.

The scenario is made up of two I-AUV's Girona 500 AUV underwater vehicles, each one equipped with a CSIP Robot arm5E (4 DOF arm with a parallel yaw gripper). The final goal is to successfully coordinate the robots in such a way that the peg, hold by both manipulators, is inserted correctly in the hole, fixed in the environment. In the literature, this problem is known as *peg-in-hole*.
One robot is equipped with a force torque sensor that permits to understand forces applied on the peg, caused during the insertion phase. This information is provided to both robots. A third robot estimates the hole pose in a preliminary phase. The figure 4.1 shows what has just been described.
The chosen strategy divides the problem in two phases: Hole Detection and Insertion. In the first, preliminary steps are done to detect the hole. A third robot, not used for manipulation task, is in charge to exploit computer vision algorithms to estimate the pose of the hole. Detail about this are given in section 5. The second phase explores the problems inherent to transportation of the tool, the interaction between the peg and the hole, and the communication between the carrying agents. This is described in this chapter.

4.1 Choosing the Simulator

A bit effort has been spent to choice a suitable simulator for the case. At the end, UWSim [Prats *et al.* (2012)] was chosen. It is a simulator largely used for this kind of scenarios, which visualize a virtual underwater scene. It provides a different variety of useful sensors (e.g. the used force-torque sensor and the cameras), but also others can be added. It is fully integrate in ROS, which made it really easy to use. ROS is used as simulator interface: through ROS messages, we can send commands to the robots and we can receive information from the going on test. Contact physics is implemented integrating the physics engine Bullet with OSG through OSGBullet. To further details about how the simulation is implemented, especially the contact physics part, please refers to the documentation of the cited software. The cons in using UWSim is that the simulations is fully kinematic, so no dynamics interaction ar present. This means, for example, that velocity sent to the robot are immediately accomplished, and that we can't simulate the real physics while grasping a real object. For the scope of this thesis, this lack is not important because dynamics is not considered. Furthermore, the only needed dynamic part, i.e. how the contact between the tool and the hole affect the whole manipulator chain, can be simulated at kinematic level thanks to the information provided by the force-torque sensor, as explained in section 4.3.
To fill the lack of dynamic of UWSim, a good alternative can be FreeFloatingGazebo [Kermorgant (2014)]. In truth, this simulator is a plug-in for Gazebo and UWSim; it integrates them in order to achieve both dynamic (thanks to Gazebo) and visually

realistic I-AUV simulation (thanks to UWSim). The interface used to communicate with the simulation is the same of UWSim, so ROS and its messages, which make it easy as UWSim to use.
This plug-in has been taken into consideration for dynamic test, that are not evaluated due to the lack of time, but can be certainly used for further works. Gazebo is a generic simulator widely used in all robotics fields. It is the de-facto simulator for ROS. Seen its purpose, it is not a ready-to use simulator for underwater environment, and can be only a starting point to build a software to simulate this particular scenario (as it is done by FreeFloatingGazebo).
Also other simulators, V-REP [E. Rohmer (2013)] and Webots [Michel (2004)] have been taken into consideration but discarded for same "not ready-to-use" reason like Gazebo.
An interesting simulator is USV simulator [Paravisi *et al.* (2019)] which takes the best from UWSim, Gazebo and FreeFloatingGazebo to implement realistic simulation. This is a really recent and in development project, and however it is focused more on surface vessels dynamics.

More details and comparisons are available in Cook *et al.* (2014) and Paravisi *et al.* (2019), and a schematic recap taken from Paravisi *et al.* (2019) is visible in fig. 4.2.

Simulator	Waves	Buoyancy	Water Currents	Wind Currents	Thruster Underwater	Thruster above Water	Foil
UWSim	√	√	×	×	√	×	×
Gazebo	×	×	×	×	√√	√√	×
Freefloating Gazebo	√	√	√	×	√√	√√	×
VREP	√	√	×	×	√	√√	×
RobotX Simulator	√	√√	×	√	√√	√√	×
USVSim	√√	√√	√√	√√	√√	√√	√√

Figure 4.2: Schematic recap of simulation comparison taken from Paravisi et al. (2019). × stands for no implemented feature; √ for a feature that is a discrete representation of the real one; √√ for a good representation of the real one. More details on how each feature is evaluated are available in the original paper.

4.2 Simulating the Firm Grasp Constraint

Due to the limitation of the used simulator (explained in section 4.1), some tricks have to be made. Without dynamics, simulate correctly the grasp of the peg is impos-

sible. The simulator permits to fake the grasping with an *object picker* sensor: when an object is sufficiently near to the point where this sensor is, it becomes "grasped" and it will rigidly move with the whole robot. The problem here is that we have two robots that must take the tool, so the object can't rigidly move with both, but only with the first who catch it. Furthermore, external forces applied to an object (grasped or not) can't be detected with the force-torque sensor, because, as it is implemented, it only detects forces acting on a vehicle part.
To solve this, a peg is modelled as additional fixed joint for each robot. In this way, each peg is rigidly attached to its own robot. Now, the problem is how to maintain the two pegs perfectly coincident during the whole mission. This is needed because the control architecture assumes a *firm grasping*. This means that the end-effector does not move respect to the peg, and, consequently, the end-effectors of the robots do not move respect themselves.
In the simulation, collisions between the "pegs" and the hole cause them to drive apart. This is because collisions are propagated to the robots with a formula which use Jacobian (detailed in section 4.3). Jacobian derives from approximation of non-linear relationship, so results are not perfect. So, during the transportation, but especially during the collision propagation in the insertion phase, the two pegs distance themselves a bit. So, the control point for one robot is in a different position of what it expect, that will cause even more diverging behaviour.
In real scenario, firm grasp act like a "glue": if the end effector tends to go away from the grasping point, friction acts to maintain it to the contact point. This is true for very small errors; if the cooperation performance is bad, the common tool falls down or something breaks.
In the simulation, to fake the firm grasp, an additional routine is implemented: it simply calculates the distance between the two peg, and generates robot velocities to zeroing this distance. It is important to note that this is an help that we would have also in real scenario, as explained before. The only difference is that, in real scenario, if the errors are too big the end-effector begins to slip, and it will never return to its original grasping point. In this case, it returns always to the initial point. The velocity generates by this routine are not so big to hide bad cooperation; so the tests are suitable to evaluate the proposed architecture, and to simulate real situation.

4.3 Collision Propagation

When a robot interacts with the environment, each contact generates forces on it. Mission about assembling objects can't be studied in a properly manner without some considerations about these forces. In a peg-in-hole Mission, collisions between the peg and the hole will be transferred through the whole kinematic chain until the

floating base, causing disturbance to the whole robotic system. Thus, it is necessary to simulate these behaviours.

Let us define $\boldsymbol{f} \in \mathbb{R}^3$ and $\boldsymbol{m} \in \mathbb{R}^3$ as:

$$\boldsymbol{f} = \begin{bmatrix} f_x \\ f_y \\ f_z \end{bmatrix} \qquad \boldsymbol{m} = \begin{bmatrix} m_x \\ m_y \\ m_z \end{bmatrix} \tag{4.1}$$

being the $\boldsymbol{f}$ and $\boldsymbol{m}$ the resultant forces and torques (projected on the tool frame $\langle t \rangle$) of all the forces and torques acting on the tool. These disturbances generate joint velocities $\dot{\boldsymbol{y}}_\delta \in \mathbb{R}^l$ [Siciliano *et al.* (2009)]:

$$\dot{\boldsymbol{y}}_\delta \triangleq \begin{bmatrix} \dot{\boldsymbol{q}}_\delta \\ \boldsymbol{v}_{1\delta} \\ \boldsymbol{v}_{2\delta} \end{bmatrix} = \begin{bmatrix} k_q \\ k_{v1} \\ k_{v2} \end{bmatrix} \left[({}^{lin}\boldsymbol{J}_t)^T \boldsymbol{f} + ({}^{ang}\boldsymbol{J}_t)^T \boldsymbol{m} \right] \qquad 0 < k_q, k_{v1}, k_{v2} < 1 \tag{4.2}$$

where J_t is the Jacobian which express how Cartesian velocity $\dot{\boldsymbol{x}}_t$ of the tool are affected by the system velocity vector $\dot{\boldsymbol{y}}$; lin, ang superscripts refer to *linear* (top three rows) and *angular* (bottom three rows) parts of J_t; $\dot{\boldsymbol{q}}_\delta$ is the velocity vector for joints caused by the collisions; $\boldsymbol{v}_{1\delta}$ and $\boldsymbol{v}_{2\delta}$ are the linear velocity and angular velocity of vehicle caused by the collisions; k_q, k_{v1}, k_{v2} are positive gains smaller than 1, in general different from each other because we are considering different types of velocities.

4.4 Assumptions

It is important to detail the assumptions made during the simulation. Some problems, that are necessary to be taken into account in a real environment, are not explored. This is necessary due to the difficulty of the particular scenario chosen. In this section, the more important assumptions are summarized.

- Simulation is only kinematic. This implies, for example, that the commanded velocity to the vehicle and the arm are accomplished *instantaneously* and *perfectly*. Another implication is that the movements of arm and of the vehicle don't influence each other at all. The only "dynamic" implemented is caused by collision between the peg and the hole, which "transfer" the forces and torques acting on the peg along the whole arm (as described in 4.3).
- The initial configuration shows the peg already *correctly* grasped by both robots. Also, the position of where the end effector have grasped the tool and the peg

dimensions are known. This implies that relative position between each robot and peg's tip is *perfectly* known. Such a initial configuration has been chosen because the grasping phase and problems arising during cooperative transportation have been explored in others already cited project like MARIS and ROBUST (e.g in the work Simetti & Casalino (2017)) and they are also part of different studies of the on-going project TWINBOT.

- Pose (linear and angular displacement) of the two carrying robots and of the vision robot respect a common inertial frame (denoted as *w - world* in the whole thesis) is known. In real situation, the pose underwater is always an issue and it is never really precise. Good precision can be provided, for example, after some works in mapping the seafloor, which will provide a common reference point somewhere. Note that it is not important know the pose of the robot respect to a point above the water surface (that can be done thanks to information shared with surface vessels, for example as explored the WiMUST project [Abreu *et al.* (2016)]). The important thing is to know relative pose of the robots to a common node, that can also be underwater. This is needed to make the vision robot share correctly the estimated hole's pose with the carrying robots.

- No real communication issues between the two carrying robot are taken into account. The presence of water puts important issues in real situation: *full-duplex* communication (i.e. sharing data *at the same time*) is impossible, and, in general, there is a lower bandwidth than in the air. Some experiments in simulated environment with different methods of underwater communication are detailed in Simetti & Casalino (2017).
  However, these issues are considered by the cooperative scheme (explained in section 2.5); in fact it permits to exchange very few information between the two carrying agents.

- The two robots firmly grasp the peg. There is no sliding caused by robot movements. This point is detailed in section 4.2.

- During the insertion phase, the architecture resolve alignment errors *only if* the peg is inside the hole. If the peg touches the external hole surface, no routines are implemented to deal with the problem of *looking* for the hole on the surface.

- The sensor is positioned on the tip of the peg, and it provides forces and torques caused by contacts with the whole peg. This would obviously not possible in real applications. In real scenario the sensor is usually put on the wrist and provide forces respect to this point. However, we could project the force-torque sensor information on another frame, if we know the relative pose.

This assumption is also necessary because the chosen simulator can give force-torque information only on the part where the sensor is positioned.
Also, both robots have access to the sensor data, without uncertainties (except numerical errors due to how almost all physics engines compute collisions, that it is done with approximations to improve the performance).

Others assumptions, more related to the vision part, are detailed in section 5.1.

4.5 Control Loop

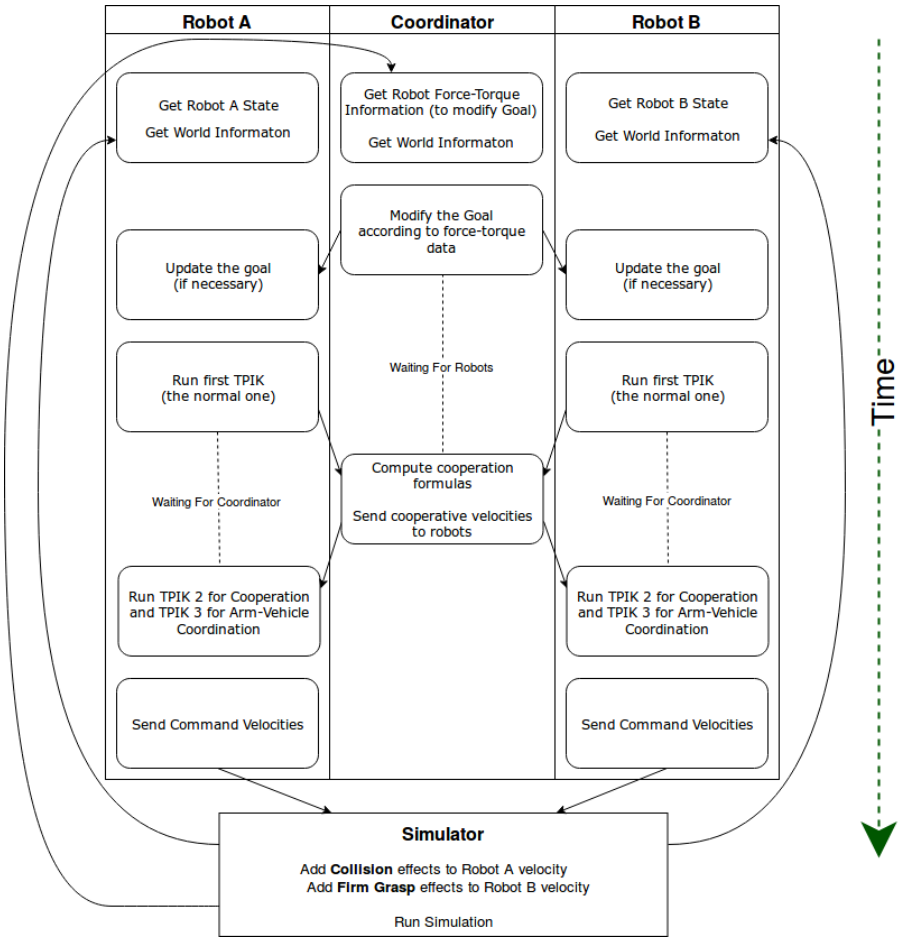

Figure 4.3: A flow scheme showing the main step of a single control loop for the robots and for the coordinator. Blocks at the same horizontal level are executed at the same time. Arrows indicate sharing of data between blocks of different nodes. Note here that the vision robot is not considered.

This section is made to give a better idea on how the control architecture works.
The Vision Robot, which job is to estimate the hole pose, acts in a preliminary phase. It *tracks* the hole, thanks to stereo-cameras, and it sends the estimated pose to the two carrying robots (and to the Coordinator). Due to its nature, no complicated control is implemented for this agent: when the pose is sent, we simply move it away from the hole with keyboard (like a ROV) to not interfere with the insertion mission. This part is described in Chapter 5.

The two carrying robots are completely autonomous: as soon they get the hole pose, they start, *without user intervention*, the main mission. There are three nodes: the two Robots (*A* and *B*) and the Coordinator. The latter is not a real *physical* agent: it is only a software routine. So, it can be physically inside one robot, let's say Robot A. In this way, communication issues (due to the underwater scenario) happen only between the two robots, and not among all the three nodes.
Initially, the Agent A, the Agent B and the Coordinator synchronize themselves, i.e. each one waits that the other two are ready. After this initialization phase, the normal routine starts, as can be seen in figure 4.3, where the main instructions of the control loop are depicted.

- At the beginning of the control loop, each node gets the updated simulation state, e.g. pose of the robots, pose of the tool, information from force-torque sensor, and so on.
- The Coordinator, which (as said previously and without loss of generality) is a software routine inside the Robot A, modifies the goal's linear position (as explained in 3.3), if some forces are detected. If the goal is updated, the two Agents get this new information.
- In the third block's row, the Robots run the first TPIK procedure. Then, they send the necessary data to the Coordinator, which computes the cooperative velocities and sends them back to the robots. Finally, the two Agents run another two TPIK procedures, one for the cooperation and the other for the vehicle-arm coordination. This routines are described in Section 2.4 and Section 2.5. In all the TPIK procedure, the Force-Torque objective (Section 3.1) is used.
- At the end, the two Agents send the outputs (i.e., the system velocity vectors) to the simulation.
- Before sending the velocities to the "real" simulation, some disturbances must be added to the commanded system velocity vectors. For the Robot A, this means adding effects of collisions between the peg and the hole (Section 4.3).

Instead, for the Robot B, effects of the firm grasp constraint are added (Section 4.2).

- After the simulation performs a step, the routine starts again.

It can be noticed that the two added physical interactions (collisions and firm grasping constraint) are added only for one robot (A and B, respectively) and not for both. This is done to not add simulation errors that can occur, and that would not happen in real scenario. For example, in real situation there are not two coincident pegs (as in this simulation) and so they can't really distinguish themselves. Putting the firm grasp constraint only on one robot helps to reduce disturbances that in real scenario are not present. Also, it is sufficient to fake a real firm grasping.
About the collisions, they affect, *directly*, only the first agent. In truth, they also affect the other one, *indirectly*, because the latter is *dragged* by the firm grasp constraint. So, practically, collisions affect the behaviours of both agents.
It is important to notice that these physical interactions do not hide control problems: if the control is setted badly, the whole mission fails (e.g. the two peg diverge and/or compenetrate visibly with the hole).
Another thing to notice is that, when the Force-Torque objective (Section 3.1) is used, both Robots need the sensor data. Being the force-torque sensor only on Robot A, this means that additional communication between Robot A and Robot B is needed. As known, underwater transmission is difficult and slow, and the general amount of the exchanged data should be keep as small as possible (from this problem it derives the used coordination policy).
An alternative can be to use another sensor on the Robot B. The problem following this direction could be that different sensors give not exactly same data. So, the two robots run each TPIK with different information. This problem is not explored here.
Another solution can be simply to avoid using this objective: it would decrease the performance of the mission (as we will see later) but results are good anyway.
It must be noticed that also to update the goal additional information has to be exchanged between the two robots.

4.6 Results

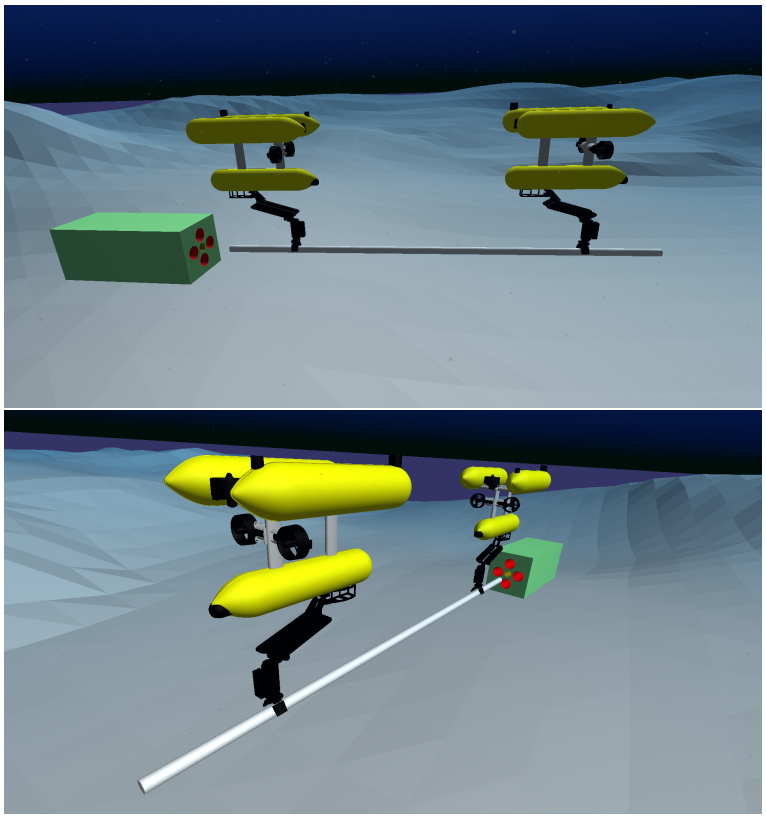

Figure 4.4: Two different points of view of the scenario for the results presented in this section. The pose estimation with vision is neglected here.

The first experiments do not take into consideration the vision part, to have a hole's pose error arbitrarily settable to discuss the performance of the methods used. The figure 4.4 shows the robots initial position. Below, a list of important details about the simulations:

- The **Peg** is a six meters long cylinder, with a diameter of 0.10 meters.
- The **Hole** is a cylindrical cavity with a diameter of 0.14 meters
- The initial position of the agents is near the hole: the peg's tip is almost aligned perfectly to the hole, and it is at almost 0.44 meters from it. To be precise, the vector from peg's tip to the hole has components : $[0.441, -0.008, -0.018]$ where x-component is along the length of the peg, y-component lies on the tip's surface and it points to the left, and z-component points downward (as

in fig. 4.5). Considering the peg's tip frame described by these components, the orientation from the peg's tip frame to the hole frame is described by these Euler angles: $[0, 0, 1.942]$ (*roll, pitch, yaw*, in degrees).

- The **goal** is to drive the peg inside the hole with a depth of 0.2 meters.
- All the vectors displayed in the plots are projected in the world frame (which orientation is visible in fig. 4.5).

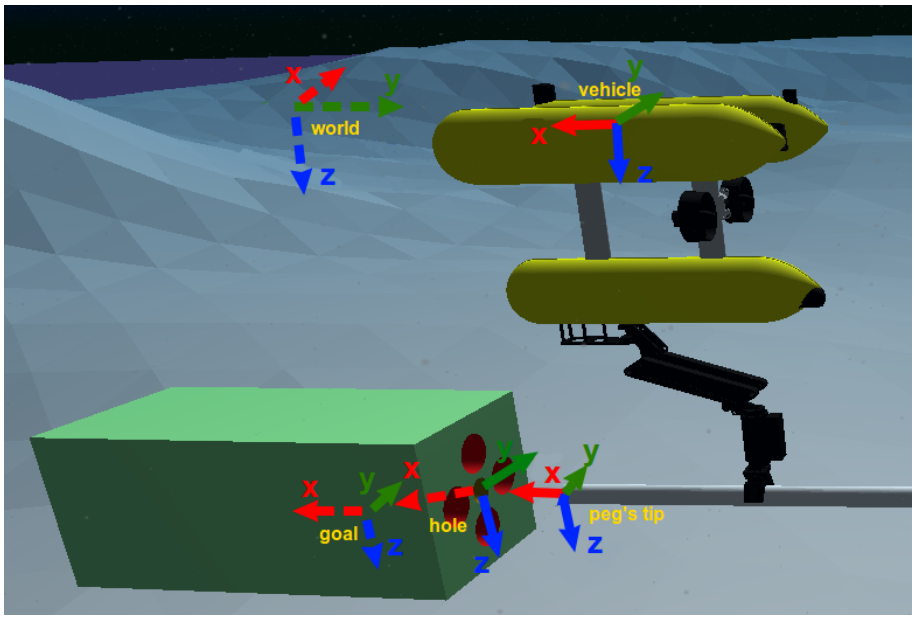

Figure 4.5: Detail of a screenshot where the main frames are drawn. The world frame is present only to clarify its orientation; its origin is not in that point. For the hole frame, the x-axis goes inside the cavity. The goal frame $\langle g \rangle$ has the same orientation of the hole frame, and it is shifted of 0.2 meters in the direction of hole's x-axis.

In the following results, only a few plots (fig. 4.14 and fig. 4.15) are related to the cooperation scheme of section 2.5, and no long discussions are made for them. This choice has been made because no robot has difficulty in tracking the ideal common tool velocity $\dot{\boldsymbol{x}}_t$, so no very interesting plot occurs. Experimental results about this particular scheme used can be found in Simetti & Casalino (2017) and Wanderlingh (2018).

The focus of the results is on the implemented methods for helping the insertion phase: the Force-Torque objective (section 3.1) and the Change Goal routine (section 3.3). Further outcomes are presented about the added simulation procedures:

the Firm Grasp constraint (section 4.2) and the Collision propagation (section 4.3). These last two extensions are important to improve the simulation in an otherwise pure-kinematic scenario.

4.6.1 Perfectly known Hole's pose

In the first experiment, the hole's pose and the goal frame $\langle g \rangle$ are known without uncertainties. The plots of figure 4.6 show how the forces and torques act on the peg, the converging positional error from the goal to the peg's tip, the tool velocities generated by the collisions, and the tool velocities caused by the firm grasp constraint.

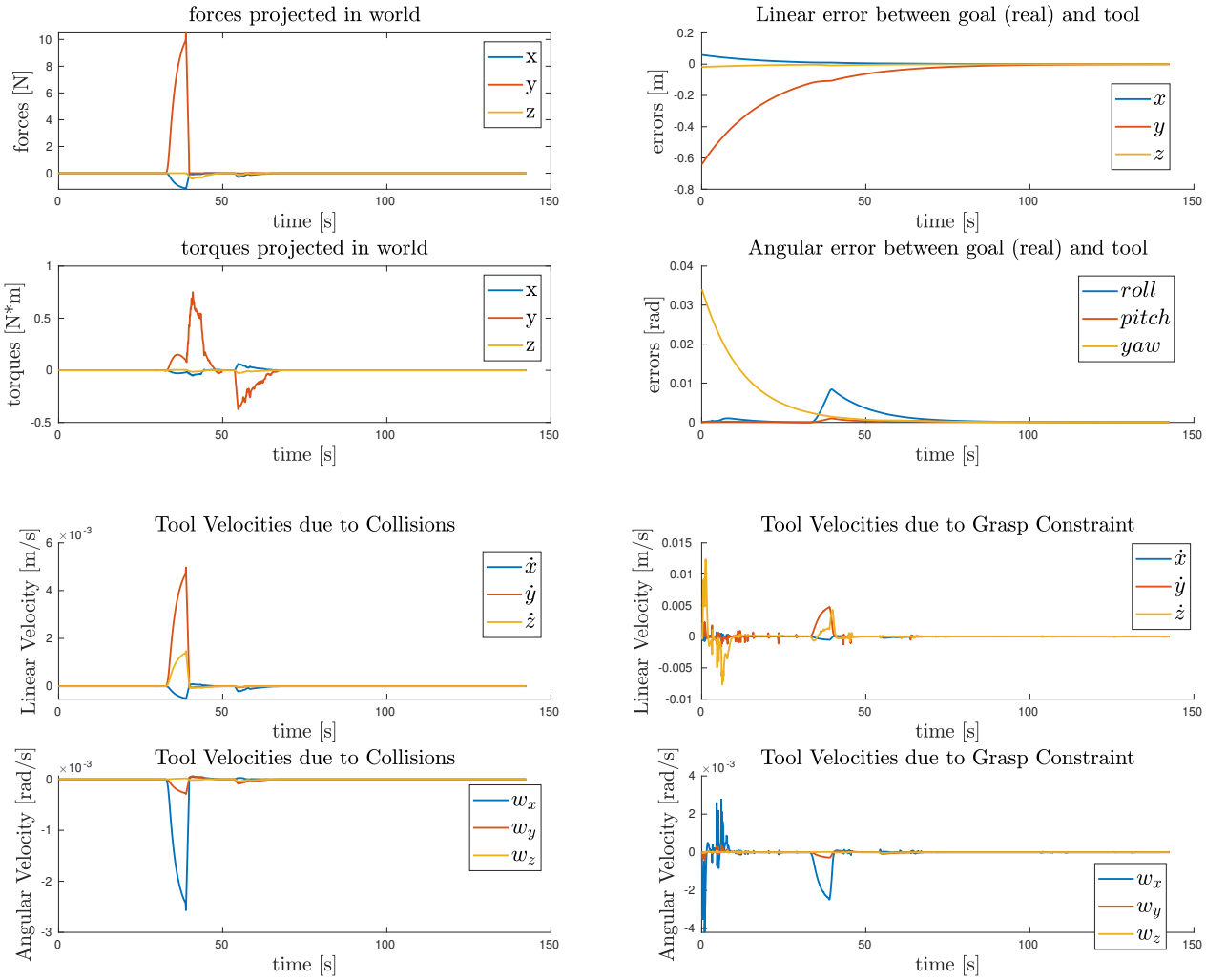

Figure 4.6: The results with the hole's pose known without errors. The upper left plot shows the forces and torques acting on the whole peg: they are the components of the total resultants projected on world. The high peak in y is due to the first contact between the peg and the hole surface. The upper right plot shows the convergence of the error between goal frame and tip frame. The lower left plot displays the tool velocities generated by the system motions caused by the collisions propagation. The lower right plot shows the tool velocities generated by the firm grasp routine.

4.6.2 Error on the Hole's pose

In general, a perfect pose estimation is never achievable, so the control should take into account that errors can be present. In this experiment, an error of 0.015 meter is added along the x-component of the goal (considering the goal projected in the world frame). So, the peg is driven a bit on the right respect to the centre of the hole, causing lot of collisions with the right side of the cavity.

4.6.2.1 Change Goal routine results

As explained in section 3.3, it has been implemented a routine to change the goal according to the forces and torques detected by the sensor. A Comparison of the results without this method is visible in figure 4.7. Here, it can be seen that the goal is changing, and at the end of the experiment the added error is compensated.

4.6.2.2 Force-Torque objective results

Besides changing the goal, it is useful to exploit the force-torque sensor also at kinematic level, using the provided information in the TPIK approach. The new added objective is described in section 3.1.
In figure 4.8 the three different methods are compared. It is visible that, when also the new objective is used, the forces and torques have the smallest peaks. Meanwhile, convergence of the error between the goal and the peg's tip is maintained as good as previously thanks to the presence of the same change goal routine.
In figures 4.9 and 4.10 details on how this new objective works are shown. When some collisions happen, the reference and the activation grow to make the tool move to reduce the force and the torque magnitude. The figure 4.10 shows the velocities generated by the objective *as if it was the only one* acting on the system, so they are not the real velocities given to the system.

Error of 0.015 meter on x-axis of the goal
Linear and Angular component of the goal frame and the tool's tip frame

Without Change Goal routine

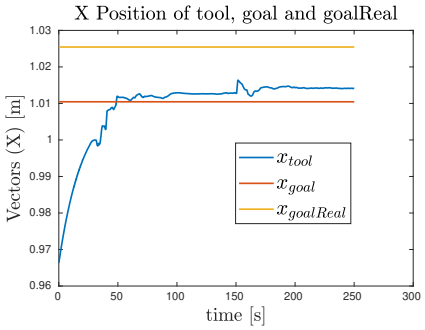

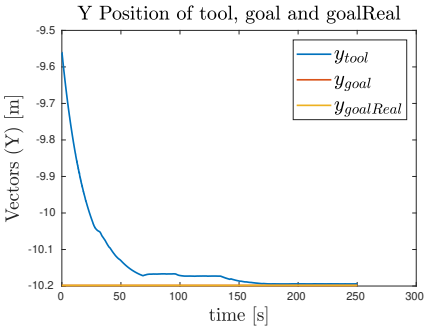

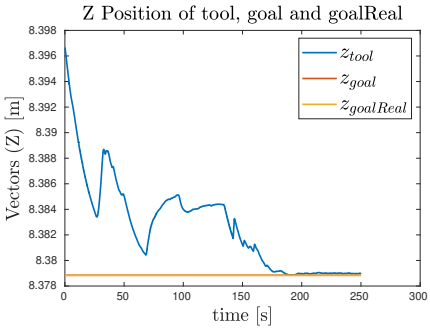

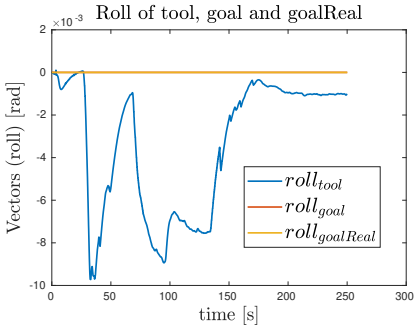

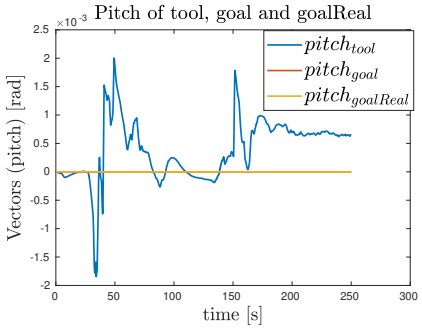

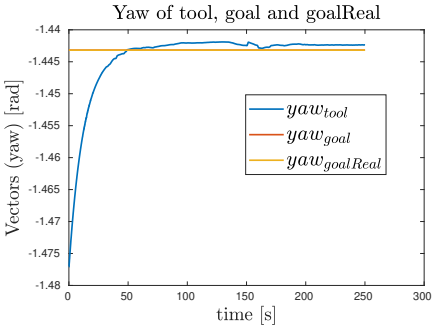

With Change Goal routine

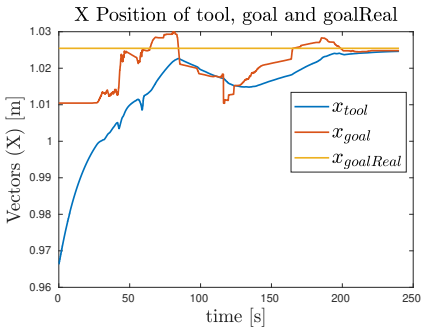

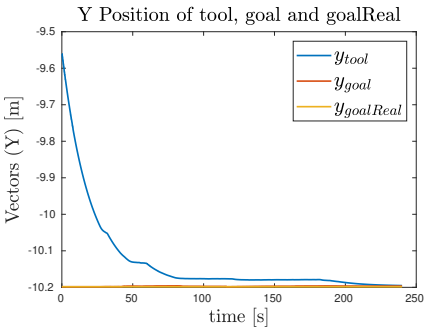

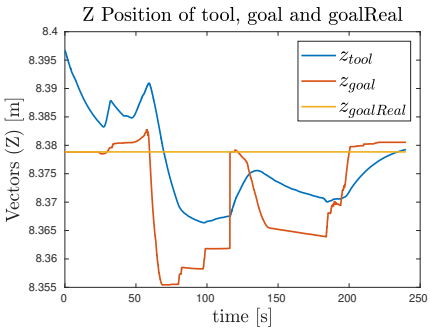

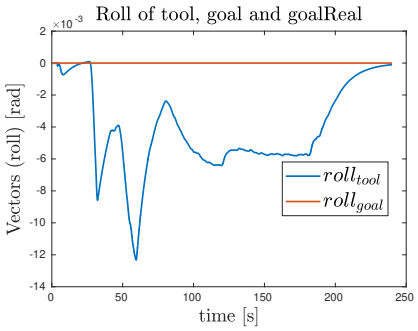

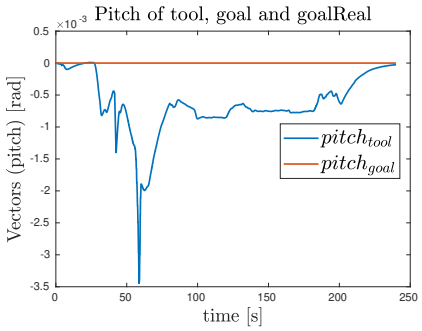

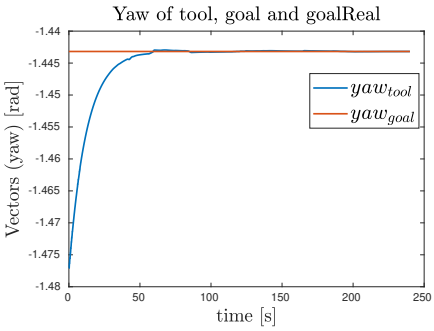

Figure 4.7: Results of the two experiment without and with the Change Goal routine (both without the Force-Torque objective). The plots show the pose of the goal frame $\langle t \rangle$ and of the tool's tip frame divided into their linear and angular components. The upper six plots show results without the routine which changes the goal position, the bottom ones show results with the routine. All the component are respect to the world frame. For the linear part, the yellow lines represent the position of the goal without errors. The red lines represent the position of the goal that the controller uses. Please note that in some plots the red and yellow lines are coincident because the component is know without errors and *it is not modified. It is clearly visible that, when the goal is modified, the red line goes toward the yellow one, correcting the initial hole's pose error.*

Error of 0.015 meter on x-axis of the goal

Norm of the forces and torques acting on the peg

Without Change Goal routine

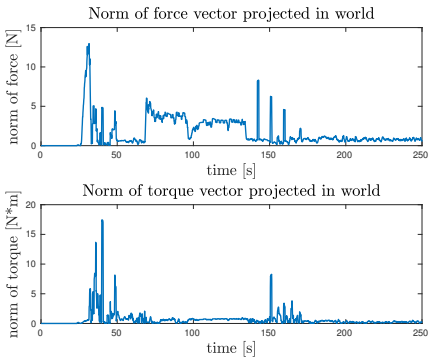

With Change Goal routine

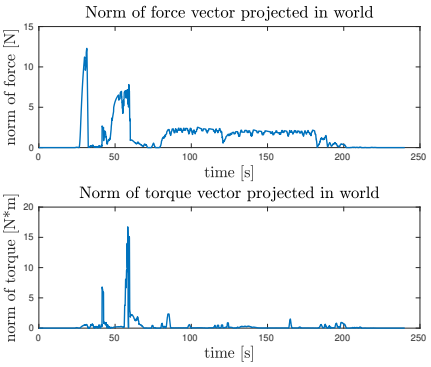

With Change Goal and Force Task

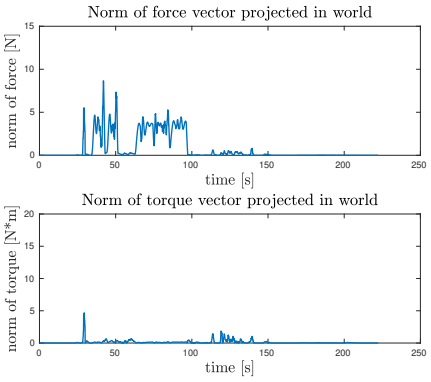

Norm of the error between ideal goal (without the added error) and tool's tip

Without Change Goal routine

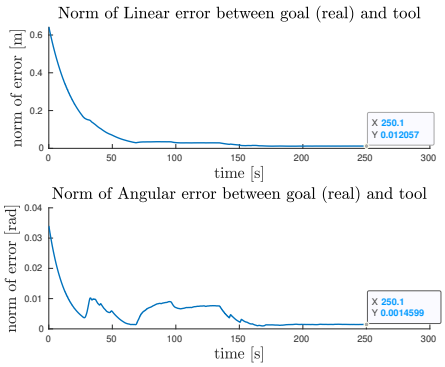

With Change Goal routine

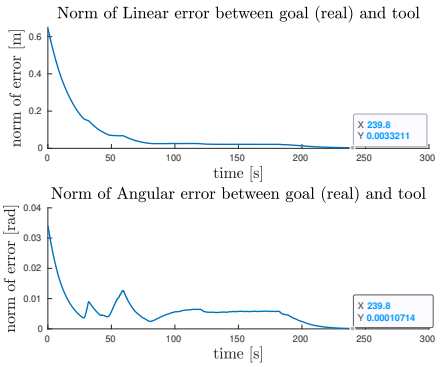

With Change Goal and Force Task

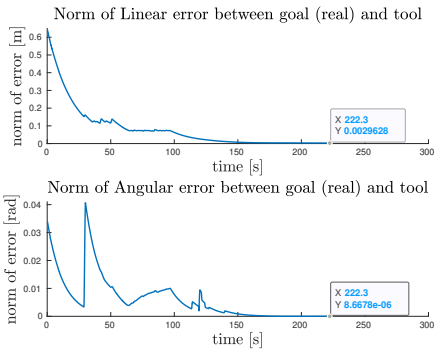

Figure 4.8: Comparison of results of the three methods: vanilla, Change Goal and Change Goal with Force-Torque objective. The three upper plots show the norm of the force and of the torque acting on the peg. It can be noticed that, in the cases where the goal is modified, at the end their norms goes to zero. The three lower plots show the norms of the error between goal and tool's tip. In the case without the Change Goal routine, the norms converge anyway but to a slightly bigger value than the one of the other two cases. In fact, when the Change Goal routine is used, the initial pose error tends to be corrected.

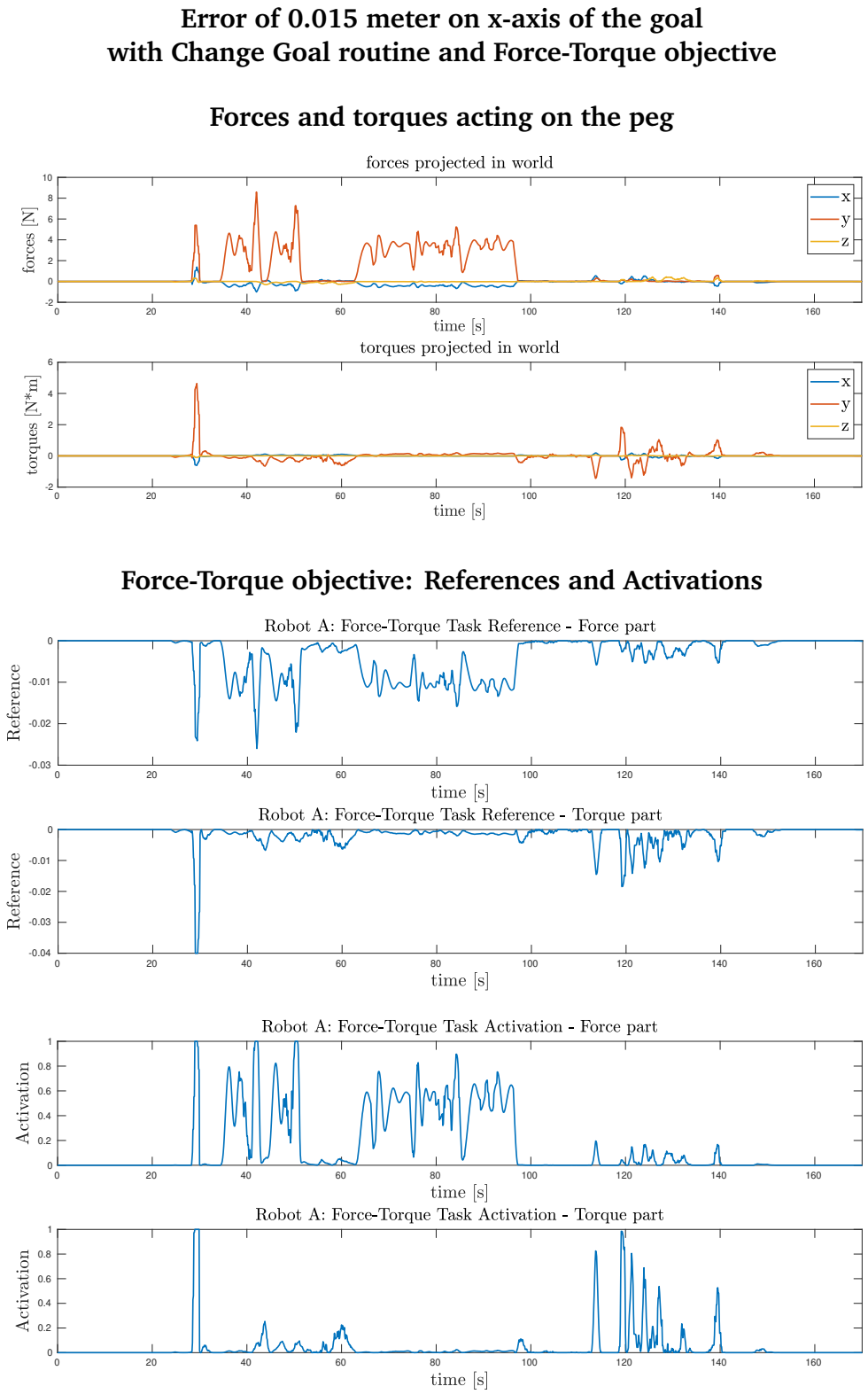

Figure 4.9: The forces and torques acting on the peg (above), and the corresponding generated references and activations of the Force-Torque objective (below); they are calculated by robot A, but for robot B they are the same.

Results with error of 0.015 meter on x-axis of the goal with Change Goal routine and Force-Torque objective

Velocities generated by the Force-Torque objective only

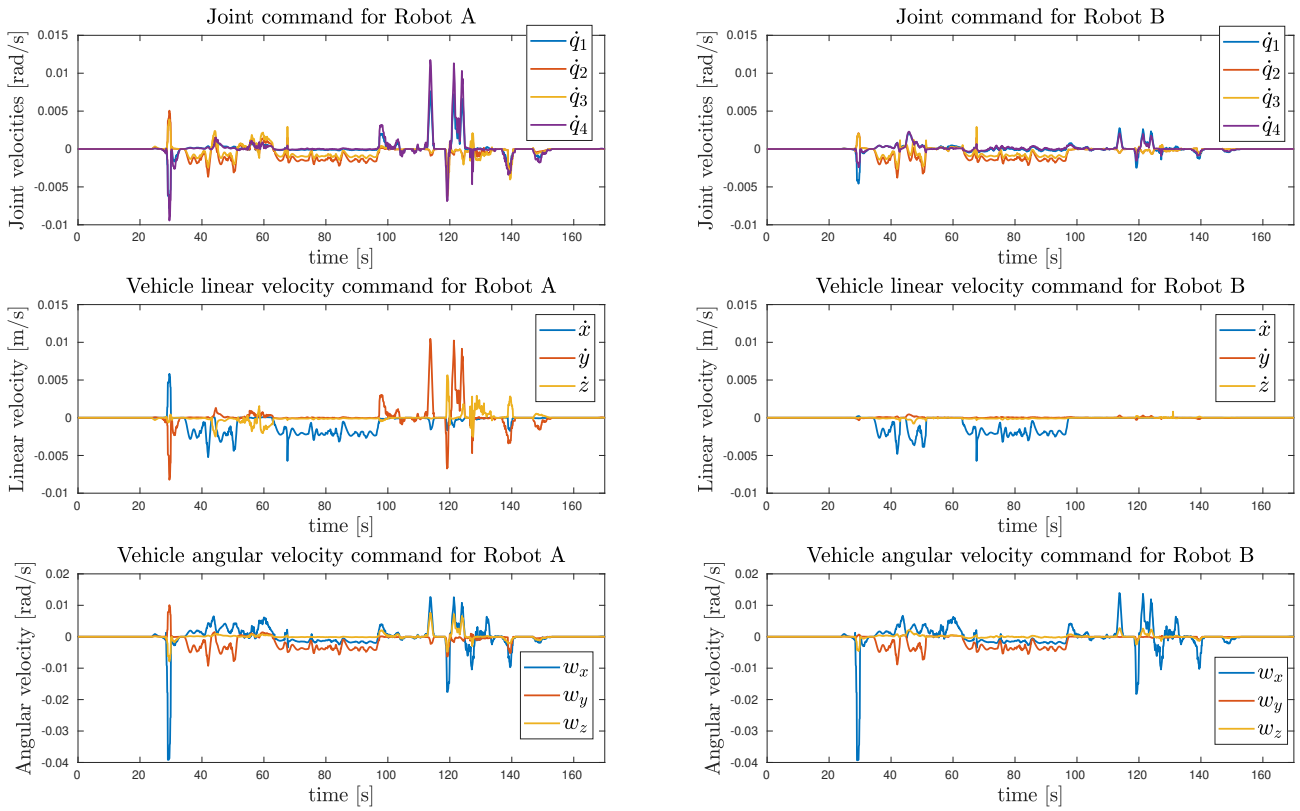

Figure 4.10: The velocity command generated by the Force-Torque objective, for the Robot A. These are the velocities that the task generates; the vectors depicted are simply the result of $\boldsymbol{J}_{ft}^{\#}\,\dot{\boldsymbol{x}}_{ft}$ to show how the objective works. So they are not the real one applied to the system because with this formula higher priority objectives are not taken into consideration. For the two robots, the reference $\dot{\boldsymbol{x}}_{ft}$ is the same because they act with the same data, it is the Jacobian $\boldsymbol{J}_{ft}^{\#}$ which is obviously different and which makes the two plots dissimilar.

4.7 Results with the Hole's pose estimation by Vision

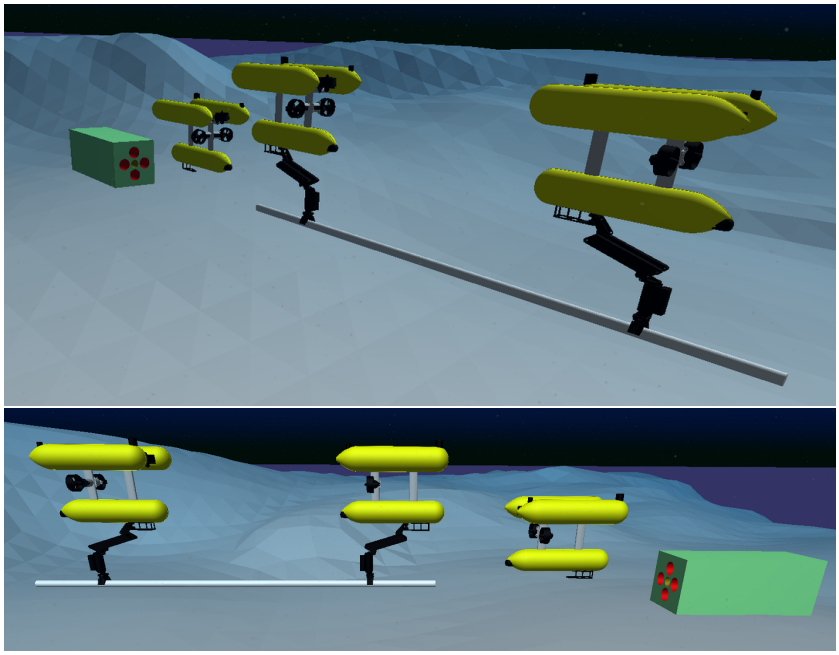

Figure 4.11: The starting position of the robots for the final experiment, where it is used the preliminary phase to estimate the hole's pose with vision.

Here, results with the preliminary vision phase are shown. Differently from the previous experiments of section 4.6.2, the error of the hole's pose when using the Vision Robot is not so influential on the mission. In norm, the pose estimation error is less than 0.006 meters for the linear part and 0.01 radians for the angular part (with the best method, as shown in figure 5.5 of section 5.4.4).
However, the experiment is interesting not only because it puts all the mission phases together, but also because it shows the outcome when the error is "spread" among all linear and, especially, angular component (which was not considered before). Even more, the carrying robots start farther from the hole than before. In this simulation, both the Change Goal routine and the Force-Torque objective are used.
The test's details described at the beginning of section 4.6 are still valid, except for the initial position of the two carrying robot. This time, the distance between hole and peg's tip has component $[3.590, 0.039, -0.041]$ for the linear part (and the same as previous for the angular part: $[0, 0, 1.942]$ *roll, pitch, yaw*, in degrees).
Some screenshots that show the main phases of the simulation are visible in figure 4.12. The interesting plots about the performances are shown in figure 4.13. To give an idea of the magnitude of the velocities involved, cooperative system velocities $\dot{\hat{\boldsymbol{y}}}_a$

and $\dot{\hat{\boldsymbol{y}}}_b$, and cooperative tool velocity $\dot{\hat{\boldsymbol{x}}}_t$ are displayed in figure 4.14 and figure 4.15. Please note that these velocities do not include the collision propagation and the firm grasp constraint, they are only the output of the kinematic layer.

Screenshots from the final experiment

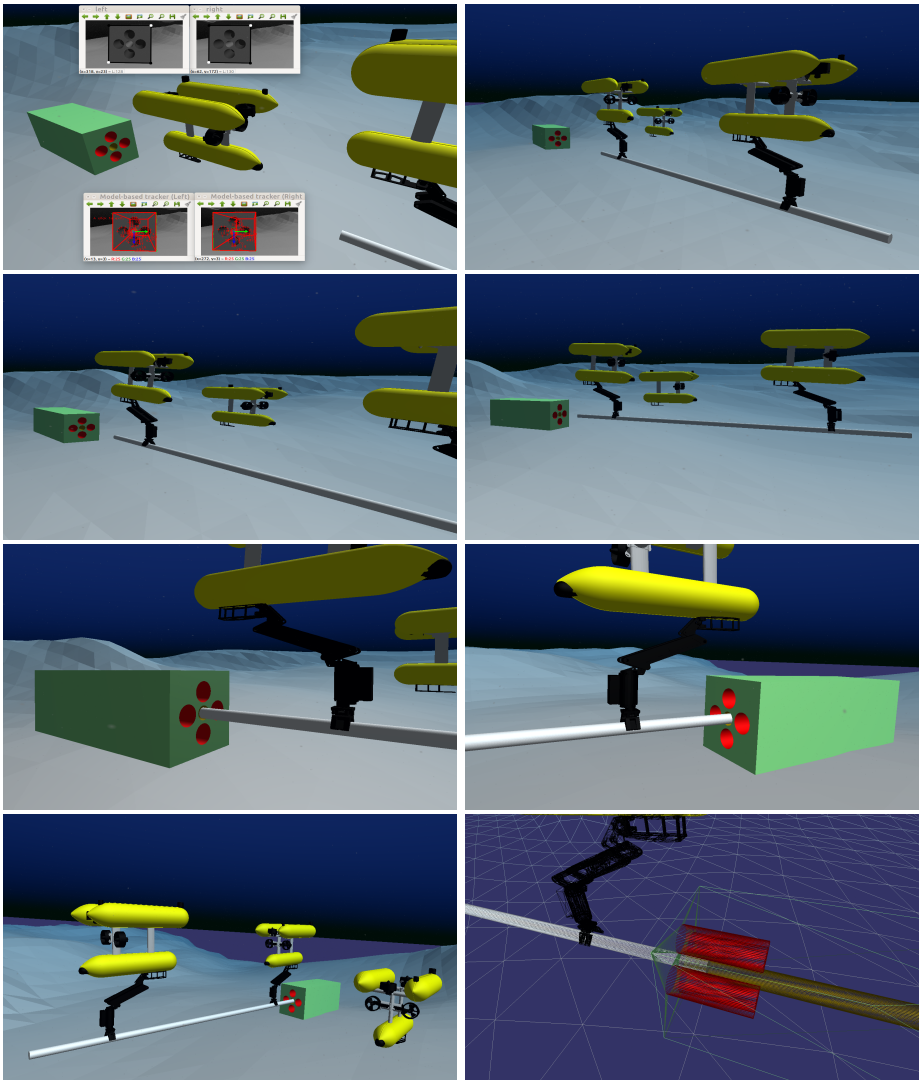

Figure 4.12: Screenshots from the final experiment with Vision. From the top to the bottom, from the left to the right: a) The Vision robot has detected the squares and it is tracking the hole's pose; b) The Vision robot is driven away and the carrying robots are ready to begin; c,d) the two robots are cooperatively transporting the peg to the hole; e) The first "contact" between the peg and the hole; f) The peg is being inserted; g) The robots stop because the tool has reached the desired depth (0.2m); h) A polygon wire-frame view mode of the simulator to see the peg inserted.

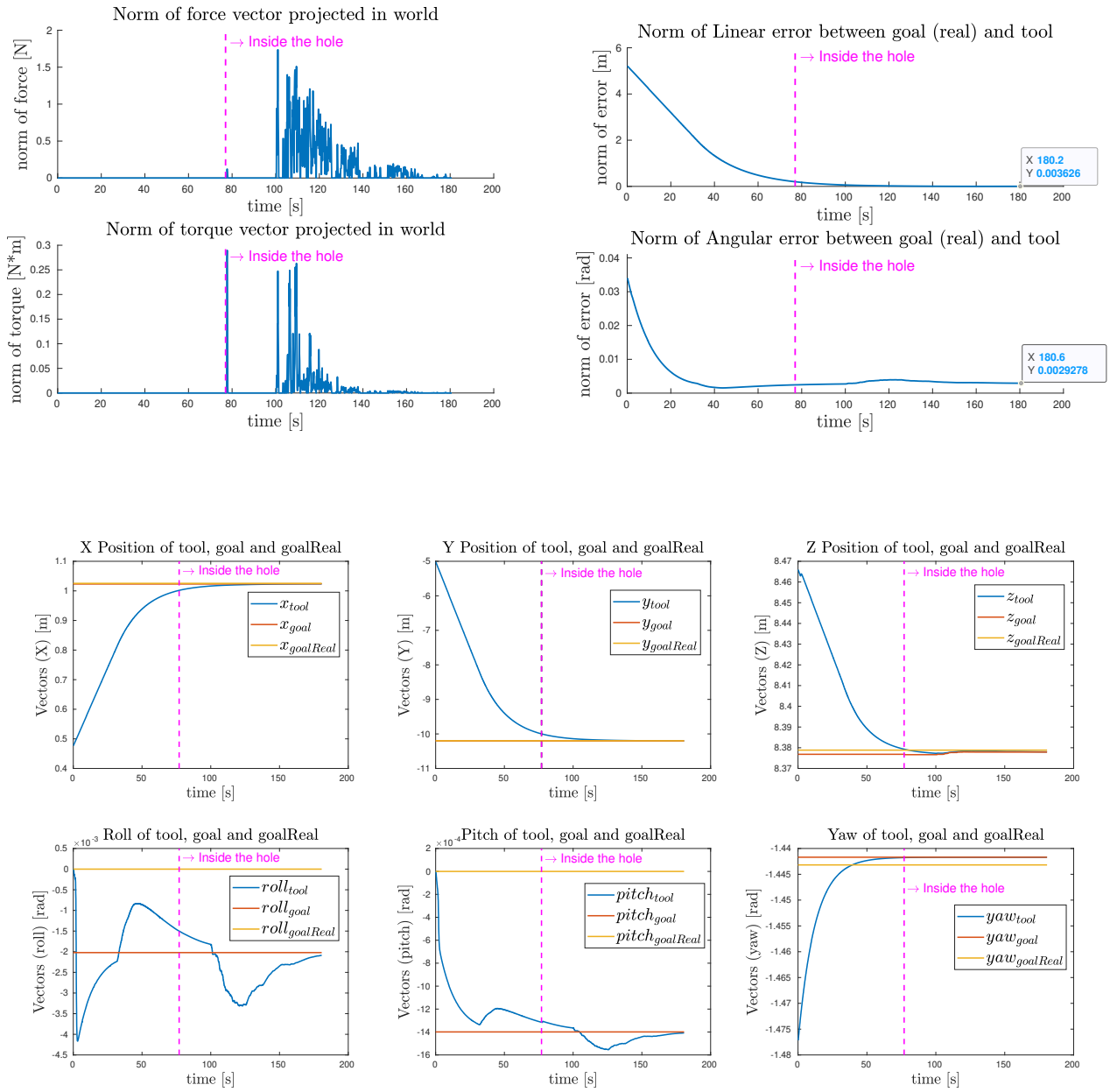

Figure 4.13: Results with the hole's pose estimated by the best one of the tested vision algorithms. At second 77 the peg's tip goes inside the hole (magenta vertical lines). Being the pose estimation really good, forces and torques are not so big as in the previous test (upper left plot). Furthermore, modification of the goal are almost not noticeable (lower plot). The positional error from goal to peg's tip converges to a small value (upper right plot). The visible error for the angular part is due to the fact that the orientation of the goal frame has some imprecisions, due to not perfect hole's pose estimation.

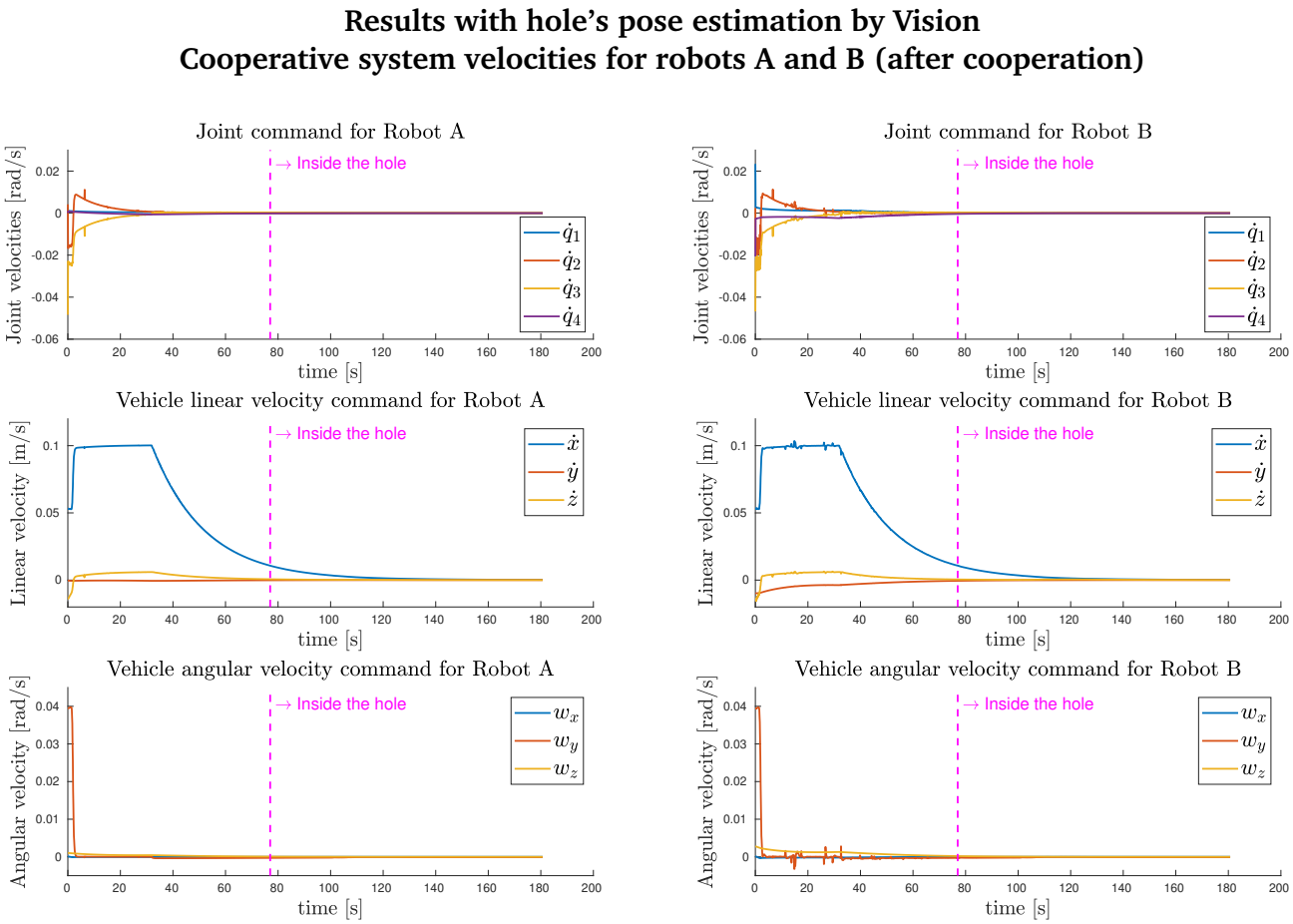

Figure 4.14: The system velocities $\dot{\hat{\mathbf{y}}}_a$ and $\dot{\hat{\mathbf{y}}}_b$, outputs of the kinematic layer after the cooperation policy (section 2.5) and the arm-vehicle coordination scheme (section 2.4). These are not always the real *robot velocities because they do not include velocities caused by collisions (for robot A) and by firm grasp constraint (for robot B).*

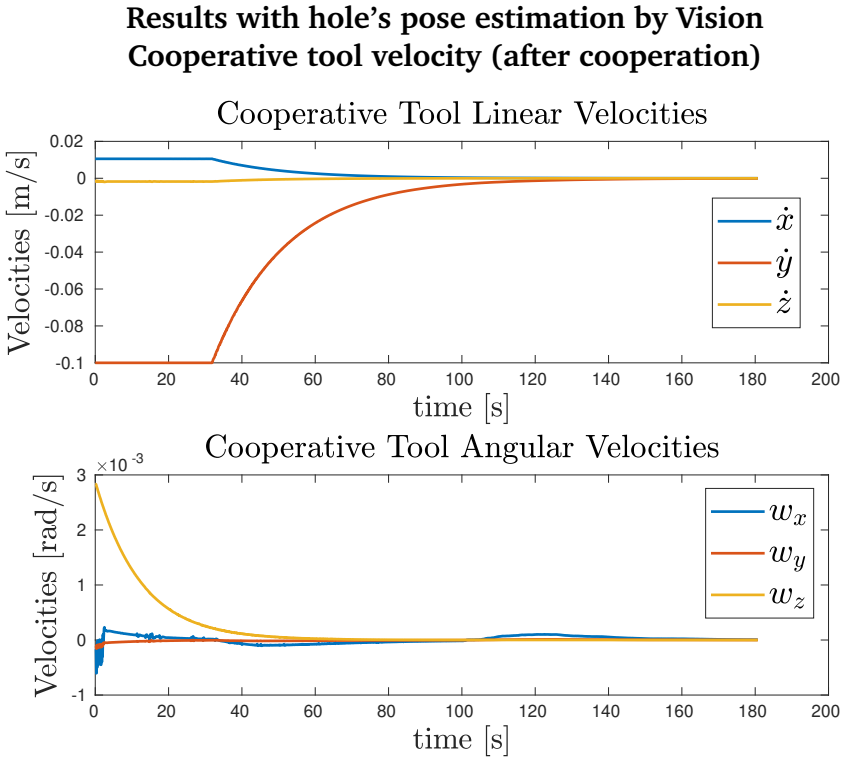

Figure 4.15: The tool velocity $\dot{\tilde{\boldsymbol{x}}}_t$, the one that the coordinator sends to both robots during the coordination policy. It is the feasible *one that* both *robots provide to the tool (section 2.5), and it is caused by the system velocities of figure 4.14. So, it is not always the* real *velocity that the tool has because collisions and firm grasp constraint are not included.*

4.8 Results Discussion

In this section, considerations about the results shown in the previous pages are made.

When the goal frame is know without error, the results are good even without the Force-Torque objective and the Change Goal routine. This is clearly visible in figure 4.6. Despite no presence of errors, some collisions happen anyway. This is due to the fact that the peg is driven directly toward the goal (inside the hole), without considering that there is the hole structure. Anyway, the forces and torques acting on the peg "help" the insertion phase because they drive *naturally* the tool inside the

hole. The peaks of the magnitudes are due to the first contact with the hole: even if the pose is perfect, this does not mean that a perfect alignment is present *before* reaching the goal frame. The lower left plot of figure 4.6 shows the tool velocities caused by the collisions, and in the lower right one we can see that the second tool "follow" the velocities of the first one, due to the firm grasp constraint (around second 40). In other words, it is as if the robot B would be dragged by motions causes by collisions on robot A. In the same plot, the chaotic velocities caused at the beginning are due to a not-perfectly coincident initial position of the two tools, that is impossible to achieve due to numerical errors of the simulation. Anyway, after a while they go to zero, so this initial error does not affect the rest of the experiment. The upper right plot shows how the error converges along its components. The small peak in roll is caused by the initial collisions with the hole.
Even if a perfect goal pose is obviously impossible to have, this experiment is useful to understand how the peg is inserted if ideal conditions are present. This is important: from now we know that in any case, the forces and torques acting on the peg may help *naturally* the insertion phase.

When an error in the goal pose is present, the results obviously get worse. The first noticeable thing is in figure 4.8: due to the error the collisions are more present during the insertion (first plot). An interesting thing is that the peg is inserted at the wanted depth anyway (as can be seen in the right lower plot, where the norm converges to a small value). An issue is that the forces are not nullified at the end, which means that continuous pressure between the peg and the hole is present.
The first idea to reduce the number of the collisions is to introduce the routine which change the goal frame. From the plots in the middle of figure 4.8, we see that the overall behaviour is improved: the forces and torques have a littler norm in general (upper plot) and the final position of the tool is more precise (lower plot). In fact, from figure 4.7 the six lower plots show us that the error in x is corrected by the routine. It can be noticed that also the z component is modified, even if it has no initial error. This is caused by the fact that the routine is active: so all the components are modified in the direction of the detected forces. Obviously, we can't assume to have an error only along a single axis, so we can't modify only the axis where we know there is the error (x-axis in this case). In truth, also the y-component is modified, even if the change is very little because the component of the force acting along the length of the peg is neglected to not modify the wanted depth of insertion (as explained in 3.3).
From the same figure 4.7, another thing to notice is that the routine does not correct perfectly the error in all the components, in fact the goal along the z-component is a bit erroneous. This is because the peg has reached a point where the forces are zero, and so no more modifications can be done. This is caused by the fact that

the peg has a smaller diameter than the hole, and so there is a tiny tolerance zone inside the hole where collisions do not happen.

In general, the goal changes slowly: this means that, especially when the first contact happens, the forces and torques magnitudes are big as in the vanilla case. The Force-Torque objective helps to reduce these peaks: as soon as a force (or torque) is detected, the objective responds to it and generates a reference velocity that moves the peg away from the walls of the hole. The reduction of the magnitudes is visible in the third plot of figure 4.8.
In the lower plots of the same figure 4.8, it is shown that the positional error between the goal and the tool is not affected so much by this objective. In truth, the convergence of the norm to a small value is a bit slower than the one of the case where this objective is not used. The first factor is that now the collisions are considered by the kinematic layer. So, being the new objective at an higher priority respect to the reaching goal objective, the kinematic control tends *first* to nullify the forces and torques and *then* to drive the tool toward the goal. This, sometimes, could increase the time to accomplish the mission (as in this case). Anyway, some other times it can *decrease* the mission time because less stalemates happen, thanks to the fact that this objective may help drive the peg away from the collision. In the second plot of figure 4.8, we can see that the norm of the force stays at almost a constant value around the interval $80s - 180s$, as well as the norm of the error in the plot below. This shows a situation of stalemate that is then solved. Presence of standoffs like this one are discussed later. A second factor is simply that, being the particularity of the problem, each experiment is different from the others, so sometimes the mission is "lucky" and it has less difficulties.
Figure 4.9 shows how the new introduced objective generates references and activations in correspondence of the forces and the torques detected: obviously the references and activations shapes (lower four plots) are similar to the shape of the forces and of the torques (depicted in the two upper plots). In this case they are even more similar because the norm (which is the quantity that the objective controls) is given by almost only one component, the y one.
In the lower plots, the activation is a function which assumes only values from 0 to 1, so it is always positive. The references instead, have opposite sign respect to the forces and the torques. This is because the objective wants to *nullify* the forces and the torques, so it provides a velocity in the opposite direction.
In the reported plots reference and activation are the ones calculated by robot A, but for the robot B they are the same. The agents receive the same data from the sensor (except small synchronization problems that can happen), so the reference $\dot{\tilde{\boldsymbol{x}}}_{ft}$ and the activation $\boldsymbol{A}_{ft}$ are the same.

Figure 4.10 shows the results of $\boldsymbol{J}_{ft}^{\#}\ \dot{\boldsymbol{x}}_{ft}$, for both robots. These are the system velocities that we would give if the objective was the only one in the TPIK list, without considering the activation, and a simple pseudoinverse for the Jacobian was used (without any regularization). So neither the collision propagation, the firm grasp constraint, nor the cooperation are included. As explained before, the reference $\dot{\boldsymbol{x}}_{ft}$ is the same vector for both agents. The thing that makes the two velocities so dissimilar, is the Jacobian $\boldsymbol{J}_{ft}^{\#}$, which is obviously different for each agent because they have different poses. This difference, at this point, it is not a problem for the cooperation because we have still to deal with the coordination policy.
These plots are shown only to point out that the velocities are not so big to be not feasible. In truth, at least for the vehicle part, they could be even too small to be followed well. This can be solved to make the objective control only the arm, or by increasing the gains (but taking into account that bigger gains would mean bigger risks of bad behaviours). Another thing we can see is that they are not so smooth, and they have lot of fast changes. However, firstly we have to consider that the activation, which the main work is to smooth the behaviour, are not present. Then, magnitudes are so little (in the $0.01 rad/s$ order for joints, and in the $0.01 m/s$ and $0.04 rad/s$ order for vehicle) that these fast changes are not so important. Last, we can't do so much because these changes are given by external data (the forces and the torques) that we have to deal with.

The final test of section 4.7 (which includes the Vision part) is interesting for two main reasons. The first one is that the peg does not start so near the hole (but it is almost aligned to it as before). This shows that the transportation phase is done in a good manner by the cooperative robots, even if no difficulties (e.g. difficult trajectories, an obstacle, a joint limit, and no vehicle and arm dynamics) are encountered. The second reason is that here we have hole's pose error also with some angular component, that affect the orientation of the goal frame where the peg is driven to. Anyway, this error is small and do not influence too much the insertion. In fact, as we can see in figure 4.13, the norm of the forces and of the torques is smaller than previous (upper left plot); the error converge smoothly (upper right plot); and little modifications are done to the frame goal, because its origin is almost with no error (lower plots). The bigger error in the angular norm is obviously due to the fact that now there are also some imprecisions in the orientation of the hole.

Figure 4.14 shows some plots about the cooperation. No big difficulties are met by the robot during the transportation and the insertion. So, the system velocities, that are the outputs of the final TPIK procedure (after the cooperation policy and

the arm-vehicle coordination), are similar between the two robots. It must be remembered that these velocities are not the applied one because the disturbances caused by collisions and firm grasp are not included. However, for the robot B (right plot) we can see that tiny peaks are present around the interval $20s - 40s$. These can be caused *indirectly* by the firm grasp constraint. When the tool of robot B is driven away a bit, in the next control loop the kinematic layer must do a little more effort in recovering the trajectory, causing these tiny peaks. Being the cooperation policy included, if these peaks are high (as around second 8) the Robot A helps the other one, in fact a little peak is present also for this one.
The last figure 4.15 shows the *feasible cooperative* tool velocity $\dot{\tilde{\boldsymbol{x}}}_t$, that is the one that the coordinator sends to the two agents, after assuring that is achievable by both (as explained in section 2.5). Even if disturbances of collisions and of firm grasp constraint are not present, this plot gives an idea about the tool's speed during the mission. It is driven slowly because the problem needs so: the insertion phase, made by two kinematic cooperative manipulators, puts big challenges and we can't afford to have too big gains.

A last thing to report is that some experiments meet a standoff situation at some point during the insertion. This happen when the collisions continuously make the peg to "bounce" on the inner hole walls, making it moving back and forth. The "bounce" is due to a bad peg alignment inside the hole, so the tip continuously touches the inner wall. In these cases, sometimes, the methods used do not manage to solve the stalemate in a reasonable time. The problem can be due to different factors. One could be that the simulation, being only kinematic, is not precise. So, even if the gain are really small, in any case the velocities are instantaneously provided to the system, and this causes always a bit chattering. This complicates the work of the simulator (to calculate the collisions) and of the whole mission (that could meet almost instantaneously a strong force or torque). Another problem could be a not so good setting of the many gains that we have to put. Other one can be that we have two robots that are carrying the peg, which makes the whole experiment much more difficult, considering also that the collisions propagate through Jacobians (that are mappings from linear approximations of non-linear things) on the system. Other one can be that, with the Change Goal routine, orientation modifications are not made, so no correction is doable for the angular part. Additional issue to take into account is that some synchronization issues may happen. The coordination policy, in the way it is implemented, assures the synchronization (section 4.5), but we have also other kinds of exchanged information. For example, the force-torque sensor data is shared using ROS topics in a simple way, so with the actual software we can't know exactly when information arrives to each node. Considering also that on a single machine we run the simulation and the two robot software (plus the coordinator)

this could cause more synchronization problem. This may be solved with further code improvement, but it goes out of the scope of this work and it is not so useful for the real application (where we don't run everything on a single machine).
The standoff problem is more influential when the hole's pose error is bigger, or, for example, when we have also orientation error such as in the last experiment. However, the methods show a good starting point to improve the current state of art in this unexplored problem underwater.

Chapter 5

Vision: Methods & Results

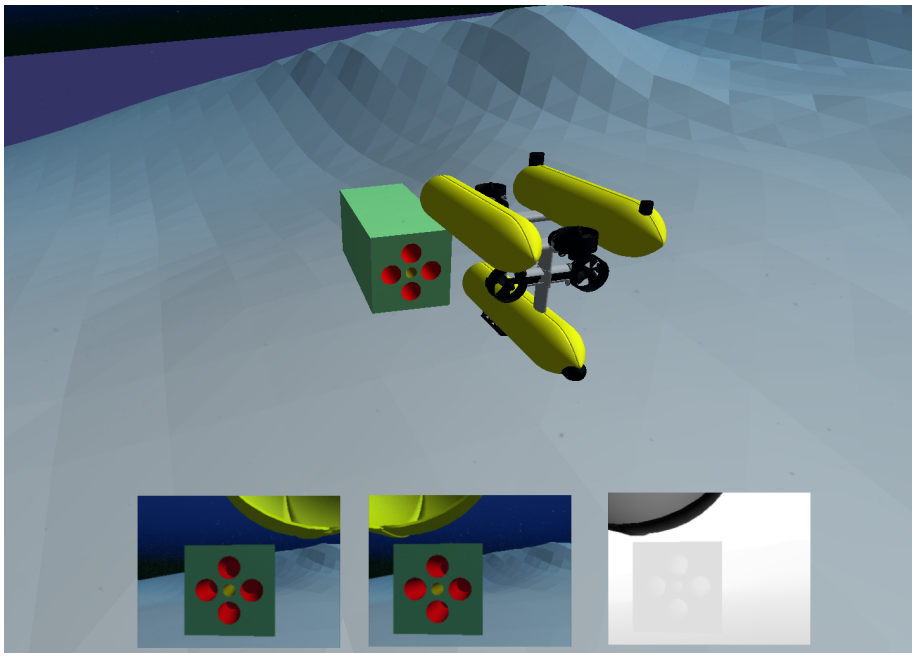

Figure 5.1: The vision Robot watching the hole. The hole is in the centre of the cuboid. The red holes are only present to help vision algorithms. Below, what the right and left camera are seeing. Note that also a depth left image is provided, but the left RGB camera and the depth camera are not used together.

Before the twin robots can approach the hole, its position must be know, at least roughly. In this chapter, the pose estimation of it is discussed.
In the considered scenario, a third robot is present. Its duty is exclusively to *detect* & to *track* the hole. In the simulation, another Girona 500 AUV is used for this job, without the arm. Is evident that, in real scenario, a littler and more efficient robot

should be used for the vision, see that no manipulation task are needed. In fact, in the original TWINBOT [TWINBOT (2019)] simulation, a smaller BlueROV is present, as can be seen in (TODO) However, in this case, another Girona 500 is used to not deal with another robot model.
The *vision* robot is equipped with two identical cameras which point in front of it. They are used as:

- Two distinct cameras, independent one of the other.
- As stereo cameras, thus exploiting stereo vision algorithms.
- As RGB-D camera, i.e., a stereo vision couple where the left one is a RGB camera and the right one a Depth camera.

The job is done into two phases: *Detection* (section 5.3) and *Tracking* (section 5.4).

5.1 Assumptions

For the sake of simplicity, some assumptions are made:

- Known *intrinsic* camera parameters. These parameters are used by algorithms to take into account how the single camera see the scene. The (known) distortion is zero.
- Known *extrinsic* camera parameters, i.e. the position and orientation of cameras (respect the vehicle), and thus the relative pose (the transformation matrix) from one camera to the other (needed for stereo vision algorithm).
- No external disturbances for the images, such as light reflections underwater or bad visibility.
- Hole model known. This means that dimensions of the cuboid which contains the hole are known. Further explanation about this are given successively in section 5.4.
- A "friendly" cuboid structure of the hole. The front face is coloured and additional holes are present, as can be seen in fig. 5.1. This help both the *detection* phase and the *tracking* phase.

About the robot, other assumption are:

- the pose of the vehicle respect the inertial frame is known. (TODO?AS explained?? se si linka sez). This permits to know the estimation of the pose of the hole respect the inertial frame, to directly send the robot which are carrying the peg.

- The initial position of the robot is such that it is facing the front face of the hole. It must be noticed that methods explained in the next sections can be adapted to relax this hypothesis. For example, the robot could turn around z-axis until the hole is detected. (TODO?? Also, good results are obtained when the robot not exactly face directly the cuboid, but, for example, it is on its side, looking at front face and a side one.

- Once the robot has tracked the hole and the pose sent to the twin robots, it must go away to not interfere with the insertion phase. This is done through keyboard (as a ROV) but it is not difficult to improve the code to let him go away autonomously. It must be noticed that, thanks to the *tracking* algorithms, if the robot moves (because it is commanded to do so, or for water currents) the pose estimation is still good.

5.2 Tools

To deal with the pose estimation, some external tools are used. In this section they are listed.

- **OpenCV** (Open Source Computer Vision Library) [Bradski (2000)], an open-source BSD-licensed library that includes several hundreds of computer vision algorithms. It is used mostly for the detection part, even if some of its functionalities are used also by ViSP (for example for keypoint tracking).

- **ViSP** (Visual Servoing Platform) [Marchand *et al.* (2005)], another open source library that allows developing applications using visual tracking and visual servoing techniques. It is helpful because is more specific for robotic fields and easier to use than OpenCV. It is used for the tracking phase.

- **PCL** (Point Cloud Library) [Rusu & Cousins (2011)] a library for 2D/3D image and point cloud processing. In this work, is used by ViSP when depth images are used. However, further works can used as another help to deal with the vision part.

5.3 Detection

Object Detection means detecting a particular shape (i.e. the *object*) in the scene. This is important to initialize the tracking algorithm used. In fact, for the tracking algorithm used successively, the detection part must provide a correspondence between some pixels in the 2D image and some points in the 3D object shape. It is

important to notice that the needed 3D coordinates refer to the object frame, and not to an "external" frame. Seen that the object model is assumed to be know, the 3D coordinates of some point directly derive from this assumption.
Four points is the minimum number of point accepted by the tracking algorithm. The more the point are, the more the tracking is good. Plus, point should lying on different surfaces of the object, to have better results. Anyway, good tracking result are obtained also not considering these two aspects. The four points chosen are the corners of the front face of the cuboid, where there is the hole.
As an example, the .init file with the 3D coordinates is like the one in file 2.

File 2 The .init file describing the position on the 4 corners of the front face, respect to a frame positioned in the centre of the hole, with x-axis going inside the hole, y lying along the surface pointing on the right, z pointing down to the seafloor.

```
1: 4              # Number of points
                  #xyz with x going in, y on the right, z down. Measure is meter
2: 0 -0.4 -0.4    # top right corner
3: 0 0.4 -0.4     # top left
4: 0 0.4 0.4      # bottom left
5: 0 -0.4 0.4     # bottom right
```

The work of Detection is to provide 2D coordinates of the image pixels that correspond to the 3D points of file **??**. This must be done for each camera, except for the Depth one (when used).
Two methods are evaluated: *Find Square* (section 5.3.2) and *Template Matching* (section 5.3.3). A third method, in which the 2D coordinates are precise as much as possible (selecting by hand the four pixels containing the corners), is used to have a benchmark for the other two and to analyse the tracking when 2D Coordinates are almost perfect (section 5.3.1).
Details of how each function works and explanation of the computer vision algorithms used are not provided here, to not go outside the scope of the thesis.
Other methods and functions are briefly explained in Appendix B. Another, not explored, method can be to use tags code on the cuboid surface. However, in underwater situations this can be difficult to be put in practice.

5.3.1 Already known Coordinate Method

As explained, with this method the 2D coordinates are perfectly known. This is done by letting the user to click on the 4 pixel which contains the corners. Given that the image is made by discrete pixels, is impossible to have an ideal point which is exactly the corner, but the errors for this are not noticeable.

5.3.2 Find Square Method

This method is taken from an OpenCV tutorial.
A rough explanation of how the method works is presented:

- This method looks in each image channel (unique if is a gray image, three if is a colored image) to find squares.
- First, it pre-processes the image to reduce noise, down and up scaling it.
- Then, *findContours()* is called to retrieves contours of the shape with the algorithm described in Suzuki & Be (1985).
- Each contour is approximated to be more like a regular polygon, with less vertices and edges.
- Finally, the algorithm looks if the shapes are similar to squares/rectangles. This is done checking if the internal angles are almost 90 degrees.
- The returned shapes are described by their four corners, that is what we are looking for. An additional function is called to be sure that the order of the returned corners is the same order of the points described in the .init file, otherwise correspondences are obviously erroneous.

5.3.3 Template Matching Method

Template Matching means to find a pattern (in this case, the face of the hole) inside a scene. So, an additional image of the square face of the hole is needed.
The code developed follow an OpenCV tutorial.
In brief, *template matching* finds the point in the scene which as more similarity (or less dissimilarity) with the provided template. This is done considering intensity values of the pixels in the neighbourhood area of a center pixel. In practice, the template is shifted all over the scene image and some calculations for each new template shifting are done. Various formulas to compute similarity (or dissimilarity) are provided by OpenCV and are detailed here. The choosen one in the experiment is the so called *squared differences* (the first in the link).
It is important to scale up and down the template and to compute various time the similarity. This because usually template size is not equal to the size of the object in the scene. For each scaling, a best similarity point is detected. Then, all the similarity points are compared and the best one are chosen. At the end, a rectangle with the template (scaled) dimensions is build considering the best point as the centre. The corners of the rectangle are the 4 points which we were looking for.

5.3.4 Detection Results

In this case, the find square method give the best results. As can be see in fig. 5.2, differences from the ideal method and this one are barely visible. In the way it works, it should be noticeable that this method gives good results only if the camera approximately face the cuboid structure at the front. If the side face is more visible, it will be the one detected. So, we must know which side the robot is facing to give the 3D correspondence points in the .init file.
In addition, this method is suitable if no other squares of similar dimensions are present. If so, further work is needed to discriminate them. Also, is not suitable with other kind of shapes (a pipe hole, for example). It is also important to point out that sometimes the method fail to find any shape in the right image. This happened approximately 30% of the time, and could show a very bad robustness and low predictability of the method. However, the fail is obviously detectable and another trial can be done easily.
The template matching is less precise than the previous. Plus, if the face is view from a different angle, other template image is needed, with an orientation similar to what the robot is seeing. In general, lot of template images at different angles are needed. Otherwise, some processing of the template image is necessary to orient it in a different way. Also, building the shape around the centre point is more difficult, if this shape is not a square. Anyway, the template method is more general because can be used also for different shapes (e.g. a hole of a round pipe).

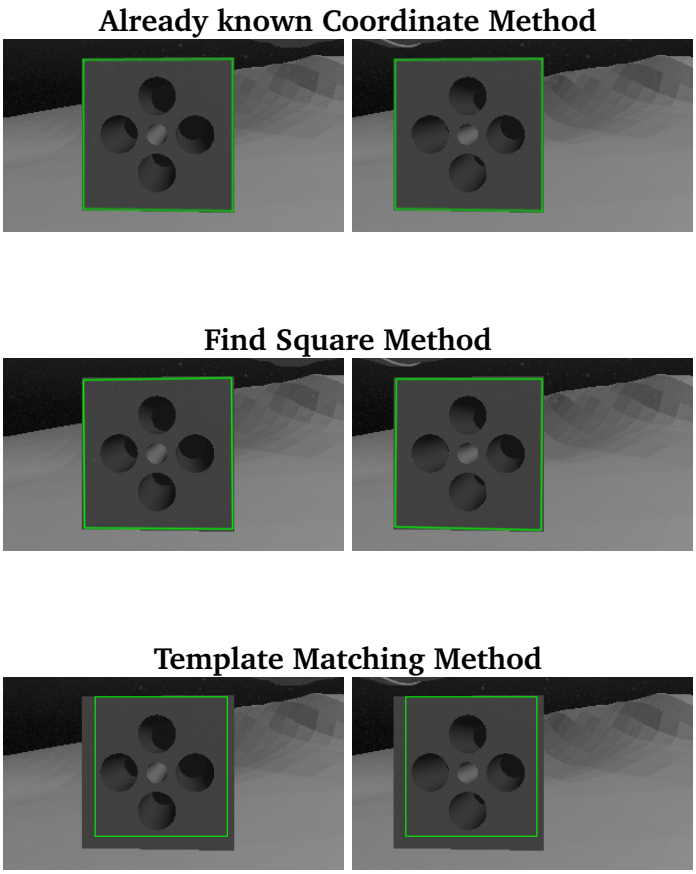

Figure 5.2: Results of the three different detection method. The green rectangle is the estimate position of the square. The output of the detection step are the four corners of the green rectangle.

5.4 Tracking

Object Tracking means to follow the motion of an object of interest during time. Both the object and the camera can be mobile, even if, in this case, only the cameras are moving (actually, the robot moves, the cameras are rigidly attached to its body). Tracking an object is usually done to estimate its pose respect to the camera frame. In this case, we speak about a *markerless model-based* tracking. Thus, the object model must be provided. In this scenario, it is sufficient to give to the algorithm the 3D dimension of the cuboid structure of the hole, with a circle in the front face. Using ViSP, the format required for the model is *.cao*, which sintax is described here. As explained in section 5.3, the algorithm must know the position of *at least* four point belonging to the cuboid. In the experiments, the provided ones are the 4 corners of the front face.

Three different trackers have been tried: *Two Mono Cameras Tracker* (section 5.4.1), *Stereo Camera Tracker* (section 5.4.2), and *Stereo Depth Camera Tracker* (section 5.4.3).
A tracker is linked to each camera. For RGB cameras, it can be of three types: *edge-based* [Comport *et al.* (2006)], *keypoint-based* [Pressigout & Marchand (2007)] or a mix of both. During the experiment, the hybrid method emerged as the most precise, so all the results in section 5.4.4 refer to this one. For the depth camera used in *Stereo Depth Camera Tracking*, the tracker type can be *normal* or *dense* [Trinh *et al.* (2018)]. Being the *dense* one more robust, it is the only one to has been considered. Please note that it is also computationally heavier for large matrix computations, but speed performance are not considered here.

5.4.1 Two Mono Cameras Tracking

This method derived from the ViSP *Markerless generic model-based tracking using a color camera* tutorial.
The implementation is straightforward: after setting the trackers (i.e. giving edge and keypoint detection parameters, camera parameters, and 2D-3D correspondence of the four corners), at each loop the tracker estimates the transformation matrix between each camera and the object.
In this method, the left and right cameras are independent. Thus, each one provides a different pose estimation. It is not so easy understand when one camera provides better results that the other. Anyway, it should be easy to understand when one camera fails completely in tracking the object.

5.4.2 Stereo Camera Tracking

This method derives from the ViSP *Markerless generic model-based tracking using a stereo camera* tutorial.
The code is analogous to the previous one, except that in this case also the relative pose between each camera must be provided. If this is unknown, some method for stereo calibration must be used.

5.4.3 Stereo Depth Camera Tracking

This method derived from the ViSP *Markerless generic model-based tracking using a RGB-D camera* tutorial.
This method is similar to the previous one, except that the right camera is now a depth one, thus providing depth images. The functions used for depth images need

the support of another library, PCL (Point Cloud Library) [Rusu & Cousins (2011)]. Another exception is that the depth camera does not need to initialize the 2D-3D correspondences, so the *Detection* step has to be done only for the left camera.

5.4.4 Tracking Results

In this section, performance of the three tracker are evaluated. For each one, the three different types of detection initialization (explained in 5.3) are considered to see the effect of detection error on each tracker.
Experiments have been conducted with lot of simplifications: no disturbance, no cameras distortions, very good visibility, nice object shape. Results described here can give only an idea on how to proceed in a more realistic scenario.
In the scenario, the robot is perfectly still while tracking the object, and it is in front of the object, slightly on the right. The original images taken from cameras are cut to delete a region where part of the vehicle is visible. This is done to make this part not interfere with the algorithm. In the depth image, this is not necessary, because there is no interference.
In fig. 5.3 the detected shape and the estimated frame are drawn on the camera images. Differences are barely visible in the first two initialization methods. With the template matching method, bad initialization (shown in 5.3.4) is paid in tracking result, especially in the depth case. This is clear in fig. 5.6. With this initialization, the depth-stereo method is even worse than the monocular case. This can be due to the fact that the depth image is not initialized with 2D-3D correspondence; thus paying more the initialization error being done only in the left image. So, it is showed that it is not always better to have a RGB-D camera instead a normal RGB. This is an interesting result and should be further explored with more realistic scenarios.
With good initialization, (fig. 5.4, fig. 5.5), the stereo methods have similar results, overall better than the mono case. which however has not bad performance. Another interesting result is that, in the monocular case, the position of the camera influence the results. This is because different view angle obviously provides different tracking performance.
In the plot of the errors (fig. 5.4, fig. 5.5, fig. 5.6), lot of variations during time can be seen, although the robot is still. This is due to the nature of the tracking algorithm, which continuously estimates the pose for each image received by the camera. However, it must be noticed that the variations are little for both linear and angular parts.

Already known Coordinate Initialization

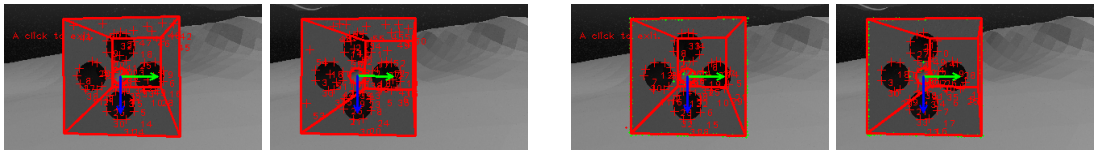

Mono Cameras Case *Stereo Cameras Case*

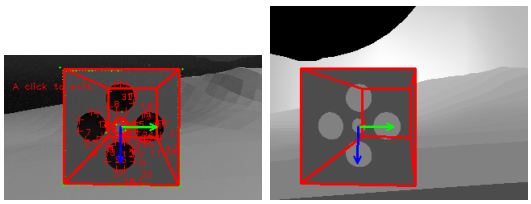

Stereo Depth Camera Case

Find Square Initialization

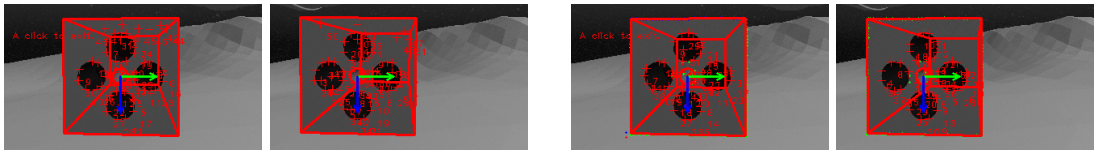

Mono Cameras Case *Stereo Cameras Case*

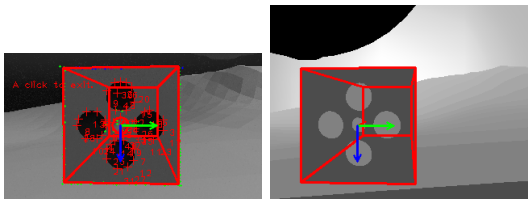

Stereo Depth Camera Case

Template Matching Initialization

Mono Cameras Case *Stereo Cameras Case*

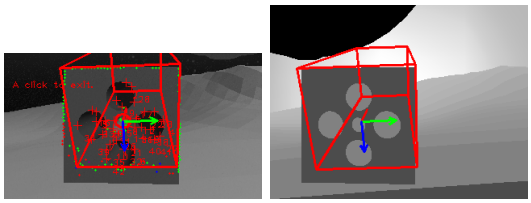

Stereo Depth Camera Case

Figure 5.3: Tracking Results. Red lines are the contours of the model where is estimated to be ; red cross are the point tracked by the algorithm. The arrows represent the estimated object frame: green for y-axis, blue for z-axis, red for x-axis (which go inside the hole and is barely visible). Green dots are the tracked correspondent points between left and right images, thus they are present only in the stereo cases.

Already known Coordinate Initialization

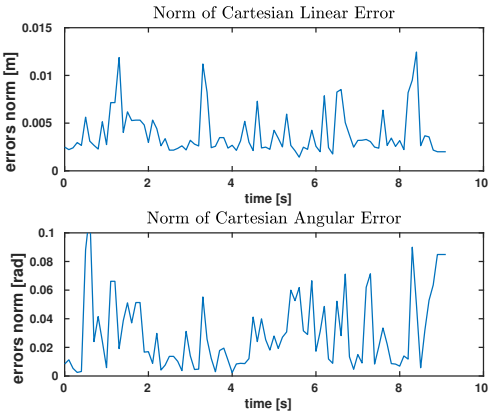

Mono (left Camera) Case

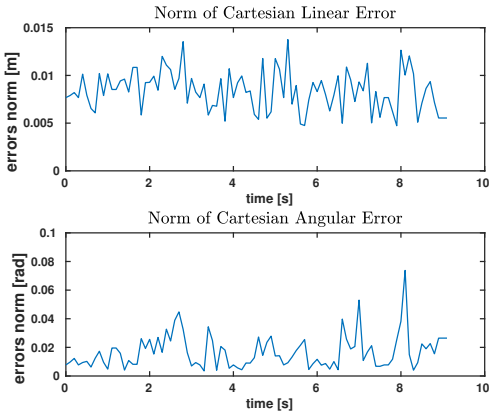

Mono (right Camera) Case

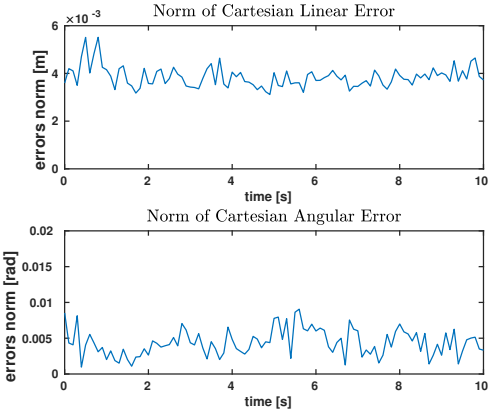

Stereo Camera Case

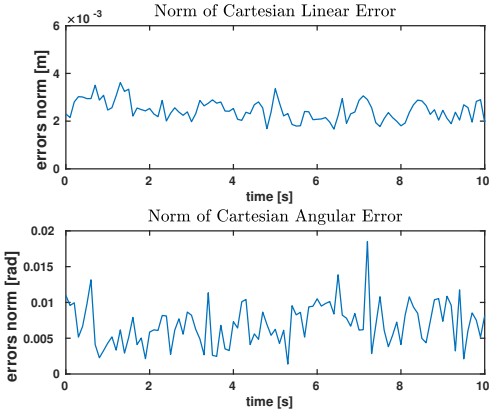

Stereo Depth Camera Case

Figure 5.4: Linear and Angular Error (in norm) between true pose and estimated pose, with the best initialization of detection step possible.

Find Square Initialization

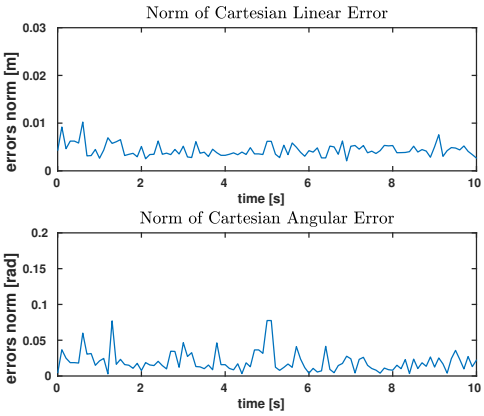

Mono (left Camera) Case

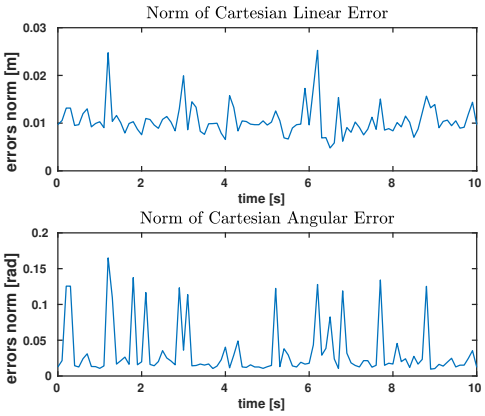

Mono (right Camera) Case

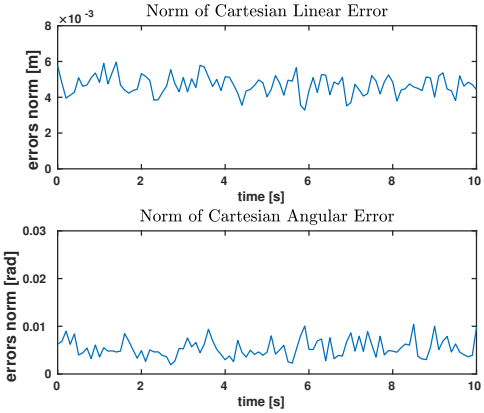

Stereo Camera Case

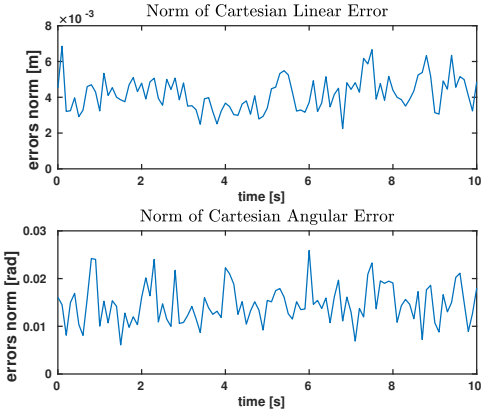

Stereo Depth Camera Case

Figure 5.5: Linear and Angular Error (in norm) between true pose and estimated pose. The detection step here uses the find square method.

Template Matching Initialization

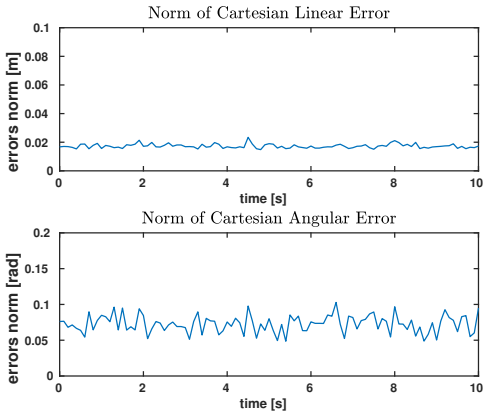

Mono (left Camera) Case

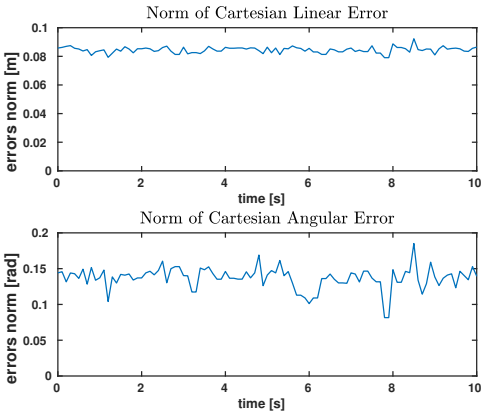

Mono (right Camera) Case

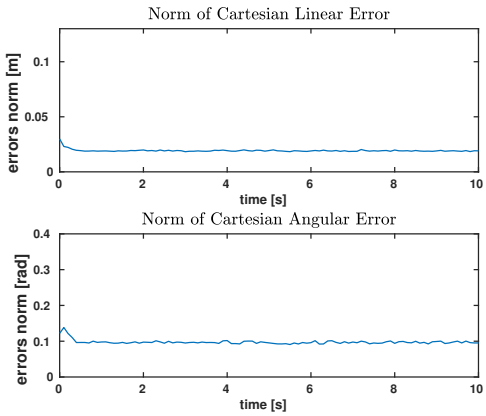

Stereo Camera Case

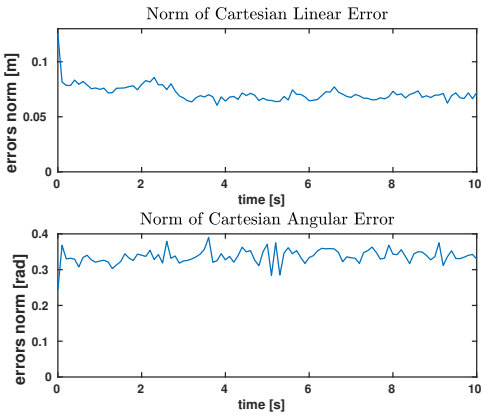

Stereo Depth Camera Case

Figure 5.6: Linear and Angular Error (in norm) between true pose and estimated pose. The detection step here uses the template matching method.

Chapter 6

Conclusions

This thesis presented a kinematic control architecture for two cooperative autonomous underwater manipulators. The cooperation is done at kinematic level, exchanging vectors and matrices to produce a common tool Cartesian velocity. The cooperation scheme takes into account that underwater communication is difficult, and makes the amount of exchanged data as low as possible. Code implementation is suited to easily manages objectives (e.g. to delete offline some objectives to try a different method). Big effort has been made in provide a modular and flexible code architecture. For example, the dependency from the Robotics Operating System (ROS) is kept at minimum to make possible to easily adapt the code to a different kind of interface and/or simulator (which do not rely on ROS to communicate).
The experimental results showed how the Task Priority Inverse Kinematic approach used can deal with an assembly task: the *peg-in-hole*. Being an unexplored problem for cooperative underwater manipulator, the problem is simulated with many simplifications and assumptions.
Part of the problem deal with Computer Vision Algorithm. The thesis shows how some detection and tracking algorithm can be exploited to estimate the hole's pose. For the insertion phase, a force-torque sensor is used to help the accomplishment of the mission.
Both the Control and the Vision part can help other works in various robotics fields, not only related to underwater intervention missions.

In the Chapter 1, an introduction about the context is given, and the previous works in the field has been recalled.
In Chapter 2 the principal points of the theory behind the Control Architecture are summarized. Here, the mathematical foundations for the Task Priority Inverse Kinematic approach are recalled, considering also a coordination policy between multiple agents that fits in the chosen approach.
In Chapter 3 the theory explained before is exploited to deal with the scenario

stated by this thesis. A Force-Torque objective is inserted in the TPIK list to reduce the magnitude of forces and torques that act on the peg during the insertion phase. This is noticeable because it is used a "dynamic" information (the force and the torque) in a pure-kinematic method. A simple, but suitable for the scenario, list of objectives is then described. An additional routine, part not of the kinematic layer but more of the Mission Managing layer, is explained. Took the goal frame where the peg is driven to by the kinematic control, this new routine shift its origin according to the direction of the force acting on the peg. This is an additional method to further exploit the information given by the force-torque sensor.
In Chapter 4 simulated environment is detailed. The chosen simulator, UWSim, is introduced, along with some other underwater simulators that can be useful for the interested reader. To make the insertion phase realistic, collisions between the peg and the hole have been introduced. These collisions propagates through the whole robotic system, thus affecting the arm and the vehicle. Another routine is implemented to fake a firm grasp of the tool by the two robots. In real environment, this constraint is assured by frictional forces, but in a kinematic simulator like the used UWSim the frictions are not present. The tuning of the gains permits to not hide bad cooperation between the agents. In the same Chapter 4, assumptions to simplify the problem are explained, and an idea of how the Control Loop runs is given. Finally, results of the experiments done are presented and discussed. Three main experiments have been carried out: without hole's pose error, with a fixed error of 0.015m along one axis, and one final test which includes the Vision part with the hole's pose error given by the *Detection* and the *Tracking* algorithms used.
Chapter 5 covers exclusively methods and tools used by the Vision Robot. No theoretical background is given because it would take out of the scope of this thesis. The Chapter gives an idea on how two computer vision libraries, **OpenCV** (Open Source Computer Vision Library) [Bradski (2000)] and **ViSP** (Visual Servoing Platform) [Marchand *et al.* (2005)], are used. The Vision part is divided into two phases: Detection and Tracking. For both, different algorithms have been tested, compared and discussed. In particular, for the Detection part, some methods have been discarded and they have not been used any more for further trials, but they are anyway presented in Appendix B. They are all OpenCV algorithms that can help in other applications.
The Appendix A gives some details on how the software is implemented, together with a list of some useful libraries used that surely can help to develop control architecture in C++ programming language.

For on-going progress in this scenario, it can be useful for the reader to follow the TWINBOT project [TWINBOT (2019)]. This thesis context derives from the scenario of this project, but it evolved independently because at the time this thesis was being

developed, TWINBOT was in a very early stage.

6.1 Further Works

Since the novelty of the applications, further works can be done in various direction. For what concerns the experiments, a dynamic simulation, along with a dynamic controller, can be introduced to better analyse the methods used. Considering this means to include effects that increase the realism of the simulation, such as buoyancy, thrusters modelling, disturbances of the arm to the vehicle and vice-versa, real tool-grasping effects, even some water currents. Some works have been done in this direction but then not pursued due to the lack of time. These efforts, even if they are not presented in this thesis, show that the first step to introduce dynamics could be using the plugin FreeFloatingGazebo [Kermorgant (2014)], mentioned in section 4.1. This one is the most simpler to use from the actual work because the scene (i.e. the file which describes the simulated scenario, such as the initial pose of objects and robots) would be the same and ROS would be always used as interface, so no big modifications on the code have to be made.

Regarding the actual chosen architecture, the force-torque task can be improved, for example considering a reference calculated not only as a proportional error between the desired force (that is zero) and the actual detected one. Another improvement can be for the Change Goal routine, to let the the forces and torques also modify the orientation of the goal frame and reduce/eliminate also the angular error from the real goal frame to the one estimated.

Additional methods can be explored regarding the insertion phase. This thesis concentrates only on collisions that may happen when the peg is already inside the hole. If some contact between the external surface of the hole's structure and the peg's tip happens, the mission fails (i.e. a stalemate where the peg bounces forever against the squared hole's surface, unable to find the hole). In the literature, various methods have been explored to find the hole on the surface. For example, researchers have considered the cases when the peg meets the hole with a bad alignment that creates a 2 or 3 points contact (as briefly explained in 1.1.3). However, to the best of this author's knowledge, the *peg-in-hole* problem has never been studied when the protagonists are two autonomous mobile manipulator (in any scenarios, not specifically underwater ones), so can be interesting to adapt old methods to this particular (cooperative and underwater) field.

Towards a more realistic intervention missions, efforts can be spent to consider methods and tools to localize the robot underwater. In this thesis, it is assumed

that all agents have a reference frame in common, but, usually, localization underwater is really an issue. Some cooperation (this time not at kinematic level) can be considered to make some surface vessels helping the underwater agents to localize themselves (a problem explored in the WiMUST project [Abreu *et al.* (2016)]).

In this thesis, some assumptions have also been made for the Vision part. Further works could consider to relax some of them, for example to increase the difficulty of the detection and tracking phases. In an underwater scenario, not always the water permits to watch from afar, and illumination and distortions can be other important issues.

In general, there is always a lot of work to increase the capacity of intervention-AUV. For example, we can consider more specifically communication issues and techniques to exchange data between agents; especially in underwater scenario, we can't share too much information among robots and with too high frequency. Also, other kinds of assembly problem can be addressed: for instance a *peg-in-hole* one where the *peg* is held by only one robot and the *hole* by another one. Some objectives of the TWINBOT project [TWINBOT (2019)] aim to study these two lasted cited problems.

Appendix A

C++ Code Scheme

Some effort has been spent to implement a flexible and modular C++ code architecture. The main focus is directed to facilitate the use of the TPIK approach. With this scheme, adding and removing tasks from the code is easy and straightforward. Furthermore, even if ROS is used as interface, other communication methods (for different simulators, or even for real robots) can be used easily, changing a little part of the code. This is due to the fact that all the ROS parts (the *interfaces*) are implemented in different files from the ones of the main blocks.
Only a rough idea about the code scheme is given here, without too much details. Further explanations can be found in the github page and in the code documentation.

A.1 Tools

The Control Architecture is implemented in C++ language, using various libraries. In this section, the most relevant libraries and tools used for the software are described. Please note that a particular section (section 4.1) is dedicated to the choice of the simulator, and another for tools used by vision (section 5.2).

- **ROS** (Robot Operating System), the well-known robotic middleware. It is used to communicate with the simulator, so to send commands to robots and receive information by the on-going simulations (e.g. robots states, information from sensors, streaming images from cameras).
- **Eigen** [Guennebaud *et al.* (2010)], a C++ library for linear algebra. It is very useful to deal with matrices computations and management in any C++ software.
- **CMAT**, another C++ library, implemented at GRAAL. It implements the core functions for the TPIK method, detailed in Simetti & Casalino (2016).

- **Orocos KDL**, a package to deal with kinematic and dynamic chains. Here it is used to compute the Jacobian of the robots, given the configurations.

A.2 The Single Robot Code Scheme

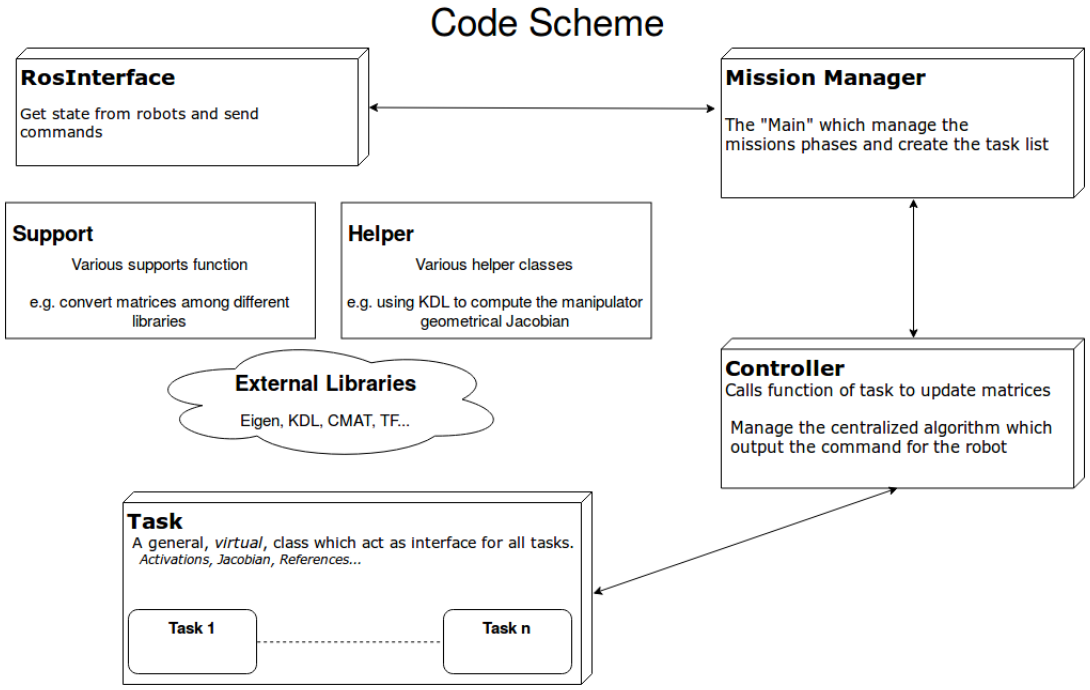

Figure A.1: The C++ code scheme that show the relationship between the main blocks of the single robot. Parallelepipeds represent the principal blocks, while rectangles contain useful functions used by them. Arrows indicate the communication between the main blocks.

Here is presented the scheme for the two carrying robots. The two robots share the same code, and they are differentiated (when necessary) thanks to their names (*g500_A* and *g500_B*).

- **RosInterface** This class is used to communicate with the simulator, e.g. sending commands to the robot, receiving state and sensor information, and so on. It is obviously ROS-dependent, and it should be replaced if another middleware is used.

- **Mission Manager** This block is the "main". It initializes all useful classes, it creates the tasks list, and it manages the whole mission.
- **Controller** This class is the core of the control; in practice it is the kinematic layer. It generates commands for the vehicle according to the prioritized list of tasks. It is where the iCAT algorithm (2.3) is used.
- **Task** This is an *abstract* class. It acts as a base class, and all the specific *concrete* classes of tasks derive from this one. In this way, the controller and the mission manager simply handle a vector of pointer to Task. The Mission Manager creates a concrete class for each task and then it fills a vector. This vector is the prioritized list of the TPIK method. The controller can iterate this vector and can call the abstact methods of Task without worrying of which real concrete task is actually inside the list.
- **Support** It is a group of various *namespaces*, used for conversions, to print to file, and to use some mathematical formulas.
- **Helper** It contains a group of classes and headers used to help the control scheme (e.g. to compute the Jacobian with KDL) and to log results.

A.3 The Whole Code Scheme

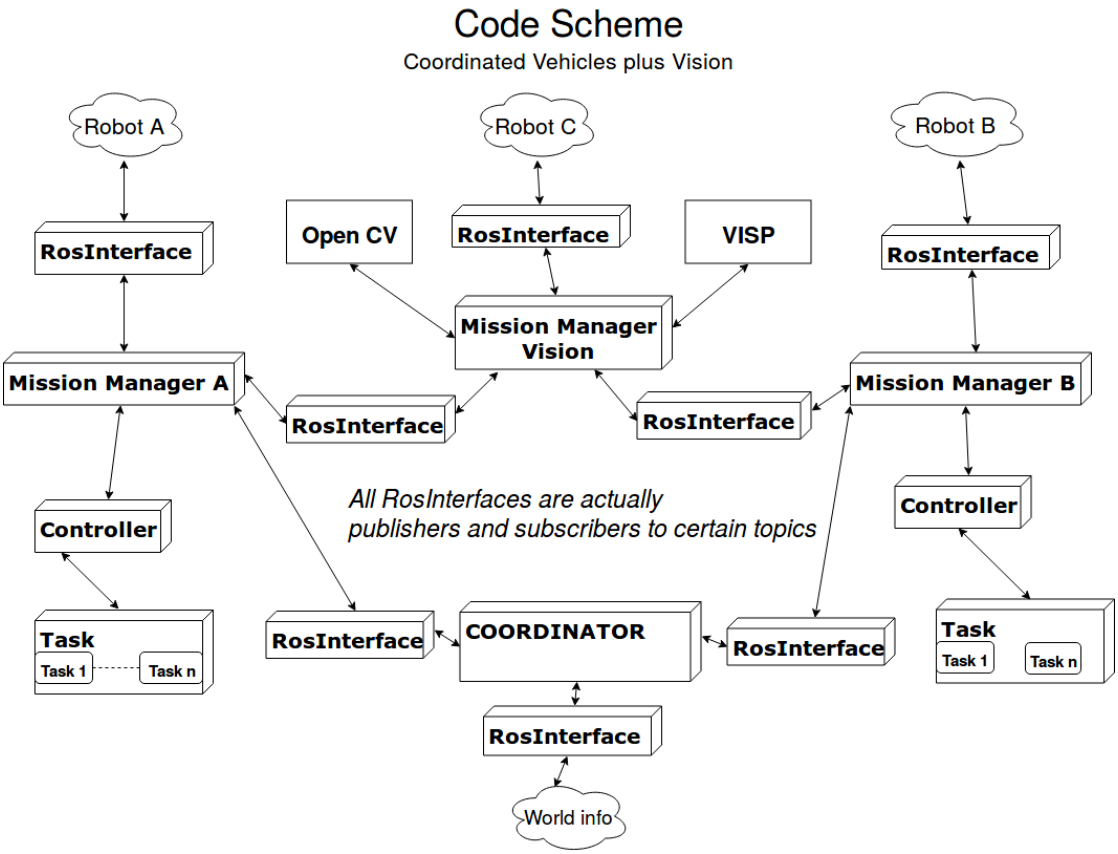

Figure A.2: The C++ code scheme that show the relationship between the main blocks of the three robots. On the left and on the right side there is a zoomed out view of the fig. A.1, for the two carrying robots. In the centre, there are the schemes for the Vision Robot (where also main tools for it are visible) and for the Coordinator.

The two robots must communicate between them and with the vision robot. Like explained before, ROS is used to communicate with the simulator, but it is also used to make different nodes (e.g. Coordinator and Robots) to communicate.
Please note that the Coordinator is not a physical object: can be put as a routine on one robot. This would help communication issues, because only information exchange between the Coordinator and the other robot will pass through the water.
The scheme for the Vision Robot is simplify because it is driven as a ROV: so it is not autonomous and no TPIK is implemented for it. Anyway, it can be turned easily into an autonomous robot, with or without TPIK (that it is not really necessary for this

robot).
The Coordinator is a node in charge of dealing with the coordination method explained in section 2.5. It also needs information from the world (i.e. the simulation) to compute the cooperative velocity.

Appendix B

Other Algorithms for Object Detection

During the simulations, several trials have been done to find a suitable algorithm for the detection of the hole structure. In Chapter 5 two methods have been discussed as the successful ones. In this appendix, others are briefly explained and discussed. Even if they are not used in the last versions of experiments, they can be useful for other purposes, such as detection of other kind of shapes. They can also be useful when the scene is different, for example while taking the hole structure from its side. Each one is taken from OpenCV Detection tutorials, where also other algorithms can be found.

B.1 Corner Detection with the Shi-Harris method

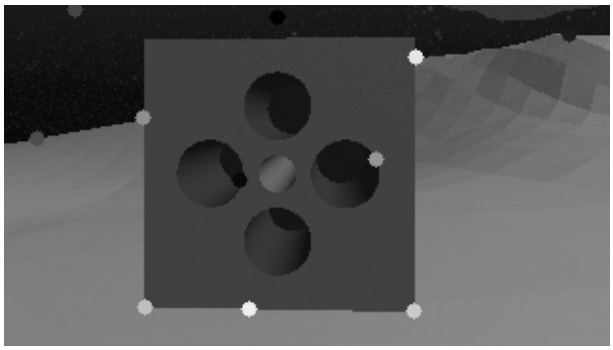

Figure B.1: goodFeaturesToTrack() result. Only two detected points are real corners, and the upper corners are not detected.

Following the tutorial, I implemented a corner detector with the Shi-Harris method [Shi & Tomasi (2000)] using the OpenCV function goodFeaturesToTrack().
This function acts as corner detector. In our case, this can be useful to find corners of the square hole structure. These points can be used successively as starting point to higher level vision algorithms (e.g. draw the square shape to then understand its pose).
The original example lets change the number of maximum points to be found. This is useful to reduce the number of false positive corners. The main problem is that the real corners of the square are not the "best" ones. So we can't simply put this parameter equal to 4. On the other side, with bigger number of points, is then difficult to discriminate the right corners from the others.
Other interesting parameters are:

- **minDistance** The minimum distance between corners to be found.
- **qualityLevel** Parameter characterizing the minimal accepted quality of image corners.
- **blockSize** Size of an average block for computing a derivative covariation matrix over each pixel neighbourhood.
- **mask** To specify a certain region of interest in the image. In such a way, corners are found only in this region. The problem in our case is that without prior works we can't know where is the hole surface.

The points detected are effectively good feature points (as can be see in B.1). But the best ones, are not the ones that we want to detect (ie, the corner of the square). This method should be used as a low level algorithm, to then help higher level ones. For example, to construct some polygons and to check if these polygons are square/rectangles. However, to follow this direction should be better to start from the edges. Another function can be to initialize a tracking by keypoints.

B.2 Canny Edge and Hough Transform

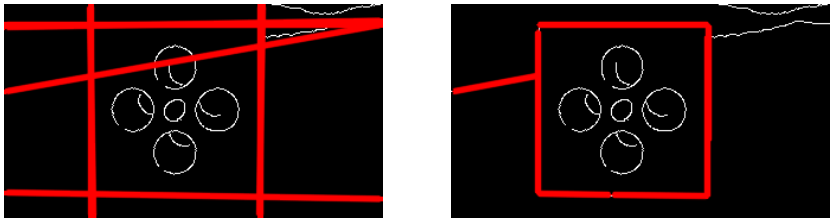

Figure B.2: Result of Hough Standard Transform (left) and Probabilistic (right). In white all the edges detected with Canny, in red the detected straight lines.

The Hough Transform [Duda & Hart (1972)] is a method to detect straight lines in an image. Usually, a preprocessing of the image with an edge detector is used to improve the results, for example with a Canny Edge Detector [Canny (1986)]. The OpenCV tutorial makes use of two types of Hough Transform: the standard *HoughLines()* and the probabilistic *HoughLinesP()* [Matas *et al.* (2000)].
Results are visible in B.2. The probabilistic method shows that this function is good to detect the square structure of the hole. Thus, this method can be used as good starting point to further process the image, to then estimate the pose of the hole, or of other objects of interest.

B.3 Bounding Boxes Detection

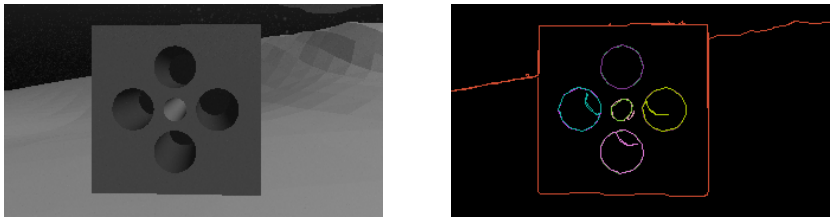

Figure B.3: Result of the algorithm: on the left the original image, on the right the contours detected.

Figure B.4: On the left, the original image. On the right, the drawn bounding boxes around the holes.

In this method, shape contours are found and then bounding boxes drawn. As explained in the previous section, finding shape contours can be a starting point to initialize higher level image processing, such as the tracking.
The code derived from an OpenCV tutorial.
First, a Canny edge detector is used to preprocess the image. Then, the function *findContours()* is called to retrieves contours with the algorithm described in Suzuki & Be (1985). Finally, rectangles are draw around as a bounding boxes.
In case of the square hole structure (already almost a "bounding box" of itself), finding the boxes is useful to reduce the noise, and to have a square/rectangle with straight lines.
The result without the bounding boxes are shown in B.3. The square is noticeable, but also other not interesting lines are shown. For this specific purpose (detection of square face of hole), the detection is worse than the algorithm of section B.2 which used probabilistic hough transform.
The thing to notice is that the holes on the surface are well visible. This may be useful for other algorithms, or to detect other kind of shapes like a tube hole (a pipe).
Results in B.4 show bounding boxes around the holes. However, it is difficult to have a precise pose estimation with bounding boxes.
In conclusion, this is a good method that can be explored. However, lot of non interesting edge are detected, so parameters have to be chosen wisely.

B.4 2D Feature Matching & Homography

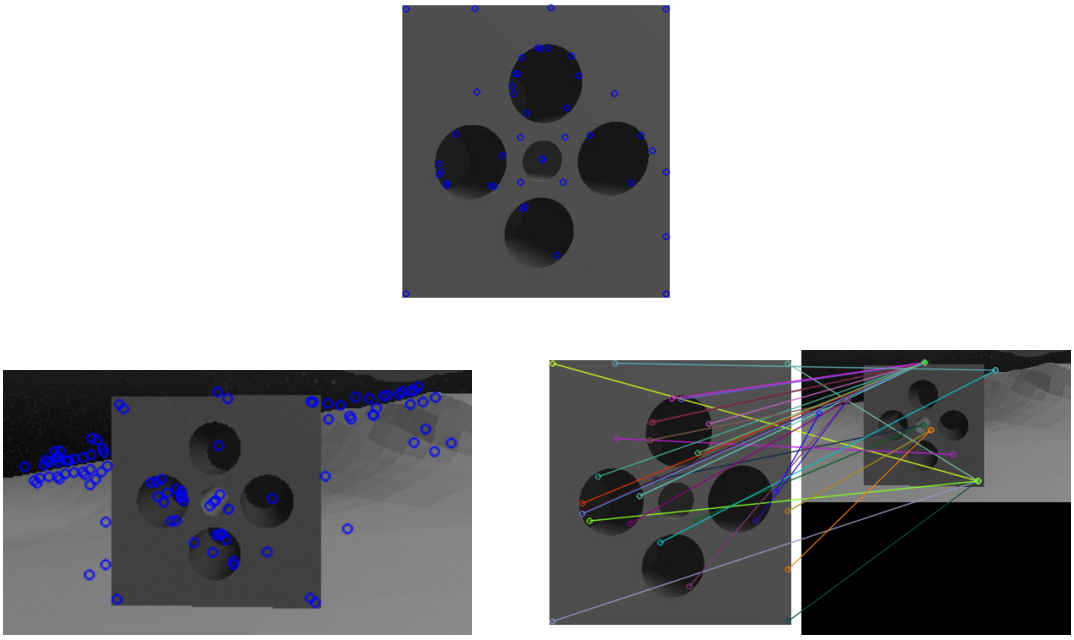

Figure B.5: Result of the algorithm. Above, the detected features (in blue) in the object image. Below, on the left, the detected features in the scene image; on the right the matched (erroneous) features.

Image features are small patches that are useful to compute similarities between images. Please note that these features are different from corner points. They indicates particular details that are different from others. Detecting these areas is important to recognize objects of interest in the image. The *descriptors* of these features contain the visual description of the patches, and they are used to recognize similarities.
This method uses a *object image* and a *scene image*. The first is a sort of template (note that this method is not a template matching as the one in section 5.3.3) which contains only the object to be found (in this case, the square face of the hole). The second is the image in which we want to detect this object (in this case, what the camera is seeing).
After good *features* are extracted from both images, the *descriptors* are used to match them, thus, detecting the object in the scene. Then, it is necessary to find the perspective transformation between object image and the scene (i.e. find homography). This is needed to take into account that usually pose and scaling of the object in the scene are not the same of the object image.
The OpenCV tutorial use different tools:

- **SURF** (Speeded Up Robust Features) Detector [Bay *et al.* (2006)] to extract features from *object image* and *scene image*, and to compute descriptors.
- **FLANN** (Fast Library for Approximate Nearest Neighbors) matcher [Muja & Lowe (2012)] to match the features.
- **Lowe's ratio test** [Lowe (2004)]to filter the best matches.
- **RANSAC** (RANdom SAmple Consensus) [Fischler & Bolles (1981)] method to find the homography with the function *findHomography()*.

In this case, results are unsatisfactory as can be seen in B.5. The main problem is that in this particular scene there are not nice distinct features. Also, the symmetry of the structure does not help, because there are a lot of particulars that are the same (like the square side and the holes). As can be seen in the tutorial, good results are obtained for food boxes. In fact, this methods is often associate to scenes where a lot of details are present (graffiti painting, supermarket shelf, ...). In our underwater case, realistic infrastructures don't have this details.
There are also lot of parameters to set for the three main tools (SURF, FLANN, RANSAC). Various trials have been tried but no-one was satisfactory. Also, different detectors (like SWIFT [Lowe (2004)]) and matchers (like Brute-force), have been tried.
The variety of tools and parameters make this method suitable for a lot of applications, and must be taken into consideration in other applications.

References

ABDULLAH, M., ROTH, H., WEYRICH, M. & WAHRBURG, J. (2015). An approach for peg-in-hole assembling using intuitive search algorithm based on human behavior and carried by sensors guided industrial robot. *IFAC-PapersOnLine*, **48**, 1476–1481. 7

ABREU, P., MORISHITA, H., PASCOAL, A., RIBEIRO, J. & SILVA, H. (2016). Marine Vehicles with Streamers for Geotechnical Surveys: Modeling, Positioning, and Control. *IFAC-PapersOnLine*. 30, 71

ANTONELLI, G. (2009). Stability analysis for prioritized closed-loop inverse kinematic algorithms for redundant robotic systems. *IEEE Transactions on Robotics*, **25**, 985–994. 5

ANTONELLI, G. & CHIAVERINI, S. (1998). Task-priority redundancy resolution for underwater vehicle-manipulator systems. In *Proceedings. 1998 IEEE International Conference on Robotics and Automation (Cat. No.98CH36146)*, vol. 1, 768–773 vol.1. 5

ANTONELLI, G. & CHIAVERINI, S. (2003). Fuzzy redundancy resolution and motion coordination for underwater vehicle-manipulator systems. *IEEE Transactions on Fuzzy Systems*, **11**, 109–120. 5

ANTONELLI, G., ARRICHIELLO, F. & CHIAVERINI, S. (2008). The null-space-based behavioral control for autonomous robotic systems. *Intelligent Service Robotics*, **1**, 27–39. 5

ANTONELLI, G., INDIVERI, G. & CHIAVERINI, S. (2009). Prioritized closed-loop inverse kinematic algorithms for redundant robotic systems with velocity saturations. 5892–5897. 15

BAERLOCHER, P. & BOULIC, R. (2004). An inverse kinematics architecture enforcing an arbitrary number of strict priority levels. *The Visual Computer*, **20**, 402–417. 6

BAY, H., TUYTELAARS, T. & VAN GOOL, L. (2006). Surf: Speeded up robust features. In A. Leonardis, H. Bischof & A. Pinz, eds., *Computer Vision – ECCV 2006*, 404–417, Springer Berlin Heidelberg, Berlin, Heidelberg. 82

BINGHAM, B., FOLEY, B., SINGH, H., CAMILLI, R., DELAPORTA, K., EUSTICE, R., MALLIOS, A., MINDELL, D., ROMAN, C. & SAKELLARIOU, D. (2010). Robotic tools for deep water archaeology: Surveying an ancient shipwreck with an autonomous underwater vehicle. *Journal of Field Robotics*, **27**, 702–717. 2

BRADSKI, G. (2000). The OpenCV Library. *Dr. Dobb's Journal of Software Tools*. 56, 69

CANNY, J. (1986). A computational approach to edge detection. *IEEE Transactions on Pattern Analysis and Machine Intelligence*, **PAMI-8**, 679–698. 79

CAPOCCI, R., DOOLY, G., OMERDIC, E., COLEMAN, J., NEWE, T. & TOAL, D. (2017). Inspection-class remotely operated vehiclesâĂŤa review. *Journal of Marine Science and Engineering*, **5**, 13. 2

CARRERA, A., PALOMERAS, N., HURTOS, N., KORMUSHEV, P. & CARRERAS, M. (2014). Learning by demonstration applied to underwater intervention. vol. 269. 4

CASALINO, G., ANGELETTI, D., BOZZO, T. & MARANI, G. (2001). Dexterous underwater object manipulation via multi-robot cooperating systems. In *Proceedings 2001 ICRA. IEEE International Conference on Robotics and Automation (Cat. No.01CH37164)*, vol. 4, 3220–3225 vol.4. 3

CASALINO, G., ANGELETTI, D., CANNATA, G. & MARANI, G. (2002). The functional and algorithmic design of amadeus multirobot workcell. In S.K. Choi & J. Yuh, eds., *Underwater Vehicle Technology*, vol. 12. 3

CASALINO, G., TURETTA, A., SORBARA, A. & SIMETTI, E. (2009). Self-organizing control of reconfigurable manipulators: A distributed dynamic programming based approach. In *2009 ASME/IFToMM International Conference on Reconfigurable Mechanisms and Robots*, 632–640. 5

CASALINO, G., ZEREIK, E., SIMETTI, E., TORELLI, S., SPERINDÉ, A. & TURETTA, A. (2012). Agility for underwater floating manipulation task and subsystem priority based control strategy. In *International Conference on Intelligent Robots and Systems (IROS 2012)*, 1772–1779. 3

CASALINO, G., CACCIA, M., CAITI, A., ANTONELLI, G., INDIVERI, G., MELCHIORRI, C. & CASELLI, S. (2014). Maris: A national project on marine robotics for interventions. In *22nd Mediterranean Conference on Control and Automation*, 864–869. 4, 7

CHANG, R.J., Y. LIN, C. & S. LIN, P. (2011). Visual-based automation of peg-in-hole microassembly process. *Journal of Manufacturing Science and Engineering*, **133**, 041015. 7

CHENG CHANG, C., YUAN CHANG, C. & TING CHENG, Y. (2004). Distance measurement technology development at remotely teleoperated robotic manipulator system for underwater constructions. 333 – 338. 2

CHHATPAR, S.R. & BRANICKY, M.S. (2001). Search strategies for peg-in-hole assemblies with position uncertainty. In *Proceedings 2001 IEEE/RSJ International Conference on Intelligent Robots and Systems. Expanding the Societal Role of Robotics in the the Next Millennium (Cat. No.01CH37180)*, vol. 3, 1465–1470 vol.3. 7

CHIAVERINI, S. (1997). Singularity-robust task-priority redundancy resolution for real-time kinematic control of robot manipulators. *IEEE Transactions on Robotics and Automation*, **13**, 398–410. 5

CHRIST, R. & WERNLI, R. (2013). *The ROV Manual: A User Guide for Remotely Operated Vehicles*. Elsevier, 2nd edn. 2

CIESLAK, P., RIDAO, P. & GIERGIEL, M. (2015). Autonomous underwater panel operation by girona500 uvms: A practical approach to autonomous underwater manipulation. In *2015 IEEE International Conference on Robotics and Automation (ICRA)*, 529–536. 4

COMPORT, A., MARCHAND, E., PRESSIGOUT, M. & CHAUMETTE, F. (2006). Real-time markerless tracking for augmented reality: the virtual visual servoing framework. *IEEE Transactions on Visualization and Computer Graphics*, **12**, 615–628. 61

COOK, D., VARDY, A. & LEWIS, R. (2014). A survey of auv and robot simulators for multi-vehicle operations. In *2014 IEEE/OES Autonomous Underwater Vehicles (AUV)*, 1–8. 27

DI LILLO, P.A., SIMETTI, E., DE PALMA, D., CATALDI, E., INDIVERI, G., ANTONELLI, G. & CASALINO, G. (2016). Advanced rov autonomy for efficient remote control in the dexrov project. *Marine Technology Society Journal*, **50**. 4

DIAZ LEDEZMA, F., AMER, A., ABDELLATIF, F., OUTA, A., TRIGUI, H., PATEL, S. & BINYAHIB, R. (2015). A market survey of offshore underwater robotic inspection technologies for the oil and gas industry. 2

DIETRICH, F., BUCHHOLZ, D., WOBBE, F., SOWINSKI, F., RAATZ, A., SCHUMACHER, W. & WAHL, F.M. (2010). On contact models for assembly tasks: Experimental investigation beyond the peg-in-hole problem on the example of force-torque maps. In

2010 IEEE/RSJ International Conference on Intelligent Robots and Systems, 2313–2318. 7

DJAPIC, V., NAÄŚ, Ä., FERRI, G., OMERDIC, E., DOOLY, G., TOAL, D. & VUKIÄĞ, Z. (2013). Novel method for underwater navigation aiding using a companion underwater robot as a guiding platforms. In *2013 MTS/IEEE OCEANS - Bergen*, 1–10. 2

DRAP, P. (2012). Underwater photogrammetry for archaeology. *Special Applications of Photogrammetry*. 2

DUDA, R.O. & HART, P.E. (1972). Use of the hough transformation to detect lines and curves in pictures. *Commun. ACM*, **15**, 11–15. 79

E. ROHMER, M.F., S. P. N. SINGH (2013). V-rep: a versatile and scalable robot simulation framework. In *Proc. of The International Conference on Intelligent Robots and Systems (IROS)*. 27

ESCANDE, A., MANSARD, N. & WIEBER, P.B. (2014). Hierarchical quadratic programming: Fast online humanoid-robot motion generation. *I. J. Robotics Res.*, **33**, 1006–1028. 6

EVANS, J., REDMOND, P., PLAKAS, C., HAMILTON, K. & LANE, D. (2003). Autonomous docking for intervention-auvs using sonar and video-based real-time 3d pose estimation. In *Oceans 2003. Celebrating the Past ... Teaming Toward the Future (IEEE Cat. No.03CH37492)*, vol. 4, 2201–2210 Vol.4. 3

EVANS, J.C., KELLER, K.M., SMITH, J.S., MARTY, P. & RIGAUD, O.V. (2001). Docking techniques and evaluation trials of the swimmer auv: an autonomous deployment auv for work-class rovs. In *MTS/IEEE Oceans 2001. An Ocean Odyssey. Conference Proceedings (IEEE Cat. No.01CH37295)*, vol. 1, 520–528 vol.1. 3

FAVERJON, B. & TOURNASSOUD, P. (1987). A local based approach for path planning of manipulators with a high number of degrees of freedom. In *Proceedings. 1987 IEEE International Conference on Robotics and Automation*, vol. 4, 1152–1159. 6

FISCHLER, M.A. & BOLLES, R.C. (1981). Random sample consensus: A paradigm for model fitting with applications to image analysis and automated cartography. *Commun. ACM*, **24**, 381–395. 82

FLACCO, F., DE LUCA, A. & KHATIB, O. (2012). Prioritized multi-task motion control of redundant robots under hard joint constraints. 3970–3977. 5

FLETCHER, B. (2000). Worldwide undersea mcm vehicle technologies. 10. 2

GILMOUR, B., NICCUM, G. & O'DONNELL, T. (2012). Field resident auv systems âĂŤ chevron's long-term goal for auv development. In *2012 IEEE/OES Autonomous Underwater Vehicles (AUV)*, 1–5. 2

GUENNEBAUD, G., JACOB, B. *et al.* (2010). Eigen v3 [online; accessed 29-june-2019]. 72

KANOUN, O., LAMIRAUX, F. & WIEBER, P. (2011). Kinematic control of redundant manipulators: Generalizing the task-priority framework to inequality task. *IEEE Transactions on Robotics*, **27**, 785–792. 6

KERMORGANT, O. (2014). A dynamic simulator for underwater vehicle-manipulators. In *International Conference on Simulation, Modeling, and Programming for Autonomous Robots Simpar*, Springer, Bergamo, Italy. 26, 70

KHATIB, O. (1986). Real-time obstacle avoidance for manipulators and mobile robots. *The International Journal of Robotics Research*, **5**, 90–98. 5

KHATIB, O. (1987). A unified approach for motion and force control of robot manipulators: The operational space formulation. *IEEE Journal on Robotics and Automation*, **3**, 43–53. 4

LANE, D.M., DAVIES, J.B.C., CASALINO, G., BARTOLINI, G., CANNATA, G., VERUGGIO, G., CANALS, M., SMITH, C., O'BRIEN, D.J., PICKETT, M., ROBINSON, G., JONES, D., SCOTT, E., FERRARA, A., ANGELLETI, D., COCCOLI, M., BONO, R., VIRGILI, P., PALLAS, R. & GRACIA, E. (1997). Amadeus: advanced manipulation for deep underwater sampling. *IEEE Robotics Automation Magazine*, **4**, 34–45. 3

LANE, D.M., MAURELLI, F., KORMUSHEV, P., CARRERAS, M., FOX, M. & KYRIAKOPOULOS, K. (2012). Persistent autonomy: the challenges of the pandora project. *IFAC Proceedings Volumes*, **45**, 268 – 273, 9th IFAC Conference on Manoeuvring and Control of Marine Craft. 4

LEE, H. & PARK, J. (2014). An active sensing strategy for contact location without tactile sensors using robot geometry and kinematics. *Autonomous Robots*, **36**, 109–121. 7

LEE, J., MANSARD, N. & PARK, J. (2012). Intermediate desired value approach for task transition of robots in kinematic control. *IEEE Transactions on Robotics*, **28**, 1260–1277. 6

LOWE, D.G. (2004). Distinctive image features from scale-invariant keypoints. *International Journal of Computer Vision*, **60**, 91–110. 82

LOZANO-PÃLREZ, T., MASON, M.T. & TAYLOR, R.H. (1984). Automatic synthesis of fine-motion strategies for robots. *The International Journal of Robotics Research*, **3**, 3–24. 8

MACIEJEWSKI, A.A. & KLEIN, C.A. (1985). Obstacle avoidance for kinematically redundant manipulators in dynamically varying environments. *The International Journal of Robotics Research*, **4**, 109–117. 5

MANSARD, N., KHATIB, O. & KHEDDAR, O. (2009a). A unified approach to integrate unilateral constraints in the stack of tasks. *IEEE Transactions on Robotics*, **25**, 670–685. 6

MANSARD, N., REMAZEILLES, A. & CHAUMETTE, F. (2009b). Continuity of varying-feature-set control laws. *IEEE Transactions on Automatic Control*, **54**, 2493–2505. 6

MARANI, G., KIM, J., YUH, J. & CHUNG, W. (2003). Algorithmic singularities avoidance in task-priority based controller for redundant manipulators. vol. 4, 3570 – 3574 vol.3. 5

MARANI, G., CHOI, S.K. & YUH, J. (2009). Underwater autonomous manipulation for intervention missions auvs. *Ocean Engineering*, **36**, 15 – 23, autonomous Underwater Vehicles. 3

MARCHAND, E., SPINDLER, F. & CHAUMETTE, F. (2005). Visp for visual servoing: a generic software platform with a wide class of robot control skills. *IEEE Robotics and Automation Magazine*, **12**, 40–52. 56, 69

MARTY, P. (2004). Alive: An autonomous light intervention vehicle. *Scandinavian Oil-Gas Magazine*, **32**. 3

MATAS, J., GALAMBOS, C. & KITTLER, J. (2000). Robust detection of lines using the progressive probabilistic hough transform. *Computer Vision and Image Understanding*, **78**, 119–137. 79

MICHEL, O. (2004). Webots: Professional mobile robot simulation. *Journal of Advanced Robotics Systems*, **1**, 39–42. 27

MIURA, J. & IKEUCHI, K. (1998). Task-oriented generation of visual sensing strategies in assembly tasks. *Pattern Analysis and Machine Intelligence, IEEE Transactions on*, **20**, 126 – 138. 7

MUJA, M. & LOWE, D.G. (2012). Fast matching of binary features. In *Computer and Robot Vision (CRV)*, 404–410. 82

NAKAMURA, Y. (1990). *Advanced Robotics: Redundancy and Optimization*. Addison-Wesley Longman Publishing Co., Inc., Boston, MA, USA, 1st edn. 5

NAKAMURA, Y. & HANAFUSA, H. (1986). Inverse kinematic solutions with singularity robustness for robot manipulator control. *Journal of Dynamic Systems, Measurement, and Control*. 4, 5

NENCHEV, D.N. & SOTIROV, Z.M. (1994). Dynamic task-priority allocation for kinematically redundant robotic mechanisms. In *Proceedings of IEEE/RSJ International Conference on Intelligent Robots and Systems (IROS'94)*, vol. 1, 518–524 vol.1. 6

NEWMAN, W., ZHAO, Y. & PAO, Y.H. (2001). Interpretation of force and moment signals for compliant peg-in-hole assembly. vol. 1, 571 – 576 vol.1. 7

OH, J. & OH, J.H. (2015). A modified perturbation/correlation method for force-guided assembly. *Journal of Mechanical Science and Technology*, **29**, 5437–5446. 7

PADIR, T. (2005). Kinematic redundancy resolution for two cooperating underwater vehicles with on-board manipulators. vol. 4, 3137 – 3142 Vol. 4. 5

PARAVISI, M., H. SANTOS, D., JORGE, V., HECK, G., GONÃĞALVES, L.M. & AMORY, A. (2019). Unmanned surface vehicle simulator with realistic environmental disturbances. *Sensors*, **19**. 27

PARK, H., BAE, J.H., PARK, J.H., BAEG, M.H. & PARK, J. (2013). Intuitive peg-in-hole assembly strategy with a compliant manipulator. In *IEEE ISR 2013*, 1–5. 8

PARK, H., PARK, J., LEE, D.H., PARK, J.H., BAEG, M.H. & BAE, J.H. (2017). Compliance-based robotic peg-in-hole assembly strategy without force feedback. *IEEE Transactions on Industrial Electronics*, **PP**, 1–1. 8

PAULI, J., SCHMIDT, A. & SOMMER, G. (2001). Vision-based integrated system for object inspection and handling. *Robotics and Autonomous Systems*, **37**, 297 – 309. 7

PEREZ, T. & FOSSEN, T.I. (2007). Kinematic models for manoeuvring and seakeeping of marine vessels. *Modeling, Identification and Control*, **28**, 19–30. 11

PRATS, M., PÃĽREZ, J., FERNÃĄNDEZ, J.J. & SANZ, P.J. (2012). An open source tool for simulation and supervision of underwater intervention missions. In *2012 IEEE/RSJ International Conference on Intelligent Robots and Systems*, 2577–2582. 26

PRATS, M., ROMAGÃŞS, D., PALOMERAS, N., GARCÃ◌A SÃĄNCHEZ, J.C., NANNEN, V., WIRTH, S., FERNANDEZ, J., P. BELTRÃĄN, J., CAMPOS, R., RIDAO, P., SANZ, P., OLIVER, G., CARRERAS, M., GRACIAS, N., MARÃ◌N PRADES, R. & ORTIZ, A. (2012). Reconfigurable auv for intervention missions: A case study on underwater object recovery. *Intelligent Service Robotics*, **5**, 19–31. 3

PRESSIGOUT, M. & MARCHAND, E. (2007). Real-time hybrid tracking using edge and texture information. *The International Journal of Robotics Research*, **26**, 689–713. 61

PROMETEO (2016). http://www.irs.uji.es/prometeo/, [online; accessed 25-october-2018]. 4

RIGAUD, V., COSTE-MANIERE, E., ALDON, M.J., PROBERT, P., PERRIER, M., RIVES, P., SIMON, D., LANG, D., KIENER, J., CASAL, A., AMAR, J., DAUCHEZ, P. & CHANTLER, M. (1998). Union: underwater intelligent operation and navigation. *IEEE Robotics Automation Magazine*, **5**, 25–35. 3

ROBUST (2016). http://eu-robust.eu, [online; accessed 25-october-2018]. 4

RUSU, R.B. & COUSINS, S. (2011). 3D is here: Point Cloud Library (PCL). In *IEEE International Conference on Robotics and Automation (ICRA)*, Shanghai, China. 56, 62

SANZ, P., RIDAO, P., OLIVER, G., CASALINO, G., INSAURRALDE, C., SILVESTRE, C., MELCHIORRI, C. & TURETTA, A. (2012). Trident: Recent improvements about autonomous underwater intervention missions. vol. 3, 1–10. 3, 7

SCHEMPF, H. & YOERGER, D.R. (1992). Coordinated vehicle/manipulation design and control issues for underwater telemanipulation. *IFAC Proceedings Volumes*, **25**, 259 – 267, iFAC Workshop on Artificial Intelligence Control and Advanced Technology in Marine Automation (CAMS '92), Genova, Italy, April 8-10. 3

SENTIS, L. & KHATIB, O. (2005). Control of free-floating humanoid robots through task prioritization. In *Proceedings of the 2005 IEEE International Conference on Robotics and Automation*, 1718–1723. 5

SHI, J. & TOMASI, C. (2000). Good features to track. *Proceedings / CVPR, IEEE Computer Society Conference on Computer Vision and Pattern Recognition. IEEE Computer Society Conference on Computer Vision and Pattern Recognition*, **600**, 593âĂŞ600. 78

SHIRINZADEH, B., ZHONG, Y., TILAKARATNA, P.D.W., TIAN, Y. & DALVAND, M.M. (2011). A hybrid contact state analysis methodology for robotic-based adjustment

of cylindrical pair. *The International Journal of Advanced Manufacturing Technology*, **52**, 329–342. 7

SICILIANO, B. & SLOTINE, J..E. (1991). A general framework for managing multiple tasks in highly redundant robotic systems. In *Fifth International Conference on Advanced Robotics 'Robots in Unstructured Environments*, 1211–1216 vol.2. 5

SICILIANO, B., SCIAVICCO, L., VILLANI, L. & ORIOLO, G. (2009). *Robotics: Modelling, Planning and Control*, 147–151. Springer-Verlag London. 29

SIMETTI, E. & CASALINO, G. (2016). A novel practical technique to integrate inequality control objectives and task transitions in priority based control. *Journal of Intelligent & Robotic Systems*, **84**. 4, 7, 15, 22, 72

SIMETTI, E. & CASALINO, G. (2017). Manipulation and transportation with cooperative underwater vehicle manipulator systems. *IEEE Journal of Oceanic Engineering*, **42**, 782–799. 4, 10, 16, 22, 23, 30, 35

SIMETTI, E., TURETTA, A. & CASALINO, G. (2009). *Distributed Control and Coordination of Cooperative Mobile Manipulator Systems*, 315–324. Springer Berlin Heidelberg, Berlin, Heidelberg. 5

SIMETTI, E., CASALINO, G., TORELLI, S., SPERINDÉ, A. & TURETTA, A. (2014a). Floating underwater manipulation: Developed control methodology and experimental validation within the trident project. *Journal of Field Robotics*, **31(3)**, 364–385. 3, 7

SIMETTI, E., CASALINO, G., TORELLI, S., SPERINDÉ, A. & TURETTA, A. (2014b). Underwater floating manipulation for robotic interventions. *IFAC Proceedings Volumes*, **47**, 3358 – 3363, 19th IFAC World Congress. 7

SIMETTI, E., CASALINO, G., WANDERLINGH, F. & AICARDI, M. (2018). Task priority control of underwater intervention systems: Theory and applications. *Ocean Engineering*, **164**, 40 – 54. 4, 10, 22, 23

SONG, H., KIM, Y. & SONG, J.B. (2016). Guidance algorithm for complex-shape peg-in-hole strategy based on geometrical information and force control. *Advanced Robotics*, 1–12. 7

SUGIURA, H., GIENGER, M., JANSSEN, H. & GOERICK, C. (2007). Real-time collision avoidance with whole body motion control for humanoid robots. In *2007 IEEE/RSJ International Conference on Intelligent Robots and Systems*, 2053–2058. 5

SUZUKI, S. & BE, K.A. (1985). Topological structural analysis of digitized binary images by border following. *Computer Vision, Graphics, and Image Processing*, **30**, 32 – 46. 58, 80

TRINH, S., SPINDLER, F., MARCHAND, E. & CHAUMETTE, F. (2018). A modular framework for model-based visual tracking using edge, texture and depth features. In *IEEE/RSJ Int. Conf. on Intelligent Robots and Systems, IROS'18*, Madrid, Spain. 61

TWINBOT (2019). http://www.irs.uji.es/twinbot/twinbot.html, [online; accessed 29-june-2019]. 1, 8, 55, 69, 71

URABE, T., URA, T., TSUJIMOTO, T. & HOTTA, H. (2015). Next-generation technology for ocean resources exploration (zipangu-in-the-ocean) project in japan. 1–5. 2

WANDERLINGH, F. (2018). *Cooperative Robotic Manipulation for the Smart Factory*. Ph.D. thesis, Università degli Studi di Genova. 10, 19, 22, 35

WYNN, R., HUVENNE, V., LE BAS, T., MURTON, B., CONNELLY, D., BETT, B., RUHL, H., MORRIS, K., PEAKALL, J., PARSONS, D., J. SUMNER, E., E. DARBY, S., DORRELL, R. & HUNT, J. (2014). Autonomous underwater vehicles (auvs): Their past, present and future contributions to the advancement of marine geoscience. *Marine Geology*, **352**. 2

XU, Q. (2015). Robust impedance control of a compliant microgripper for high-speed position/force regulation. *IEEE Transactions on Industrial Electronics*, **62**, 1201–1209. 8

YOSHIKAWA, T. (1984). Analysis and Control of Robot Manipulators with Redundancy. In M. Brady & R. Paul, eds., *Robotics Research The First International Symposium*, 735–747, MIT Press. 5

YUH, J., CHOI, S.K., IKEHARA, C., KIM, G.H., MCMURTY, G., GHASEMI-NEJHAD, M., SARKAR, N. & SUGIHARA, K. (1998). Design of a semi-autonomous underwater vehicle for intervention missions (sauvim). In *Proceedings of 1998 International Symposium on Underwater Technology*, 63–68. 3

ZEREIK, E., SORBARA, A., MERLO, A., SIMETTI, E., CASALINO, G. & DIDOT, F. (2011). Space robotics supporting exploration missions: vision, force control and coordination strategy for crew assistants. *Intelligent Service Robotics*, **4**, 39–60. 5